Distribution Agreement

In presenting this thesis or dissertation as a partial fulfillment of the requirements for an advanced degree from Emory University, I hereby grant to Emory University and its agents the non-exclusive license to archive, make accessible, and display my thesis or dissertation in whole or in part in all forms of media, now or hereafter known, including display on the world wide web. I understand that I may select some access restrictions as part of the online submission of this thesis or dissertation. I retain all ownership rights to the copyright of the thesis or dissertation. I also retain the right to use in future works (such as articles or books) all or part of this thesis or dissertation.

Signature:

_____ _____

Yannic J. Gagnon Date

UNCOVERING THE ROLE OF NEIGHBORING DOMAIN MODULUS ON THE LOCAL GLASS TRANSITION
AND SHEAR WAVE PROPAGATION IN NANOSTRUCTURED POLYMERIC MATERIALS

By

Yannic J. Gagnon
Doctor of Philosophy

Physics

Connie B. Roth, Ph.D.
Advisor

Justin C. Burton, Ph.D.
Committee Member

James T. Kindt, Ph.D.
Committee Member

Daniel M. Sussman, Ph.D.
Committee Member

Eric R. Weeks, Ph.D.
Committee Member

Accepted:

Kimberly J. Arriola, Ph.D.
Dean of the James T. Laney School of Graduate Studies

Date

UNCOVERING THE ROLE OF NEIGHBORING DOMAIN MODULUS ON THE LOCAL GLASS TRANSITION AND SHEAR WAVE PROPAGATION IN NANOSTRUCTURED POLYMERIC MATERIALS

By

Yannic J. Gagnon
B.S., University of Hawaii at Manoa, HI, 2015

Advisor: Connie B. Roth, Ph.D.

An abstract of
A dissertation submitted to the Faculty of the
James T. Laney School of Graduate Studies of Emory University
in partial fulfillment of the requirements for the degree of
Doctor of Philosophy
in Physics
2022

Abstract

UNCOVERING THE ROLE OF NEIGHBORING DOMAIN MODULUS ON THE LOCAL GLASS TRANSITION
AND SHEAR WAVE PROPAGATION IN NANOSTRUCTURED POLYMERIC MATERIALS
By Yannic J. Gagnon

In this dissertation, I use a modified fluorescence method to measure the local glass transition temperature $T_g(z)$ of multilayer polymer films, and I develop a quartz crystal microbalance (QCM) method to measure the modulus of single layer and bilayer films. My fluorescence measurements demonstrate that the local $T_g(z)$ in a glassy polystyrene (PS) film is strongly dependent on the Young's modulus of a neighboring polydimethylsiloxane (PDMS) domain. Specifically, by varying the Young's modulus from 0.9 to 2.6 MPa I find that the local $T_g(z)$ in PS at a distance of $z = 50$ nm away from the PS/PDMS interface increases by 40 K. In addition, I find that the length scale of perturbation to bulk T_g in PS near the interface is $z \approx 65$–90 nm. Although this length scale is large compared to the interfacial width for this system of $w_I \approx 1.5$ nm, it is considerably shorter than what would be expected from other systems studied previously by our group. We attribute this difference in length scale to a smaller interfacial width in our system compared to those studied previously. Gathering these results and others from the literature, we propose that acoustic impedance matching might be the control parameter influencing perturbations to local $T_g(z)$ near dissimilar polymer-polymer interfaces.

In acoustic impedance matching, acoustic waves are maximally transmitted across a boundary if the product of the density and shear moduli are similar between the layers, and if the width of the transition in the shear moduli or the density between the layers is large. In the rest of the dissertation, I develop an experimental method using a quartz crystal microbalance (QCM) and a continuum physics model to study the influence of annealing a polybutadiene (PB) / polystyrene interface on the MHz-frequency shear wave propagation through the interface. Along the way, I measure the shear modulus of PB, polydimethylsiloxane, and PS films at MHz frequencies. I find that annealing a PB/PS bilayer at 120 °C for 100 min results in a pronounced change in the QCM experimental signal associated with changes in viscoelasticity, and by applying a continuum physics layer model show that the width of the modulus profile near the PB/PS interface extends to approximately 150 nm. This broad length scale of the modulus profile across dissimilar polymer domains developed by annealing suggests an increase in the transmission of vibrational modes across the interface. This increased transmission of vibrational modes may then perturb the local vibrational modes in the polymer domains, which have been shown to be predictors of structural relaxations associated with the glass transition. These results suggest that this increased transmission of vibrational modes across the well-annealed polymer-polymer interface may be the source of dynamical coupling causing the broad, extended $T_g(z)$ profiles that are observed to develop with interface annealing.

UNCOVERING THE ROLE OF NEIGHBORING DOMAIN MODULUS ON THE LOCAL GLASS TRANSITION AND SHEAR WAVE PROPAGATION IN NANOSTRUCTURED POLYMERIC MATERIALS

By

Yannic J. Gagnon
B.S., University of Hawaii at Manoa, HI, 2015

Advisor: Connie B. Roth, Ph.D.

A dissertation submitted to the Faculty of the
James T. Laney School of Graduate Studies of Emory University
in partial fulfillment of the requirements for the degree of
Doctor of Philosophy
in Physics
2022

Acknowledgments

I would first like to thank my advisor Connie B. Roth for her tireless guidance and mentoring. The skills I learned from Connie have greatly improved my life both within and outside of my scientific interests, and I couldn't be more lucky to have had Connie as an advisor. I would also like to thank my co-advisor Justin C. Burton for his extreme generosity in including me in his group's events and for sharing his time to answer my many questions. I would like to extend a heartfelt thank you to Xinru Huang, who when I joined the Roth Lab quickly emerged as a very helpful and knowledgeable mentor. I frequently find myself striving to emulate her example in my own interactions with mentees. I would like to thank the past Roth Lab members for their work that set up my own research, and especially Benjamin L. Kasavan for orienting me to the lab and the instrumentation. I extend a hearty thank you to the current lab members Yixuan Han, James H. Merrill and Alex Couturier for their continuing friendship and for introducing me to many new ideas. In addition to growing up in the Roth Lab, I also grew up in the Burton Lab, where I found a highly supportive environment uplifted by good friends in the form of Justin himself and Nicholas L. Cuccia, Xiaolei Ma, Dana C. Harvey, and Kavinda Nissanka. A sincere thank you for being so welcoming and for brightening my time at Emory.

I would like to thank my committee members, Justin C. Burton, Eric R. Weeks, Daniel M. Sussman, and James T. Kindt for their generosity in sharing their time and expertise on my committee, and for their flexibility in scheduling my defense time.

I would like to extend my gratitude to Jason Boss for quickly and efficiently fixing any computer issue I couldn't solve myself, and to both Jason and former employee Art Kleyman for keeping our computers running without issues. Navigating the environment of reimbursements and administrative requirements can be challenging, and I gratefully acknowledge the kind help in this arena extended to me by the physics staff, especially Barbara Conner, Susan Cook, Jason Pettigrew, and former

staff member Calvin Jackson.

I would like to thank my wife, Rachel Behrend, whose unconditional support and good advice have kept me going. Finally, I would like to thank my parents, Joan M. Gagnon and Pierre D. Gagnon, and my brother, Pierre E. Gagnon, in addition to my in-laws Angeline Behrend, Richard Behrend, and David Behrend, for their kind support. There are so many others I am thinking of whose friendship and help was instrumental to my development as a scientist and as a person, and although for the sake of length of this document their names may not be included here, I gratefully acknowledge their help.

Finally, I gratefully acknowledge the support from the National Science Foundation Polymers Program (DMR-1709132 and DMR-1905782) and Emory University.

Contents

List of Figures

Chapter 1

Introduction

The problem of the glass transition remains unsolved, though considerable progress has been made in theory, simulations, and experiments. Polymers are excellent glass formers, and polymer films are a simple system to understand the effect of decreasing spatial dimension on the glass transition, or in the case of stacked polymer films, the effect of interfaces on the glass transition. This dissertation is divided between three main projects. The first project is about measuring the influence of modulus of a polydimethylsiloxane (PDMS) domain on the local glass transition temperature in an adjacent polystyrene (PS) domain. The second project is the development of a quartz crystal microbalance (QCM) setup and continuum physics model to measure the modulus of rubbery polymer films. The third project is about applying this QCM setup and extending the continuum physics model to measure the influence of annealing a polybutadiene (PB)/PS polymer bilayer on the modulus near the interface.

In this introductory chapter, I will briefly discuss the glass transition and modulus in both bulk polymer systems and polymer systems confined to the nanoscale, where properties of the interface dominate. I will also discuss how the interface between two adjacent polymers plays a key role in regulating perturbations to the glass transition in multilayer polymer systems. This should provide a summary of the field and

concepts that will be relevant for understanding my dissertation. I will end with an overview of the following chapters.

1.1 The Glass Transition in Polymers in the Bulk

Cooling a liquid to reach a solid state generally proceeds along two pathways. Some liquids, especially when cooled slowly, form an ordered solid termed a crystal, in which there is long-range order through a repeating unit cell. Other liquids form a disordered solid on cooling, termed a glass, in which there is no long-range ordering, but which is in a non-equilibrium and solid state. Interestingly, in a small window of temperature preceding the glass transition, the viscosity and modulus rise dramatically, even though the microscopic structure and density barely change.[1] Related to this phenomenon, the reorganizations of the liquid's units on cooling become more cooperative in nature, with ever larger length scales of cluster rearrangement needed for a given unit to move. Intermittent "cage breaking" events permit a given unit to escape from a cage of surrounding units to a new, lower energy state in a different cage.[1] While visualizing this cage hopping is difficult in molecular or polymeric glasses, this phenomenon has been directly observed in a colloidal glass.[2] The longer cooperative length scales required for particles to rearrange is accompanied by a longer time scale between rearrangements. These cooperative rearrangements are termed "α-relaxations," and the region over which the rearrangement is cooperative is termed a cooperatively rearranging region (CRR).[3] This notion of CRRs was introduced by Adam and Gibbs as a way of relating a length scale to the configurational entropy for glass-forming liquids. This configurational entropy is related to the glass transition by the fact that as the glass transition is approached, fewer configurational states of the particles are accessible, which results in the drastic slowdown of particle mobility. The size of a CRR for polymeric liquids near T_g is typically between 1-4 nm.[4,5] The

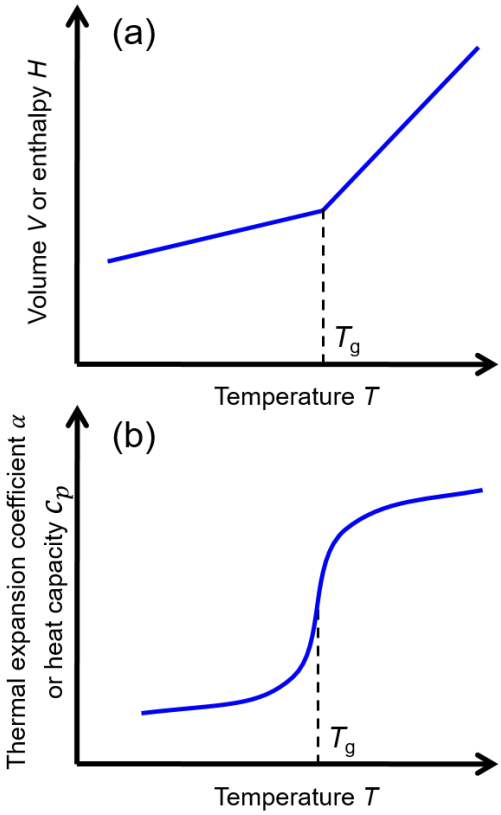

Figure 1.1: Cartoon of two common methods for measuring the average T_g of polymer systems. In (a), the change in slope of the volume or enthalpy typically measured on cooling identifies T_g. In (b), the thermal expansion coefficient α or the heat capacity c_p is measured on heating, and T_g is identified as either the temperature at the midpoint, as shown here, or the temperature at the the onset of the transition.

time interval between cooperative relaxation events grows on approaching the glass transition, before α relaxations cease altogether when the material becomes a glass. Due to experimental constraints, the glass transition is often defined in experimental systems as occurring when the relaxation time $\tau = 100$ s.

The temperature at which a given material falls out of its equilibrium liquid state on cooling is termed the glass transition temperature T_g and is a property of a material for a given cooling rate in bulk glass forming materials. Polymers, despite being long-chain molecules, have similar glass transition characteristics to small-molecule glasses, because the packing frustration in polymers associated with

the glass transition occurs at the local segmental level. The value of T_g for polymers is not dependent on molecular weight beyond a threshold of a couple of hundred monomers.[1] Polymers are excellent glass formers, inexpensive, and have a plethora of industrial applications, and are therefore often used to study the glass transition.

Figure 1.1 shows two common methods of measuring T_g experimentally. The first method is done by determining the change in slope of the volume or enthalpy as a function of temperature. Ellipsometry is a particularly common example of this method for identifying T_g in polymer films. The film thickness, which relates to the volume of the film, is monitored as a function of temperature on cooling, and the intersection of lines fit to the glassy and rubbery regimes identify T_g. The second common method of identifying T_g is by the midpoint or onset of the change in the thermal expansion coefficient or heat capacity C_p measured on heating. Differential scanning calorimetry (DSC) is a particularly common example of this method, where DSC determines T_g of polymer systems by a step change in the measured heat flow that occurs when passing through the glass transition temperature on heating.[6]

1.2 Modulus of Bulk Polymer Systems

Polymers are viscoelastic, meaning that their moduli contain an elastic term G' related to the storage of an applied strain and a loss term G'' related to dissipation in response to an applied strain. An alternate description is that the storage modulus is the portion of the modulus that is in phase with the applied strain, while G'' is the portion of the modulus that is out of phase with the applied strain.[7] The complex modulus $\widetilde{G}$ combines the storage and loss moduli: $\widetilde{G} = G' + iG''$, where i is the imaginary unit.

Figure 1.2 is a representation of the viscoelastic master curves for the storage and loss moduli and the four regimes commonly found in polymers. In practice,

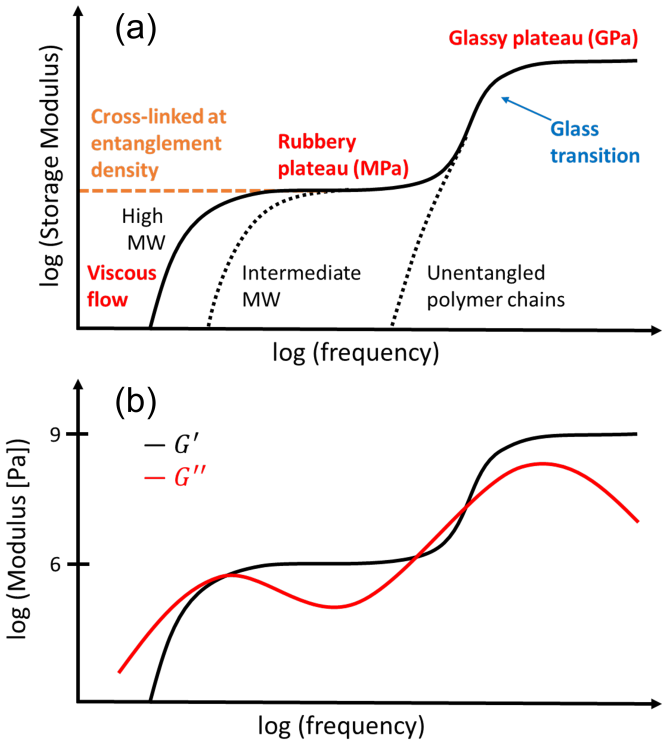

Figure 1.2: Cartoon of the frequency- or temperature-dependent elastic response of a typical polymer. (a) Storage modulus as a function of frequency, for different molecular weights. The four regions of interest are the glassy plateau at very high frequencies (typically with modulus of the order GPa), the glass-to-rubber transition, the rubbery plateau (typically with modulus of the order GPa), and the liquid flow regime. If the material is cross-linked, there is no flow at low frequencies or high temperatures. A higher molecular weight polymer will have a longer rubbery plateau regime than a polymer with intermediate molecular weight, and polymers with molecular weights below the entanglement threshold will not demonstrate rubbery plateau behavior. (b) Storage and loss moduli as a function of frequency for a given molecular weight.

such curves are produced by measuring the storage and loss moduli as a function of frequency at a series of different temperatures, then using time-temperature superposition to shift the curves to make a single master curve corresponding to the viscoelastic response at a single reference temperature.[7] Such master curves tend to describe the behavior of bulk polymers quite well within the range of frequencies that are experimentally accessible.[8] At low temperatures or high frequencies, monomers are caged by their neighbors, and motions other than local rattling of a monomer in its confining cage are effectively frozen out.[1] In this glassy state, the polymer behaves

as a solid, with $G' \sim \omega^0$ and $G''/G' << 1$.[7] In the glass-to-rubber transition, cooperative rearrangement occurs, in which multiple segmental units must move collectively to allow a trapped unit to "hop" to a new cage.[1] It is clear from Figure 1.2 that the glass transition temperature and the modulus are correlated in bulk polymers. At higher temperatures or long times, increasingly less cooperativity is needed for segmental units to rearrange. If the polymer's molecular weight is below the entanglement threshold M_c and the polymer is not chemically cross-linked, diffusion at the chain level occurs and the polymer begins to flow like a liquid. In this terminal regime, $G' \sim \omega^2$, $G'' \sim \omega$, and $G''/G' > 1$.[7]

If the molecular weight of the polymer is greater than M_c, the presence of entanglements changes the viscoelastic response and reptation begins to dominate the relaxation process. Reptation refers to the snake-like motion polymer chains must undergo to escape entanglements with nearby polymers. The presence of entanglements causes a decoupling in the time scales involving the glass transition and liquid flow. This leads to the rubbery plateau region, in which $G' \sim \omega^0$, and $G''/G' < 1$. The time scale for reptation is characterized by the reptation time τ_r, which in the tube model of reptation[7] scales with molecular weight M as $\tau_r \propto M^3$. Reptation is linearly related to the viscosity η of an entangled polymer melt, leading to a prediction of $\eta \propto M^3$. In experimental systems, the viscosity dependence scales with $M^{3.4}$, which has been explained by more complex tube models that account for additional relaxation mechanisms such as chain retraction and constraint release.[7] The rubbery plateau storage modulus G_N is related to the molecular weight between entanglements M_e by[7]

$$G_N = \frac{\rho RT}{M_e}, \tag{1.1}$$

where ρ is the density, R is the ideal gas constant, and T is the temperature. At times longer than the reptation time and for polymers which are not cross-linked, liquid flow occurs. In this regime, the moduli go as $G' \sim \omega^2$, $G'' \sim \omega$, and $G''/G' > 1$.[7] For cross-

linked polymer networks, the cross-links prevent the flow of material at time scales larger than the reptation time. The rubbery modulus of the cross-linked polymer G_x is related to the molecular weight between the cross-links M_x by[7]

$$G_x = \frac{\rho RT}{M_x}. \tag{1.2}$$

Equation 1.2 shows that the modulus of a cross-linked rubber should increase with decreasing M_x, which corresponds to increasing levels of cross-linking in the network.

1.3 The Glass Transition in Polymer Thin Films

To better understand length scales of the glass transition in polymer materials, Keddie, Jones, and Cory[9] measured the T_g of PS films atop silicon substrates as a function of film thickness h, using ellipsometry. They discovered that the T_g of PS films decreased as a function of decreasing film thickness at thicknesses below ~ 60 nm, for a total T_g depression of 30 K for the thinnest films of approximately 10 nm. This trend was not molecular weight dependent, which indicates that this "confinement effect" is not due to perturbations of the chain conformation when the chains are confined to being below their unperturbed size. A similar trend of decreasing T_g with decreasing h was measured for poly(methy1 methacrylate) (PMMA) films atop evaporated gold substrates, though the magnitude of the T_g depression was smaller, and a very slight *increase* in T_g on confinement was found for PMMA films supported on silicon.[10]

Since these studies over twenty years ago, different groups using a variety of experimental techniques such as ellipsometry, DSC, dielectric spectroscopy, X-ray reflectivity, positron annihilation lifetime spectroscopy, and local thermal analysis have reproduced the trend of decreasing T_g of PS with decreasing h, as reviewed in Ref. [11]. Meanwhile, polymers with strong interactions with the substrate such as

poly(2-vinylpyridine) (P2VP) display an increased T_g with confinement,[12] and polymers with weak interactions with the substrate such as PMMA on silica display little change in T_g with confinement.[10] These different trends in polymer films supported on solid substrates can be understood on the basis of a competition of effects from the interfaces at the top and bottom of the film. At the top of the film is a free surface, and due to the reduced number of neighbors at the free surface, polymer mobility is increased. This increased mobility means that the polymer near the free surface can relax more readily than polymer in the bulk, which leads to a decrease in the measured averaged T_g. At the bottom of the film is the substrate. If there is not a strong interaction energy between the polymer and the substrate, such as the case of PS and silica, the presence of the substrate only perturbs the polymer by altering the chain conformation from its ideal state locally near the substrate.[13,14] While the presence of a hard wall boundary condition is predicted to influence the chain conformation and entanglement density near the substrate,[14] it does not alter the local segmental mobility relevant for altering cooperative motion and thus T_g. However, this situation changes if there is an attractive energy of interaction between the polymer and the substrate, such as for P2VP and silica. In this system, hydrogen bonding occurs between the nitrogen-containing group in the P2VP monomer and the hydroxyl groups on the silica surface, which reduces the local segmental mobility and increases the measured T_g of thin films.[12]

In an effort to better understand the magnitude and the spatial extent to which interfaces *locally* influence the glass transition in polymer films, Ellison and Torkelson devised a method using the fluorescence of pyrene to measure the T_g of PS locally at the free surface and substrate interfaces.[15] To measure the local T_g in PS using pyrene, the pyrene molecule cannot be allowed to diffuse away during the experiment. In Ref. [15], the pyrene molecule was connected to a butyl methacrylate monomer which was chemically attached to the backbone of PS of sufficiently high molecular

weight so that the pyrene connected to the PS did not diffuse more than 1-2 nm on the timescales of the experiment. The pyrene was added in sufficiently low concentrations that the T_g of unlabeled, neat PS was within ∼1 K of the pyrene-labeled PS (PS-Py). To measure the local T_g, a thin (12-14 nm thick) PS-Py layer was inserted at the top of a ∼270 nm PS film to measure the local T_g of PS at the free surface. To measure the local T_g of PS at the substrate, a thin PS-Py layer was inserted between the quartz substrate and the PS film. Finally, to measure the local T_g of PS in the bulk, a thin PS-Py layer was inserted between two 270 nm PS films. Additional measurements varied the thickness of the PS-Py layer at the free surface or the thickness of the PS underlayer. The overall multilayer stack was annealed at 130 °C for 10 min prior to collecting fluorescence measurements to erase thermal history, which also smoothes over the abrupt interface between the PS and the PS-Py layers by causing some interfacial broadening between these layers. The results of these measurements were that the local T_g at the free surface was 32 °C less than the bulk PS T_g, and this effect propagated ∼30 nm from the free surface into the PS. The local T_g at the substrate was the same as the bulk T_g of PS, and the local T_g measured in the bulk of PS was the bulk T_g of PS. These results demonstrated that the length scales of perturbations to T_g near the free surface interface are tens of nm. This length scale stands in contrast with the much smaller 1-4 nm associated with the size of a cooperatively rearranging region. This difference in length scales showed that the perturbation to the local average cooperative motions that affect T_g in a region of a polymer film is determined primarily by the nature of the interface (polymer-free surface or polymer-substrate), although the sizes of CRRs likely play an additional role in the length scales of perturbation.[16]

1.4 Current Theoretical Understanding of the Glass Transition in Confined Polymer Systems

A range of theories have been put forward to model the glass transition behavior of polymeric materials in confined geometries. A recent paper by Schweizer and Simmons[17] provides an excellent review of some of the most well-known theories to date. Some theorists who prefer a thermodynamic treatment of the glass transition have extended the Adam-Gibbs concept of relating the slowing dynamics on approaching the glass transition with configurational entropy. Theories in this category include the Random First Order Theory (RFOT), which incorporates elements from nucleation theory rather than CRRs to describe the growing length scale for structural relaxation,[18] and the "string model" by Starr and Douglas[19,20] that uses a string-like geometry of CRRs to encode a length scale of cooperative motion. Different theories based on free volume approaches attempt to connect the gradient in free volume or density near an interface to the relaxation times in the material, often including the concept of CRRs but grounding these concepts in a free volume rather than configurational entropy basis.[21–24] Other models emphasize a kinetic approach to the glass transition. The "limited mobility" (LM) model of Tito, Milner, and Lipson[25–27] is a purely kinetic lattice model where free volume and local mobility in a fluid near interfaces are transferred to adjacent lattice sites according to specific rules and with specific probabilities. Importantly, free volume and mobility are decoupled, so that their individual evolution can be observed as the liquid approaches the glass transition. A "kinetic arrest" transition, beyond which mobility is arrested and free volume is kinetically trapped, is used as an analog to the glass transition.

A theory of the glass transition in polymer systems that has been particularly successful in modeling experimental data is Schweizer's Elastically Collective Nonlinear Langevin Equation (ECNLE) theory. The ECNLE theory has seen great success in

modeling glass formation in small molecule systems,[28–30] and bulk[31] or confined[32–35] polymer systems. The ECNLE model received its inspiration from the earlier Shoving model by Dyre,[36,37] which was a primarily continuum mechanics-based model applied to bulk glasses. The key aspect of these "elastic activation models" is the introduction of a long range elastic field that couples to local structural relaxation events. In the ECNLE model, spontaneous strain fluctuations in cooling liquids can create extra volume locally, which facilitate local incompressible structural relaxation events. These structural relaxation events correspond to the cage breaking and particle hopping events discussed earlier. The energy barrier of the strain fluctuation is set by the glassy plateau shear modulus $G'(T)$. In many cases the ECNLE model is able to demonstrate quantitative agreement between theory and experiment with calculations using no adjustable parameters, which suggests the importance of long-ranged strain fields and of the glassy plateau shear modulus $G'(T)$ on the glass transition in glass forming polymer systems.

1.5 Modulus of Thin Polymer Films

Measuring the modulus of thin polymer films is an especially difficult task, since conventional methods of measuring the viscoelasticity of bulk systems such as dynamic mechanical analysis typically involve applying a stress that can damage or break apart thin films. Determining reliable values of the modulus of polymer thin films from indentation methods such as nanoindentation are also difficult, because the stress field produced by the indenter tip can travel farther than the tip itself and sample the hard substrate beneath the polymer thin film.[38–40] With these difficulties in mind, a non-indentation method of measuring the modulus in thin polymer films is desirable, so that the indenter does not sample the modulus of the substrate or adhere to the film.

There are a variety of methods of measuring different forms of moduli that have been developed over the years. One method, developed by Stafford et al.,[41–44] is a particularly well-known and useful method for measuring the Young's modulus E of glassy polymer thin films, although it can also be applied to measure the Young's modulus of thin rubbery films.[45] This method, termed the "buckling" or "wrinkling"-based method, causes a strain-induced buckling instability of a glassy polymer film atop a cross-linked rubbery PDMS substrate that has been held under tension prior to placing the polymer film on top. On release of the tension, the PDMS/film system buckles, forming periodic wrinkles of wavelength λ. This wavelength is measured via optical microscopy or light scattering[45] and is related to the film's Young's modulus and the Young's modulus of the PDMS substrate with a simple equation from buckling mechanics. The buckling-based measurements of the glassy Young's modulus of PS measure a decrease in modulus with decreasing film thickness occurring at $\sim$40 nm, with E decreasing by over a factor of 3 for the thinnest films of 5 nm.[42] A similar trend was observed for the modulus of PMMA films, also supported on PDMS. The trend in decreasing modulus of polymer thin films with confinement to sub-40 nm thicknesses (without strong interactions with the substrate) is similar to the trend of decreasing T_g of polymer thin films with confinement, which is suggestive of T_g and E of thin polymer films being correlated, as they are in the bulk. However, this correlation in length scales was not observed for poly(n-propyl methacrylate) (PnPMA) films measured with the buckling method, for which the modulus varied at thickness scales up to $h = 80$ nm but the T_g was invariant at the measurable thicknesses of $h > 50$ nm.[43]

The buckling method presents a very useful method for measuring the Young's modulus of thin polymer films, but it is not without limitations. There must be a significant modulus mismatch between the rubbery substrate layer and the glassy top layer, which restricts the measurement to only being able to measure certain polymers.

Also the viscoelastic Young's modulus of polymers is temperature and rate-dependent, and is comprised of the storage and loss moduli: $\widetilde{E}(\omega, T) = E'(\omega, T) + iE''(\omega, T)$; however, the modulus determined by the buckling method is the zero frequency and room temperature real component of the Young's modulus, E. To obtain a full picture of the viscoelasticity of a polymer thin film, the buckling method therefore needs to be complemented by a different technique to access a different rate or temperature scale of the polymer's response.

A number of other methods of measuring the modulus of thin films have been proposed, each with its own particular strengths and drawbacks. The Uniaxial Tensile Tester for UltraThin films (TUTTUT) method was recently developed as a way to conduct a tensile test measurement with a cantilever system to collect full stress/strain curves on a glassy polymer thin film floating on a liquid.[46] This method obtained results in good agreement with the buckling-based method, with the glassy Young's modulus E for PS thin films decreasing precipitously with decreasing h starting at $h \approx 25$ nm. In addition, the collection of tensile measurements which collect full stress/strain curves allowed investigation into the failure mechanisms of thin PS and polycarbonate (PC) films. The TUTTUT method has been recently adapted to measure the modulus of freestanding polymer thin films with a method termed the "Tensile tester for Ultrathin Freestanding Films" (TUFF).[47] The TUFF method bypasses the weakness of the liquid-substrate TUTTUT method, for which the water may alter the measured modulus of the polymer, and which can only be used for hydrophobic polymers that float on the surface of water. Unfortunately, the difficulty in preparing and measuring freestanding films limited the TUFF method to measuring polymers of thicknesses of $h \geq 30$ nm, which is above the thickness at which the standard TUTTUT method measured differences in the modulus with decreasing film thickness.

To obtain the temperature-dependent biaxial rubbery modulus of thin polymer films, the "bubble inflation" method was created by O'Connell and McKenna.[48,49]

Pressurized air channeled through an array of 5 μm diameter holes expands a polymer film placed over the holes, creating nanobubbles in the polymer film. An atomic force microscope (AFM) images the nanobubbles as a function of time, temperature, and film thickness. The stress and strain are related by simple expressions to the pressure, film thickness and the radius of curvature of the nanobubble. Since the measurement involves measuring the time-dependent strain due to constant applied stress, the viscoelastic property measured is the compliance. The bubble inflation method has been applied to a range of polymers such as PS, PC, poly(n-butyl methacrylate) (PnBMA), poly(ethyl methacrylate), (PEMA), and poly(vinyl acetate) (PVAc), and has revealed a dramatic stiffening effect of polymer thin films in the rubbery plateau regime, with rubbery stiffness in the thinnest films being $2-3$ orders of magnitude larger than the bulk rubbery plateau stiffness.[48,50] The McKenna group also developed a method using nanoparticle embedding to measure the surface compliance of bulk PS and poly(α-methylstyrene) (PαMS) films.[51,52] This method measures the depth via an atomic force microscope (AFM) that nanoparticles placed on the polymer film's surface embed, which is related to the surface compliance of the polymer. Refs. [51, 52] found that the surface compliance of PS and PαMS in the glassy regime decreased, while the surface compliance of PS and PαMS in the rubbery regime increased.

The current consensus in studies of the confinement effect on the viscoelasticity of polymer thin films is that the glassy state modulus of thin polymer films decreases with decreasing thickness beyond a threshold thickness that is typically between $20-80$ nm.[38] For the most commonly studied system of PS, this change in viscoelasticity manifests as a decrease in the modulus with decreasing thickness as measured by the buckling-based method and the TUTTUT method.[41,42,44,46] These experimental results are in agreement with computer simulations that observe the emergence of a heterogeneous local stiffness in model glassy polymer systems on confinement[53,54] that results in a decrease in Young's modulus with decreasing feature size for polymer

nanostructures without strong interactions with the substrate,[53] a decrease in E near the free surfaces of a glassy freestanding polymer film,[55] and an increase in stiffness via a decrease in the Debye-Waller factor near the substrate for a model system of PMMA films supported on an attractive substrate.[56] However, this consensus is not universal across all experimental techniques, and other measurements, such as those conducted with Brillouin light scattering (BLS),[57] nanoindentation, and a different method using the surface wrinkling of thin (down to 10 nm-thick) PS films floating on water[58] report no modification to modulus with confinement.

1.6 Influence of Polymer-Polymer Interfaces on the Glass Transition

The enthalpy of mixing dissimilar polymers is positive: like polymers prefer to associate with like polymers.[7] The entropy of mixing two dissimilar polymers is inversely proportional to the degree of polymerization–the number of monomers per chain–so that dissimilar polymers do not have as much of an entropic drive to mix, in contrast to dissimilar small molecules. Therefore, when two dissimilar polymers A and B are placed next to each other, an interface forms between them. The properties of the interface are determined by a competition of forces. First, there is a relative attraction of A with A and B with B, which seeks to drive A from B. But there are cohesive forces even between A and B that prevent a gap in the interface from forming. The shape of the density profile of the interface is dictated by a balance between the low probability of a high energy conformation that explores the dissimilar other phase, and the conformational entropy increase on exploration of the other phase.[59] The degree of relative repulsion between different chain segments, which determines the favorability of mixing, is encoded in the temperature-dependent interaction parameter χ, often written as an expansion in temperature of the form $\chi = A + \frac{B}{T} + \frac{C}{T^2}$,

where A, B, and C are constants.[60] Experimentally, χ is typically measured from small-angle neutron scattering (SANS) experiments of binary polymer blends.[61,62] The interaction parameter in turn relates to the width of the compositional interface w_I between two immiscible polymers. This interfacial width for two high molecular weight polymers with similar statistical segment lengths b and densities is given by[63]

$$w_I = \frac{2b}{\sqrt{6\chi}}, \tag{1.3}$$

for a composition profile

$$\phi(z) = \frac{1}{2}\left[1 + \tanh\left(\frac{2z}{w_I}\right)\right]. \tag{1.4}$$

The glass transition in polymer blend systems is conventionally related to the composition and individual glass transition temperatures of the homopolymers.[64,65] The Fox equation is the most simple equation that has been successful in predicting the T_g of polymer blends,[64] although a number of more complicated equations have been developed to better fit experimental data. The sample-averaged T_g of a binary blend of polymers A and B is given by the Fox equation as:[64,65]

$$\frac{1}{T_g(A+B)} = \frac{x_A}{T_g(A)} + \frac{x_B}{T_g(B)}, \tag{1.5}$$

where x_i is the mass fraction of polymer i ($x_B = 1 - x_A$), and $T_g(i)$ is the glass transition temperature of the homopolymer i. Other equations have been developed to model the presence of other factors such as hydrogen bonding on the T_g of polymer mixtures,[65,66] and together with the Fox equation this series of equations predicting T_g of polymer blends or copolymers as a function of composition tend to be quite accurate.[67] More recent developments such as the Lodge-McLeish model[68] treat polymer systems in a more sophisticated manner by taking into account the increased

probability of a given monomer to be next to a monomer of the same species due to chain connectivity.

Based on the Lodge-McLeish picture for local T_g, near and within the interface between two polymers, one would expect that the local T_g should depend on the local mass or volume fraction of the two polymers and their respective T_g. However, the physics of how polymer-polymer interfaces perturb local material properties is quite nuanced, and a variety of experimental, simulation, and theory work suggest that such a simple relation is not sufficient. Recent experimental work by Baglay and Roth[69,70] used a local fluorescence probe method derived from that developed by Ellison and Torkelson[15] to measure the local T_g near polymer-polymer interfaces in a multilayer film geometry.

Recent experimental work by Baglay and Roth measured the local T_g near and across polymer-polymer interfaces in a multilayer film geometry,[69,70] demonstrating that the local T_g as measured by pyrene fluorescence in a PS domain is perturbed to long length scales of 225-250 nm when near an interface formed between PS and a lower T_g polymer domain. A shorter ranged length scale of 100-125 nm was required to reach bulk T_g of PS near an interface formed between PS and a higher T_g polymer. These results were determined for weakly immiscible PS / polymer pairs, with the interfacial width of the composition for these systems ranging from 5-7 nm. Interestingly, progressive annealing above the T_g of PS for a PS / polysulfone (PSF) system demonstrated that the long length scales of local T_g perturbation are only observed when the interface is sufficiently annealed.

As discussed in Ref. [70], annealing a polymer-polymer interface changes the system in three main ways. First, annealing broadens the interfacial region, resulting in an equilibrium interfacial width determined by the interaction parameter χ. Second, annealing increases the interfacial roughness. Third, annealing increases chain connectivity across the interface. Later work demonstrated that roughness of an interface,

studied by measuring the local T_g in PS near silica surfaces roughened by exposure to corrosive hydrogen fluoride vapor,[71] does not play a large role in varying the local T_g in PS. Other work with grafted polymer chains suggests that chain connectivity may be a relevant parameter.[72] However, the length scales of T_g perturbation in a PS domain next to a lower T_g^{bulk} polymer domain were demonstrated to be independent of molecular weight of the lower T_g^{bulk} polymer.[73] It is therefore unclear as to how important increased chain connectivity across a dissimilar polymer-polymer interface caused by annealing is to producing the effect of long length scales of T_g perturbation.

A known effect of annealing a dissimilar polymer-polymer interface is broadening the interface, and this interfacial broadening may be an important factor in altering local T_g near the interface. This expectation is in good agreement with theoretical results from Mirigian and Schweizer that demonstrated that increasing the width of the polymer-air interface of free standing films from a step-function to a finite, more realistic interfacial width for a polymer-air interface leads to an approximate doubling of the length scales of perturbation to the local glass transition.[74]

Similar to the previous discussion of the confinement effects on T_g and mechanical properties, property changes near polymer-polymer interfaces can often depend on the measurement method and the property being measured. Block copolymers, which consist of alternating layers of different domains, are one model system used to measure property changes in polymer systems due to interfaces. When the average T_g of block copolymers are measured by DSC, typically small T_g shifts are observed with decreasing domain size.[75] Recently, Christie, Register, and Priestley used a similar local fluorescence probe method as that developed by Ellison and Torkelson to measure the local T_g in a block copolymer that was self assembled into alternating layers of poly(butyl methacrylate) and PMMA.[76] They found that bulk T_gs of the individual polymers were recovered at a distance of less than 5 nm from the interfaces, with a larger length scale required to reach bulk T_g in the glassy PMMA domain than

in the poly(butyl methacrylate) domain. In addition, the Fox equation presented a reasonable model for the local T_g in the rubbery poly(butyl methacrylate) domain, but was not able to model the local T_g in the glassy PMMA domain.

A number of open questions remain from Baglay and Roth's work. First, what is the relevant parameter describing hard vs. soft confinement? Modulus, especially the high frequency shear modulus,[17,77] is a likely candidate, but simply comparing the moduli of the polymers in these studies cannot be done without also accounting for the different chemistry of the polymers. Chapter 2 of this dissertation disentangles the effect of modulus with different chemistry of a polymer on local T_g perturbations in adjacent PS. This is accomplished by using cross-linked PDMS, which can be prepared with different moduli tuned by the level of cross-linking. While the modulus of PDMS is varied by changing the cross-link density, the underlying chemistry is preserved. Second, what is the mechanism responsible for the large length scales of hundreds of nm of perturbation to local T_g near weakly immiscible polymer-polymer interfaces? This length scale is much broader than the local composition, is larger than intrinsic length scales of the polymers used such as the radius of gyration (up to $\sim$50 nm for Baglay and Roth's systems), and is unaffected by molecular weight. In Chapter 2, I propose the source of these long length scales relate to the transmission of acoustic vibrations / phonon modes across the polymer-polymer interface. In Chapter 3, I design an experimental circuit that transmits acoustic shear waves into an adjacent polymer film and develop the necessary continuum mechanics analysis to measure the modulus and film thickness of the film. In Chapter 4, I use this circuit and adapt the continuum physics model to measure the transmission of shear waves across a polymer-polymer interface under varying stages of interface formation, controlled by annealing time. I find a long length scale of the width of the modulus profile near the interface, which demonstrates a large spatial extent in the local modulus variation near glassy-rubbery polymer interfaces, which causes increased transmission

of acoustic waves through the interface, may be responsible for the long length scales in local $T_g(z)$ perturbations near dissimilar polymer interfaces.

1.7 Experimental Methods

The main experimental techniques used in this dissertation are fluorescence spectroscopy, and a quartz crystal microbalance method that will be described in detail in Chapter 3. In addition, I use ellipsometry to measure the film thickness of polymer thin films.

The fluorescence spectroscopy method used in this thesis to measure local T_g in polymer films was originally developed by Ellison and Torkelson.[15] The fluorescence probe used is pyrene, which has a fluorescence spectrum that is highly sensitive to the local environment's polarity, density, and rigidity.[78,79] The temperature dependence of the fluorescence intensity of pyrene within a polymer matrix reflects changes in the quantum yield of the dye due to a competition between radiative and non-radiative decay. At higher temperatures, increased thermal energy results in more non-radiative decay through vibrational or rotational modes, while at lower temperatures, an increased rigidity of the surrounding polymer matrix decreases the non-radiative decay and increases the fluorescence intensity.[15,80] As established by Torkelson and co-workers,[15,81] the T_g values from fluorescence agree well with ellipsometry and differential scanning calorimetry (DSC) for bulk samples. The fluorescence method used by Baglay and Roth was developed by Rauscher et al.[82] to allow for more data to be collected and to automate the data collection process, while also minimizing photobleaching of the pyrene fluorophore. The protocol used a Photon Technology International QuantaMaster spectrofluorometer with a sample mounted on a heater stage. Samples were thermally equilibrated at temperatures above the bulk T_g of all layers in the sample for times sufficient to consolidate the material and

remove potential air gaps but still smaller than the reptation time of the polymer chains labeled with the pyrene fluorophore.[69,70,82] Measurements of the fluorescence intensity of pyrene at the first emission peak corresponding to an emission wavelength of 379 nm were collected on cooling at 1 °C per minute for 3 s every 30 s. The local T_g measured by the fluorescence of the pyrene-labelled layer was identified by the intersection of linear fits to the glassy and rubbery regime data.

Throughout this dissertation, I use ellipsometry to measure the film thickness of polymer thin films. Ellipsometry measures the change in polarization of elliptically polarized light upon reflection from a film. Fresnel reflection coefficients describe the portion of reflected light polarized parallel r_p and perpendicular r_s to the plane of incidence. An ellipsometer measures the wavelength-dependent quantities ψ and Δ, which relate to the magnitude $\tan\psi$ and phase $e^{i\Delta}$ of the ratio of the Fresnel reflection coefficients:[83]

$$\frac{r_p}{r_s} = \tan\Psi e^{i\Delta}. \tag{1.6}$$

Polymer films are typically transparent in the visible light range, and we used the wavelength range $400 - 1000$ nm (in the visible to infrared range) to avoid optical absorption by the film at smaller wavelength radiation and to maximize the signal to noise ratio. A layer model is used to fit the experimental data to determine the film thickness h and index of refraction n of the film. I used a Cauchy layer model[83] to model the index of refraction of a polymer film atop a semi-infinite silicon substrate with a 1.25 nm native oxide layer:[84]

$$n(\lambda) = A + \frac{B}{\lambda^2} + \frac{C}{\lambda^4}, \tag{1.7}$$

where A, B, and C are fit parameters. Fitting for the film thickness and index of refraction was done in the CompleteEASE or WVASE software, in which the mean squared error (MSE) between the experimental data and the model data were

minimized by varying the model's h, A, B, and C until the minimum of the sum of residuals from the calculated and experimental $\psi(\lambda)$ and $\Delta(\lambda)$ was reached. The best fit film thickness and index of refraction are the thickness and index of refraction that correspond to the minimized MSE. There is a change in slope in the film thickness as a function of temperature that occurs on passing through T_g, which relates to the different thermal expansion coefficient in the glassy and rubbery states of the polymer.[84] By measuring the thickness as a function of temperature, the T_g of a polymer film can be determined by the intersection of linear fits to the regions above and below T_g. In this dissertation, ellipsometry is used only to measure the thickness of films at room temperature.

1.8 Outline of Dissertation

This dissertation consists of five chapters on my research that developed a better understanding of the role that modulus plays in regulating perturbations to the local T_g near a polymer-polymer interface, the development of a QCM circuit and a continuum model to measure the shear modulus of rubbery polymers, and the application of the QCM circuit and continuum model to investigate the influence of annealing on the modulus and acoustic wave propagation in polymer bilayer systems.

Baglay and Roth's work suggested that the modulus of a polymer may be important in altering the local T_g in an adjacent polymer,[69,70] but the modulus was not decoupled from the chemistry of the polymer underlayers. In Chapter 2, I use PDMS to vary the Young's modulus of a substrate while retaining the chemistry to determine the effect of substrate modulus on local T_g in adjacent PS, measured using the same fluorescence method as that in Refs. [69, 70]. I find the surprising result that the local T_g in PS next to PDMS at 50 nm from the interface varies by 40 K when the Young's modulus of PDMS is varied from 0.9 to 2.6 MPa. Measuring local

T_g at varying distances from the interface, I find that the local T_g profile extends to ≈65-90 nm before bulk T_g is recovered. I demonstrate that the reduction in this length scale compared to the hundreds of nm length scales from systems with $5-7$ nm interfacial widths studied by Refs. [69, 70] is likely due to the smaller interfacial width of the PS/PDMS pair of ≈ 1.5 nm, which provides experimental evidence that the interfacial width between immiscible polymer pairs plays a key role in governing the extent of alterations to local dynamics characterized by local T_g shifts. A version of this chapter was published as:

> Yannic J. Gagnon, and Connie B. Roth. "Local Glass Transition Temperature Tg(z) Within Polystyrene Is Strongly Impacted by the Modulus of the Neighboring PDMS Domain." *ACS Macro Letters* **9**, 1625-1631 (2020).

Baglay and Roth's results, as well as my own, together with intriguing results from the literature demonstrating that the thickness-dependent T_g of thin PS films floating on glycerol follow a similar quantitative trend in T_g reduction as PS films on silica,[85,86] suggest that a concept such as acoustic impedance matching might be the control parameter influencing perturbations to local T_g. In acoustics, the concept of impedance matching states that transmission of a transverse acoustic wave across a boundary is maximized if the product of the density and shear moduli are similar between the layers.[87] Also, reflections are reduced if there is a gradual change in the material; i.e., if the interfacial width is large between the materials. Given the similarities between the impedance matching concept and the strong impact of interfacial width on local T_g perturbation length scales, theory demonstrating the connection between cage breaking events and elastic fluctuations,[17,74,88] and simulations demonstrating the importance of the relative high-frequency shear moduli between adjacent polymer domains in altering T_g of the domains,[77] these T_g perturbations and potentially modulus perturbation length scales may be related to acoustic shear wave transmission across the polymer-polymer interface.

A QCM is a promising device to investigate shear wave transmission or changes in modulus in polymer films, because it produces MHz frequency shear waves that are extremely sensitive to changes in the overlayer material.[89] In Chapter 3 I develop an experimental QCM circuit in collaboration with Emory's Burton Lab that measures resonance frequency traces of the QCM. Shifts in these resonance frequencies and bandwidths on loading the QCM with a film correspond to the thickness and modulus of the film. I illustrate the use of a simple continuum physics model that provides the frequency-dependent storage and loss moduli of a polymer film on a QCM, in addition to the film thickness. An advantage to our approach is that we are able to collect and analyze data over a larger frequency range than other groups, which is especially important for measurements of rubbery polymer films. We also contribute a physically intuitive continuum model to the literature that numerically solves the relevant continuum equations without mathematical simplifications. I measure the modulus of rubbery PB and PDMS at MHz frequencies within the glass transition regime and find excellent agreement with literature values collected by more conventional means. A version of this chapter was published as:

> Yannic J. Gagnon, Justin C. Burton, and Connie B. Roth. "Physically Intuitive Continuum Mechanics Model for Quartz Crystal Microbalance: Viscoelasticity of Rubbery Polymers at MHz Frequencies." *Journal of Polymer Science* **60**, 244-257 (2022).

In Chapter 5, I use the QCM method developed in Chapter 4 to investigate the acoustic shear wave transmission through a PB/PS interface, and demonstrate that annealing the interface at 120 °C produces a broad shear modulus profile of width $\approx$ 150 nm near the interface after sufficient annealing times. This result provides strong evidence that the long-ranged modulus gradient may be responsible for the long-ranged local $T_g(z)$ perturbations observed in Refs. [69, 70, 73, 90]. A version of this chapter is in preparation for publication.

Chapter 2

Local Glass Transition Temperature Tg(z) Within Polystyrene Is Strongly Impacted by the Modulus of the Neighboring PDMS Domain

2.1 Synopsis

Profiles in the local glass transition temperature $T_g(z)$ within polystyrene (PS) next to polydimethylsiloxane (PDMS) domains were determined using a localized fluorescence method. By changing the base to cross-linker ratio, we varied the cross-link density and hence Young's modulus of PDMS (Sylgard 184). The local $T_g(z)$ in PS at a distance of $z = 50$ nm away from the PS/PDMS interface was found to shift by 40 K as the PDMS modulus was varied from 0.9–2.6 MPa, demonstrating a strong sensitivity of this phenomenon to the rigidity of the neighboring domain.

The extent the $T_g(z)$ perturbation persists away from the PS/PDMS interface, $z \approx$ 65–90 nm before bulk T_g is recovered, is much shorter for this strongly immiscible system compared with the weakly immiscible systems studied previously, which we attribute to a smaller interfacial width as the χ parameter for PS/PDMS is an order of magnitude larger.

2.2 Introduction

High performance multicomponent materials have nanostructured morphologies where the desired global properties are obtained from an amalgam of local property changes caused by the multitude of internal interfaces. Studies on thin polymer films have demonstrated a host of property changes with decreasing film thickness attributed to interface effects,[15,17,38,91,92] including polymer-polymer interfaces.[69,70,77,82,92–101] The efficient design of multicomponent materials requires the understanding of how these interface effects perturb local properties. Glassy-rubbery interfaces between polymer domains impart material toughness and flexibility,[102,103] and can be used to tune phononic transport.[104] Although a range of different processing methods have been developed to create morphologies with sub-100 nm domain sizes,[105–108] studies of simplified systems with a single interface can directly inform the underlying mechanisms behind such applications by mapping local properties as a function of distance from the interface.

In 2015, Baglay and Roth mapped how the local glass transition temperature $T_g(z)$ changed across a glassy-rubbery polystyrene (PS) / poly(n-butyl methacrylate) (PnBMA) interface, finding this profile in local dynamics to be much broader and asymmetric relative to the composition profile,[69] with follow-up work demonstrating a similar behavior for a range of weakly immiscible polymer pairs.[70,73] The range the dynamical perturbation persisted away from the dissimilar polymer-polymer inter-

face before bulk T_g was recovered for these semi-infinite bilayer systems depended on whether the neighboring polymer domain had a higher T_g^{bulk} ("hard confinement"), extending to $z \approx 100$–125 nm, or lower T_g^{bulk} ("soft confinement"), extending to $z \approx 225$–250 nm. An important observation from these studies was that these broad $T_g(z)$ profiles only formed upon annealing the dissimilar polymer interface to equilibrium, suggesting that some factor during polymer-polymer interface formation was responsible for the coupling of T_g dynamics across the interface.[70] More recent work has identified that chain connectivity across the interface appears to play a dominant role,[72] as opposed to interfacial roughness.[109] However, a number of open questions remain: Does the breadth of the compositional interface impact the range of the dynamical $T_g(z)$ perturbation? Is the modulus of the neighboring domain an important factor in dictating the $T_g(z)$ response?

In the present work we test both these open questions by experimentally measuring the $T_g(z)$ profile in PS next to polydimethylsiloxane (PDMS) by varying cross-link density to alter the modulus of the PDMS neighboring domain without changing the chemistry of the dissimilar polymer interface. A localized fluorescence method is used to measure the local $T_g(z)$ of a thin pyrene-labeled PS probe layer placed at a distance z from the PS/PDMS interface. These findings demonstrate that the breadth of the compositional interface between the two dissimilar polymers and the modulus of the neighboring domain are key factors controlling the $T_g(z)$ behavior, providing insight for related theoretical efforts in the field[17,26,34,35,77,99,100,110–112] into the control parameters responsible for this phenomenon. Characterization of the local properties near the interface of PS/PDMS, in particular, are relevant for a range of applications from mechanical reinforcement of polymers[102,103] to the buckling-based metrology used to measure the modulus of ultrathin glassy films.[41–43]

2.3 Experimental Methods

Figure 2.1a illustrates the multilayer sample geometry assembled for the fluorescence measurements that places a 10-15 nm thick pyrene-labeled PS probe layer (M_w = 672 kg/mol, M_w/M_n = 1.3, 1.4 mol% pyrene[69,70,72,113]) at a known distance z from the PS/PDMS interface by changing the thickness z of a neat PS (M_w = 1920 kg/mol, M_w/M_n = 1.26) spacer layer between the underlying PDMS and pyrene-probe layer. An additional thick (>500 nm) neat PS layer is placed atop the probe layer to eliminate T_g shifts caused by the free surface. Layer thicknesses were measured using ellipsometry.[84] By assembling samples with different z-layer thicknesses, the local $T_g(z)$ value can be mapped out as a function of distance from the PS/PDMS interface. We ensure that the PS/PDMS interface is annealed to equilibrium by first assembling the z-spacer layer atop the PDMS and annealing these two layers for 90 min at 140 °C before adding the remaining layers. The entire multilayer stack is further annealed for 20 min at 120 °C immediately prior to the start of the fluorescence measurements to ensure thermal history has been erased, and to consolidate all the layers into a continuous material while still maintaining the morphology of the assembled structure shown in Figure 2.1a.[69] High molecular weight polymers have been used to limit the diffusion of the pyrene-labeled probe layer and keep it localized at the position z by making the reptation time longer than the measurement time.[15,69] PDMS layers (50–180 μm thick) were made from Sylgard 184 (Dow Corning) where the base to cross-linker ratio was varied from 6:1 to 17:1 by weight and cured at 70 °C for 2 h following Refs.[42,45]. The same $T_g(z)$ values were also obtained for samples with 2 μm thick PDMS layers formed by spin-coating, prior to curing under the same conditions. Thus, the measured $T_g(z)$ values are independent of the thickness of the PDMS layer. Further experimental details are provided in the Appendix along with various control measurements.

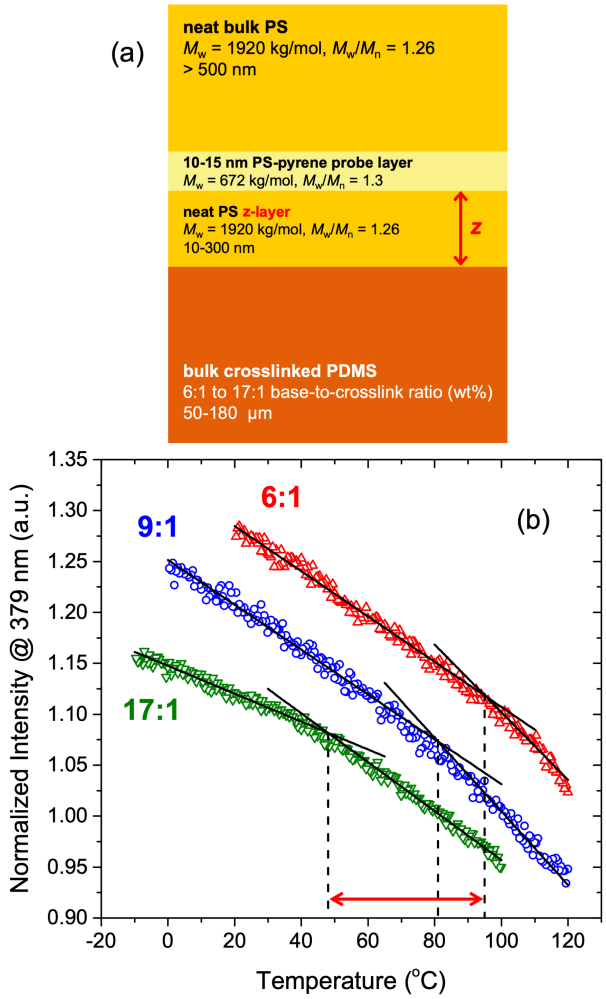

Figure 2.1: (a) Schematic of sample geometry assembled to place the 10-15 nm thick pyrene-labelled PS (PS-Py) probe layer at a distance z from the PS/PDMS interface by varying the thickness z of the neat PS spacer layer. (b) Temperature dependence of fluorescence intensity of PS-probe layer at $z = 50$ nm for all three samples of varying PDMS cross-link density: $T_g(z = 50\text{ nm}) = 48 \pm 2$ °C (17:1), 81 ± 2 °C (9:1), and 95 ± 2 °C (6:1).

2.4 Results and Discussion

Fluorescence measurements to determine the local $T_g(z)$ were done on cooling at 1 °C/min by monitoring the pyrene emission intensity at a wavelength of 379 nm for 3 s every 27 s, exciting at a wavelength of 330 nm.[82] The temperature dependence of the fluorescence intensity is shown in Figure 2.1b for three representative

samples with varying PDMS cross-link densities, where the pyrene probe layer has been placed at a distance $z = 50$ nm. Following previous works,[15,69,70,72,73,82] the glass transition temperature $T_g(z)$ is determined from the intersection of linear fits to the data above and below the transition. It is well known that pyrene fluorescence is extremely sensitive to the local environment's polarity, density, and rigidity, where the temperature dependence of the fluorescence intensity of pyrene within a polymer matrix reflects changes in the quantum yield of the dye due to the local rigidity of the surrounding matrix that is influenced by the polymer's thermal expansivity.[78,79,81] As established by Torkelson and co-workers,[15,81] the T_g values from fluorescence agree well with ellipsometry and differential scanning calorimetry (DSC) for bulk samples. For the intensity vs. temperature curves shown in Figure 2.1b, the glass transition temperatures for these three samples are $T_g(z = 51 \text{ nm}) = 95 \pm 2$ °C for PDMS with 6:1 base to cross-linker ratio, $T_g(z = 53 \text{ nm}) = 81 \pm 2$ °C for 9:1, and $T_g(z = 51 \text{ nm}) = 48 \pm 2$ °C for 17:1. These data demonstrate that the local $T_g(z)$ of PS at $z = 50$ nm is strongly reduced relative to the bulk T_g value for PS of $T_g^{\text{bulk}} = 101.5 \pm 2.0$ °C and extremely sensitive to the properties of the neighboring PDMS layer, with the $T_g(z = 50 \text{ nm})$ values shifting by approximately 45 K as the PDMS base to cross-linker ratio is varied from 6:1 to 17:1.

The PDMS underlayers were fabricating using Dow Corning's Sylgard 184 elastomer kit by mixing the base prepolymer with the curing agent at different ratios n to create PDMS with different cross-link densities. Sylgard 184 has frequently been used in this manner with several groups characterizing the resulting modulus.[45,114–117] In Figure 2.2, we plot the Young's modulus E as a function of base to cross-linker ratio n measured by these various studies that used comparable curing conditions to our own, 70 °C for 2 h. Remarkable consistency is found for the measurements of Young's modulus $E(n)$ using a range of different methods: tensile,[45,114] compression,[115] indentation,[116] dynamic mechanical analysis (DMA),[117] and buckling-based

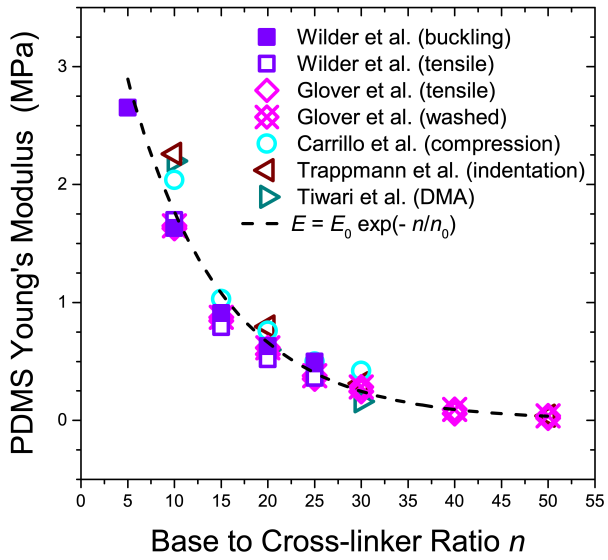

Figure 2.2: PDMS Young's modulus E for Sylgard 184 as a function of base to cross-linker ratio n measured using different methods as compiled from literature: Wilder et al.,[45] Glover et al.,[114] Carrillo et al.,[115] Trappmann et al.,[116] and Tiwari et al.[117] Glover et al.'s data marked as X-diamonds represent samples washed in good solvent to extract unreacted small molecules.

metrology.[45] We find these $E(n)$ data are well described by an exponential decay

$$E(n) = E_0 \exp\left(-\frac{n}{n_0}\right) \quad \text{(in MPa)}, \tag{2.1}$$

where $E_0 = 4.73 \pm 0.36$ MPa and $n_0 = 10.16 \pm 0.67$.

Equation 2.1 gives values for the PDMS modulus of $E = 0.89 \pm 0.12$ MPa for 17:1, $E = 1.95 \pm 0.19$ MPa for 9:1, and $E = 2.62 \pm 0.22$ MPa for 6:1. For the data shown in Figure 2.1, this implies that a change of the PDMS modulus by nearly a factor of three generated an approximately 45 K shift in the local T_g in PS at a distance of $z \approx 50$ nm from the PS/PDMS interface. We explore this trend more fully in Figure 2.3 by plotting the local $T_g(z = 50$ nm) as a function of PDMS modulus for a range of different samples, using eq. 2.1 to determine E for the given base to cross-linker ratio n used. The trend in $T_g(z = 50$ nm) with E appears linear, showing a large decrease in $T_g(z = 50$ nm) of more than 20 °C/MPa with decreasing PDMS modulus

in the range of $E = 0.9$–2.6 MPa, suggesting that the modulus of the neighboring domain is a dominant factor influencing the properties of PS. Interestingly, the value of $T_g(z = 50\text{ nm})$ for the 6:1 ratio, when the PDMS modulus is still only $E = 2.6$ MPa, is already at 90.7 ± 3.3 °C, close to the bulk value for PS of $T_g^{bulk} = 101.5 \pm 2.0$ °C. For comparison, if we perform the same local $T_g(z = 50\text{ nm})$ measurement in PS when the underlying material is silica (a material with a modulus[118] of ≈ 75 GPa), we obtain a local $T_g(z = 50\text{ nm}) = 101.7 \pm 1.5$ °C as shown in Figure 2.3, equivalent to T_g^{bulk} as expected given that PS/silica is known to be a neutral interface not impacting the local T_g as measured by fluorescence.[15,72,109] However, a comparison between the PS/PDMS system, where interdiffusion of the two polymers has been allowed to occur, with the PS/silica interface, where no such interdiffusion is possible, may not be the most pertinent.

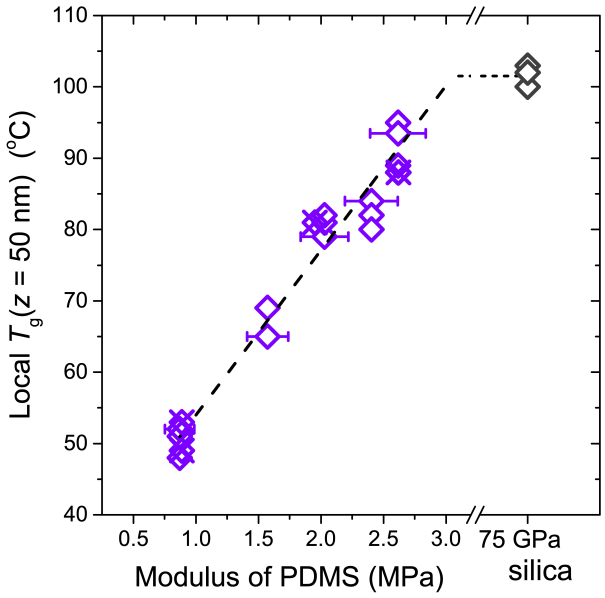

Figure 2.3: Local $T_g(z)$ in PS at a fixed distance of $z = 50$ nm from the PS/PDMS interface as a function of PDMS Young's modulus E, based on eq. (2.1). Representative horizontal error bars denote the uncertainty in E, while the symbol size indicates the vertical uncertainty of ±2 °C in any given T_g measurement. The X-diamond symbols correspond to samples where the PDMS was washed in toluene, a good solvent, to extract unreacted small molecules. Grey diamonds at 75 GPa are $T_g(z = 50\text{ nm})$ for PS supported on silica with the horizontal dotted line corresponding to T_g^{bulk}.

In our group's 2017 study,[70] we learned that the interaction between the two polymer domains that creates the broad $T_g(z)$ profile only occurs upon annealing of the dissimilar polymer-polymer interface to equilibrium. Local interpenetration of the two polymer domains at the interface is key to creating this coupling of dynamics that impacts the local properties over an extended distance from the interface. In follow-up work, we were able to show that chain connectivity plays a dominant role in this behavior,[72] while interface roughness has little to no impact.[109] However, it is worth noting that although chain connectivity across the interface itself seems to be important to at least create interfacial breadth, we are observing significant shifts in local $T_g(z)$ at distances z sufficiently far away from the interface that no individual chain can span the distance. Shown in the Appendix, we demonstrate how the $T_g(z = 50$ nm) decrease develops upon annealing of the PS/PDMS interface at 140 °C, requiring 60–90 min to reach equilibrium. All $T_g(z)$ measurements shown in Figures 2.1, 2.3, and 2.4 are for samples where the PS/PDMS interface was annealed for 90 min at 140 °C to ensure equilibrium was reached. In the buckling-based metrology method used to measure the elastic modulus of PDMS in Figure 2.2,[45] bilayer films of glassy PS atop rubbery PDMS are formed at room temperature by stretching the PDMS layer prior to placing the glassy PS layer on top. Upon release of this initial strain, the PDMS layer contracts and the glassy PS layer buckles with an undulation wavelength that depends on the modulus of both layers.[41,42,45] In this measurement, because the PS/PDMS bilayer film is never heated above room temperature, there will be little to no interpenetration between the two polymer domains. Thus, we would not expect local $T_g(z)$ changes near the PS/PDMS interface, and would anticipate the PDMS modulus to be equivalent to bulk measurements as shown in Figure 2.2. Interestingly, Vogt and coworkers have correlated a softening of the top glassy layer measured using the buckling-based metrology method as the T_g of the glassy layer is approached.[38,44] Forrest and Dalnoki-Veress have shown that some

limited interdiffusion can occur at glassy-rubbery interfaces below the T_g of the glassy polymer.[119] Thus, it is possible that as the glassy T_g is approached from below, some limited interdiffusion is occurring at the glassy-rubbery interface between the glassy polymer layer and the underlying PDMS in the buckling-based metrology, resulting in an additional source of softening for the glassy layer.

One of the concerns with using the commercial Sylgard 184 elastomer kit is that the base and curing parts also contain additional components such as a catalyst, an inhibitor, solvent diluents, and silica filler (according to the product safety data sheets),[120,121] which could affect the PDMS material formed. In addition, curing the material at a different base to cross-linker ratio from the recommended 10:1 ratio can result in unreacted small molecules still being present in the PDMS material after curing. This has been reported to be especially pronounced for $n > 30$, but for the range of $6 \leq n \leq 17$ used in our study, the percentage of unreacted mass is only ∼4–8 %.[114,121] Washing of the PDMS with a good solvent like toluene or heptane to swell the PDMS elastomer can be used to extract this unreacted material and other free small molecules.[114,120,121] Glover et al.[114] compared the modulus $E(n)$ of Sylgard 184 PDMS before and after solvent washing to extract unreacted material and found only a very small difference in the modulus E for the range of n's shown in Figure 2.2 (their washed $E(n)$ values are denoted with X-diamond symbols). Perhaps a bigger concern for our $T_g(z)$ measurements is that such free small molecules could migrate to the surface of PDMS and across to the PS domain, possibly causing plasticization of the material. We have verified that this concern is not impacting the measured $T_g(z)$ values by washing our PDMS samples in toluene to remove such unreacted free material and confirmed that we obtain the same $T_g(z)$ values pre- and post-extraction. We show these measured $T_g(z)$ values for samples where the PDMS layer has been washed in Figure 2.3 with X-diamond symbols. Thus, we have ensured that the reduction in local $T_g(z)$ near the PS/PDMS interface is not caused by plasticization,

which is consistent with our earlier publication where we also demonstrated that the local $T_g(z)$ profiles reported were not caused by plasticization from some low molecular weight component.[73]

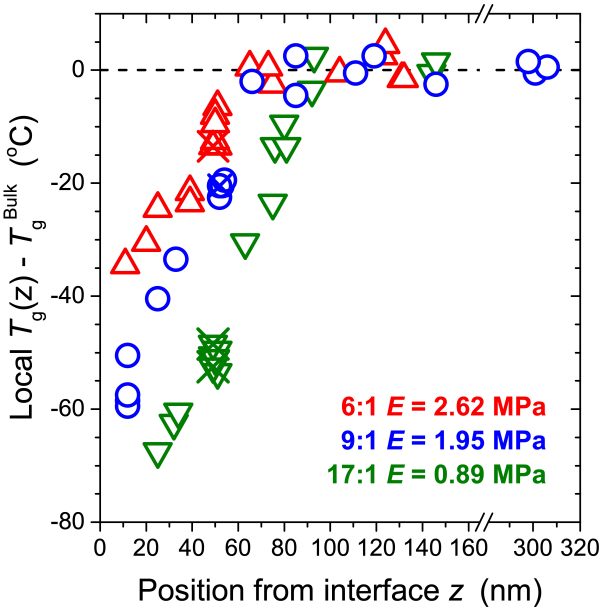

Figure 2.4: Local $T_g(z)$ profile within PS as a function of distance z from the PS/PDMS interface for PDMS with three different cross-link densities (moduli). PS T_g^{bulk} is recovered at $z \approx 65$–90 nm. Data marked with an X denote samples where the cured PDMS was solvent washed to remove any unreacted monomer or impurities. Symbol size represents the ± 2 °C uncertainty associated with any given T_g measurement.

In Figure 2.4, we plot the $T_g(z)$ profile within PS next to PDMS with varying cross-link densities: 6:1 ($E = 2.62$ MPa), 9:1 ($E = 1.95$ MPa), and 17:1 ($E = 0.89$ MPa). As the pyrene-labeled PS layer, where the local $T_g(z)$ is measured, is moved closer to the PS/PDMS interface by decreasing the thickness of the neat PS z-layer (see Figure 2.1a), the local $T_g(z)$ decreases in an apparent linear fashion by tens of degrees Celsius from T_g^{bulk} for PS, with an ≈40 K larger $T_g(z)$ decrease for the softer PDMS underlayers. The distance $z \approx 65$–90 nm from the PS/PDMS interface at which T_g^{bulk} is recovered is significantly shorter than the $z \approx 225$–250 nm observed previously for soft underlayers by Baglay et al.[69,70] for a series of weakly immiscible

polymer pairs with interfacial widths $w_I = 5$–7 nm. We believe this difference is likely due to the greater immiscibility of PS/PDMS, whose interaction parameter χ is an order of magnitude larger than the weakly immiscible systems studied previously, such that the interfacial width $w_I \sim \chi^{-1/2}$ for the PS/PDMS system would be much smaller. For PS/PDMS, we estimate the interfacial width $w_I = \frac{2b}{\sqrt{6\chi}} \approx 1.5$ nm from the interaction parameter[60] $\chi = 0.17$ at 140 °C where the PS/PDMS interface is annealed to equilibrium (b is the statistical segment length) for a composition profile $\phi(z) = \frac{1}{2}\left[1 + \tanh\left(\frac{2z}{w_I}\right)\right]$. Supporting this conclusion is the recent theoretical work by Mirigian and Schweizer that demonstrated an approximate doubling of the length scale in interface perturbations by incorporating a larger, more realistic interfacial width for a polymer–air interface compared to the infinitely narrow, step-function interface most commonly employed by theoretical works.[74] Unfortunately, theoretical difficulties and limited computational power make the modeling of polymer-polymer systems with large interfacial widths challenging.[17]

Theoretical efforts aimed at understanding T_g perturbations near interfaces have suggested that local elastic stiffness[34,35,88] or rigidity of the neighboring domain correlated with the Debye-Waller factor[77,110] may be strong controlling parameters for affecting local α-relaxations. These efforts would suggest that the high-frequency, glassy shear modulus $G(\omega)$ would then be the relevant property for correlating with local $T_g(z)$ shifts. However, varying the cross-link ratio of PDMS changes the zero-frequency, rubbery modulus of the elastomer, not the high-frequency glassy response. Tiwari et al.[117] showed using DMA that while the low-frequency elastomeric response changed with base-to-cross-linker ratio as shown in Figure 2.2, the high frequency glassy Young's modulus $E(\omega)$ was the same for ratios of 10:1, 20:1, and 30:1, as would be expected for this level of cross-linking.

2.5 Conclusions

The most puzzling aspect of these $T_g(z)$ results is the enormous 40 K change in local T_g occurring within the PS domain for such a small change in underlying PDMS modulus, varying only from 0.9–2.6 MPa. From existing literature studies we know there are limitations over which we can extrapolate the modulus-dependent data shown in Figure 2.3. As already mentioned, the PS/silica system with GPa underlayer modulus reports T_g^{bulk}.[15,72,109] However, even at the opposite extreme of PS films floating on top of liquid glycerol, the $T_g(h)$ behavior has been reported to be identical to PS on silica.[85,86] If both extremely hard (GPa) and extremely soft (liquid) underlayers report no T_g perturbation from the underlying interface, how is it that intermediate (MPa) underlayers cause such a large shift in local $T_g(z)$? One immediate difference is that both the PS/silica and PS/glycerol systems have sharp interfaces with widths ∼0.5 nm only. We have already identified that the large $T_g(z)$ profiles require a broad, well-interpenetrated interface. However, this does not address why PDMS modulus values within the MPa range would be the region to impart such large shifts in local $T_g(z)$. The pyrene dye identifies T_g on cooling as the temperature at which the local polymer matrix falls out of equilibrium as it passes from its rubbery plateau modulus ($E_R = 0.6$ MPa for PS[7]) through the glass transition to its glassy modulus ($E_G = 3.2$ GPa[122]), which might reasonably occur when the PS modulus is of order a few to tens of MPa, a value comparable to that of the underlying PDMS. In an earlier publication,[82] we introduced the idea that perhaps the coupling of local mobility across interfaces behaves in a manner analogous to impedance matching. In contrast to a sharp interface that would cause reflection of density waves (phonon modes), a sufficiently broad interface with also some amount of similarity in the mechanical properties on either side of the interface (e.g., density and modulus of the material that would impact the velocity of such acoustic waves) would allow for transmission of such waves across the interface changing the boundary

conditions of phonon mode propagation throughout the material. How exactly such a change in phonon mode propagation translates into the measured local $T_g(z)$ profiles is not quite clear at this point, but certainly much has been said in the literature associating phonon modes, so-called "soft spots", and α-relaxations.[123,124] Further work along these lines is underway.

2.6 Appendix

Sample Preparation

High molecular weight pyrene-labeled polystyrene (PS-Py) with 1.4 mol% pyrene (M_w = 672 kg/mol, M_w/M_n = 1.3) was synthesized using free radical copolymerization of styrene with 1-pyrenylbutyl methacrylate at 50 °C for 24 h under a nitrogen environment using azobisisobutyronitrile (AIBN) as initiator as described in Refs.[69,113]. Unlabeled (neat) polystyrene (PS) (M_w = 1920 kg/mol, M_w/M_n = 1.26) was purchased from Pressure Chemical and used as received. The polydimethylsiloxane (PDMS) layers were made from Dow Corning's Sylgard 184 elastomer kit. Cross-linked PDMS of varying modulus was made by mixing the base prepolymer with the curing agent at different ratios n:1 between 6:1 and 17:1 by weight. The mixture was stirred with a metal spatula for 30 s and then left to sit for 30 min to remove air bubbles introduced during mixing. The PDMS mixture was then poured into a mold formed between two glass microscope slides separated by an aluminum foil spacer of thickness 200–215 μm with a rectangular opening of 1.5 cm × 4 cm. A Teflon sheet was added between the top of the PDMS sample and the upper glass slide for ease of opening the mold after the PDMS was cured. Binder clips were placed on all four sides to secure the mold. Curing of the PDMS was done in an oven at 70 °C for 2 h to match the curing conditions of Refs.[42,45]. After curing, a scalpel was

used to slice a 1.5 cm × 1.5 cm square section of the PDMS layer and place it onto the quartz slide used for fluorescence measurements. PDMS layer thicknesses ranged between 50 μm and 180 μm, as measured by a micrometer. Much thinner PDMS layers were also made by spin-coating the PDMS mixture prior to curing resulting in thicknesses of only 2 μm, as measured by ellipsometry. The local $T_g(z = 50$ nm) values within PS were the same for spin-coated PDMS underlayers as for the mold cast PDMS, demonstrating that the measured $T_g(z)$ profile is independent of PDMS layer thickness within this range of 2–180 μm.

Figure 2.5 illustrates the individual layers and steps used to construct the multilayer sample geometry used. PS and PS-Py layers were made by spin-coating films from toluene solutions onto freshly-cleaved mica, varying spin speed and solution concentration to obtain films of the desired thicknesses. All PS and PS-Py layers were annealed individually on mica at 120 °C under vacuum for a minimum of 14 h to remove residual solvent and release any stresses imparted during the spin-coating process. Multilayer samples were then assembled by floating the individual films onto room temperature deionized water and capturing the layers from below with the portion of the sample already assembled. Between each floating step, the sample was allowed to thoroughly dry under an incandescent lamp. The top bulk PS layers were made >500 nm thick to ensure that the PS-Py layer would be unaffected by free surface effects. Annealing of the layers to create a consolidated sample with no air gaps was done in two stages to ensure that equilibrium chain interpenetration across the PS/PDMS interface was obtained, while minimizing interdiffusion of the PS-Py probe layer.[69,70] As shown in Figure 2.5, the PS z- and PDMS layers were first annealed separately at 140 °C for 1.5 h, prior to floating the PS-Py and bulk PS layers on top. A final annealing step at 120 °C for 20 min was then done immediately prior to the start of the fluorescence measurements.

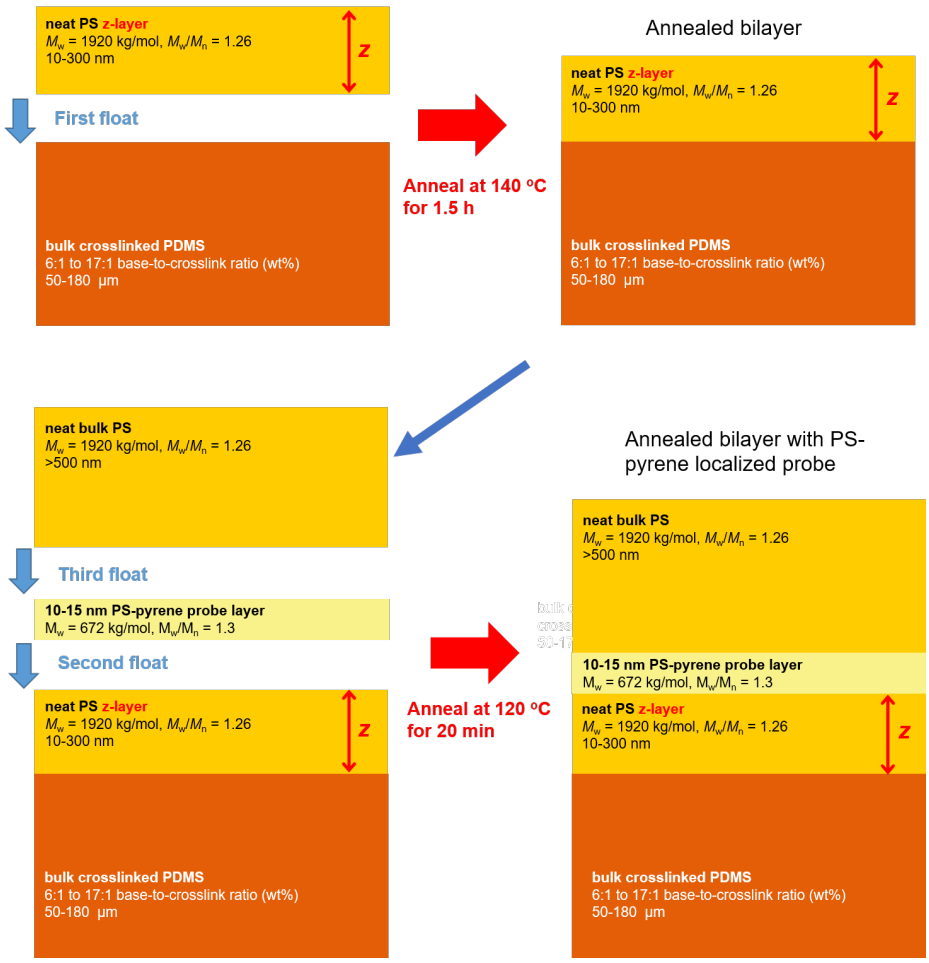

Figure 2.5: Schematic illustrating sample preparation steps. In the first annealing step, the PS z-layer and PDMS underlayer are annealed at 140 °C for 1.5 h to ensure this dissimilar polymer-polymer interface is annealed to equilibrium. The remaining PS-Py probe and bulk PS layers are then added, with a final annealing step of 20 min at 120 °C done prior to the start of the fluorescence measurements to consolidate all the layers into a single material with no air gaps, while keeping the PS-Py probe layer localized at a position z from the PS/PDMS interface.

Ellipsometry and Fluorescence Details

Layer thicknesses were determined using a variable angle spectroscopic ellipsometer with rotating compensator (J.A. Woollam M-2000). The amplitude ratio $\Psi(\lambda)$ and phase shift $\Delta(\lambda)$ of the ratio of p- to s-polarized light Fresnel reflection coefficients were measured at three angles of incidence, 55°, 60°, and 65°, for wavelengths λ spanning 400–1000 nm. The film thickness h and wavelength-dependent index of

refraction $n(\lambda)$ of the polymer layer were determined by fitting the $\Psi(\lambda)$ and $\Delta(\lambda)$ data using Woollam's WVASE software to an optical layer model composed of a transparent Cauchy layer $n(\lambda) = A + \frac{B}{\lambda^2} + \frac{C}{\lambda^4}$ for the polymer film, and a 2.0 nm native oxide layer atop a semi-infinite silicon substrate.[84] For the 2 μm thick PDMS films, an additional thickness non-uniformity parameter, typically between 3% and 7%, was modeled in the CompleteEASE software. PDMS Cauchy parameter values obtained were $A = 1.406$, $B = 0.00251$ μm^2, and $C = 0.00016$ μm^4, in good agreement with values reported in the literature.[125]

Fluorescence measurements were done using a Photon Technology International QuantaMaster spectrofluorometer following the protocol outlined in Refs.[69,70,82]. Samples were placed in a Peltier-cooled Instec TS62 heat stage with dry nitrogen gas continuously flowed through the chamber at 1.1 L/min to prevent condensation of moisture below room temperature. The pyrene dye was excited at a wavelength of 330 nm using a xenon arc lamp with an excitation band-pass of 5.5-6.0 nm and an emission band-pass of 5.0 nm. Fluorescence measurements were initiated by heating the sample to the starting temperature, typically 120 °C, and equilibrating the sample for 20 min as the final annealing step. While cooling the sample at 1 °C/min, the fluorescence intensity of pyrene was monitored at an emission wavelength of 379 nm for 3 s every 27 s, as described previously.[82] At the end of each measurement run, the sample was reheated to the starting temperature to ensure that the same emission intensity was obtain at 120 °C, verifying that photobleaching was negligible and the sample had remained stable.

The T_g value for a given run was determined from the change in slope of the fluorescence intensity I with temperature T by performing linear fits to the $I(T)$ data above and below the transition, and then identifying the temperature at which the two linear fits intersected. Figure 2.6 shows three such intensity vs. temperature curves for the 9:1 PDMS cross-link ratio for samples with the pyrene-labeled layer

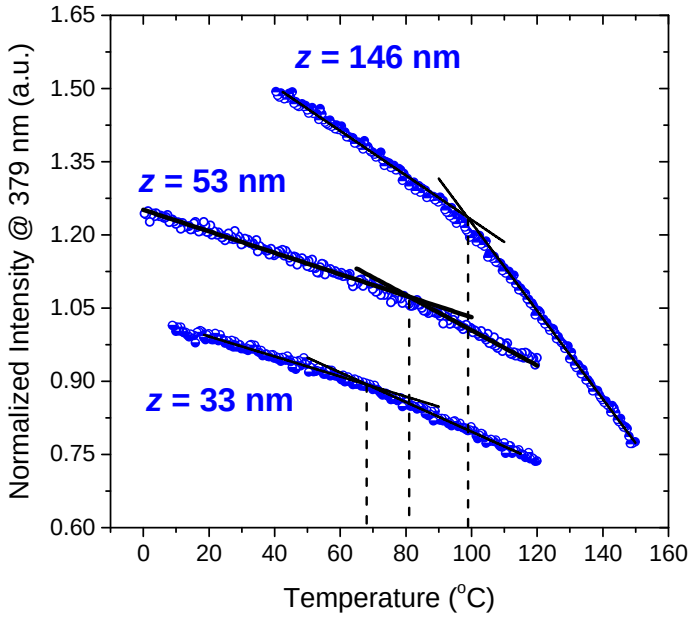

Figure 2.6: Temperature dependent fluorescence intensity measured for three different PS/PDMS multilayer samples with the 9:1 PDMS cross-link ratio where the pyrene-labeled layer was placed at varying distances z from the PS/PDMS interface resulting in local $T_g(z)$ values measured within the PS domain of $T_g(z = 146\text{ nm}) = 99\ ^\circ\text{C}$ (equivalent to T_g^{bulk}), $T_g(z = 53\text{ nm}) = 81\ ^\circ\text{C}$, and $T_g(z = 33\text{ nm}) = 68\ ^\circ\text{C}$.

placed at different distances from the PS/PDMS interface: $z = 33$, 53, 146 nm. The data ranges for the linear fits were chosen to begin at a minimum of 5 °C from the transition temperature and to include the largest amount of data, while maximizing the R^2 value for the fits. In Figure 2.6, the measured $T_g(z)$ values systematically decreased with decreasing z as the PS/PDMS interface was approached, with T_g^{bulk} being recovered sufficiently far ($z \geq 100$ nm) from the interface. As in our previous fluorescence studies of the local $T_g(z)$ as a function of position from an interface, only a single T_g value was found for a given z value no matter how wide the temperature range investigated.[69,70,72,73] As initially demonstrated by Ellison and Torkelson,[15] the change in pyrene fluorescence intensity with temperature is sensitive to the stiffness (thermal expansion) of the surrounding polymer matrix, where the T_g values measured by fluorescence for polymer films of a given thickness h are in excellent agreement with $T_g(h)$ values measured by ellipsometry, as well as onset T_g values measured

by differential scanning calorimetry (DSC) for thick (bulk) films.[81] The bulk glass transition temperature $T_g^{bulk} = 101.5 \pm 2.0$ °C shown as horizontal dotted lines in Figures 2.3 and 2.4 were determined from the average of local $T_g(z)$ values with $z \geq 100$ nm.

Effect of Annealing on Local $T_g(z)$ Profile Between PS and PDMS

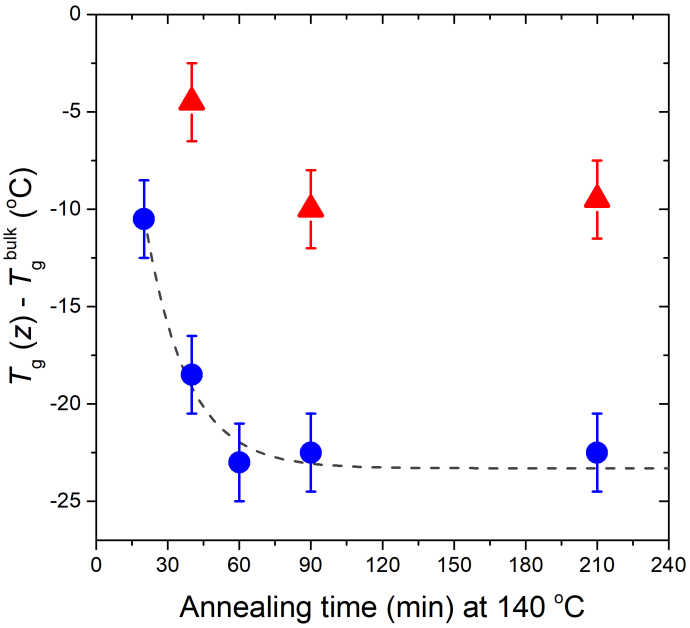

Figure 2.7: Local $T_g(z = 50 \text{ nm}) - T_g^{bulk}$ as a function of annealing time at 140 °C of the PS/PDMS interface (first annealing stage). Solid blue circles are for samples made with 9:1 PDMS, while the solid red triangles are for samples made with 6:1 PDMS. The dashed curve is an exponential decay fit to the 9:1 data. The $T_g(z = 50 \text{ nm})$ value stabilizes after 60–90 min of annealing as the PS/PDMS interface reaches equilibrium.

From our 2017 study on weakly immiscible polymers,[70] we learned that the broad $T_g(z)$ profile showing dynamical coupling across dissimilar polymer domains only develops upon annealing of the dissimilar polymer-polymer interface to equilibrium. To determine the annealing conditions necessary to obtain an equilibrium PS/PDMS interface, measurements of the local $T_g(z = 50 \text{ nm})$ were done on samples where the

annealing time of the first annealing step at 140 °C (see Figure 2.5) was increased from 20 to 210 min. Figure 2.7 shows how the local $T_g(z = 50\text{ nm})$, relative to T_g^{bulk}, decreases upon annealing of the PS/PDMS interface, stabilizing after 60–90 min as the PS/PDMS interface reaches equilibrium. Data shown are for samples made with either 9:1 or 6:1 PDMS cross-linking ratios. From these results we concluded that 90 min of annealing at 140 °C during the first annealing step of the sample assembly process shown in Figure 2.5 is sufficient and necessary to obtain reproducible and reliable $T_g(z)$ values for the PS/PDMS samples.

Calculation for the Interfacial Width between PS and PDMS Films Annealed to Equilibrium

We estimate the equilibrium interfacial width w_I attained between PS and PDMS annealed at 140 °C based on values of the interaction parameter χ from the literature evaluated at 140 °C. From values tabulated by Eitouni and Balsara in Mark's *Physical Properties of Polymers Handbook*,[60]

$$\chi(T) = A + \frac{B}{T} \tag{2.2}$$

for PS/PDMS with $A = 0.031$ and $B = 58$ K based on measurements from 165–225 °C of the order-disorder-transition temperature (T_{ODT}) for block copolymers by Ref. [126], where values have been adjusted by Eitouni and Balsara to account for a common reference volume. Based on eq. 2.2 with a minor temperature extrapolation, $\chi(T) = 0.17$ at 140 °C. The interfacial width w_I for two high molecular weight polymers with similar statistical segment lengths b and densities is given by[63]

$$w_I = \frac{2b}{\sqrt{6\chi}}, \tag{2.3}$$

for a composition profile

$$\phi(z) = \frac{1}{2}\left[1 + \tanh\left(\frac{2z}{w_I}\right)\right]. \tag{2.4}$$

Taking the average of the statistical segment lengths for PS and PDMS,[7] $b_{\mathrm{PS}} = 0.67$ nm and $b_{\mathrm{PDMS}} = 0.58$ nm, eq. 2.3 gives $w_I = 1.24$ nm. Such calculations of interfacial widths based on χ parameters often provide underestimates of w_I compared with experimentally measured values because real polymer-polymer interfaces are also broadened by interface roughening associated with capillary waves[63]. We note that the light cross-linking of the PDMS elastomer may also result in minor differences to the interfacial width. Based on these considerations, we estimate the PS/PDMS interfacial width as $w_I \approx 1.5$ nm.

Measurements To Ensure that Migration of Unreacted PDMS Monomer Across the Interface Does Not Alter $T_{\mathrm{g}}(z)$ of PS

To ensure that our $T_{\mathrm{g}}(z)$ results were not influenced by any unreacted PDMS material migrating from the PDMS to the PS domain, we also performed $T_{\mathrm{g}}(z)$ measurements for samples where the PDMS layers underwent a washing procedure of soaking the PDMS in good solvent to remove unreacted material.[114,120,121] PDMS strips with masses between 5–10 mg and thicknesses between 50–200 μm were soaked for 24 h in 200 mL of toluene, a good solvent for PDMS. The strips were then degassed and reweighed to determine the mass lost, where we also verified that further washing did not result in additional mass loss. The resulting gel fraction, corresponding to the amount of polymer participating in the network, was determined from the ratio of the mass measured post- and pre-soaking $\frac{m_{\mathrm{post}}}{m_{\mathrm{pre}}}$.[127] In Figure 2.8 we plot our measured gel

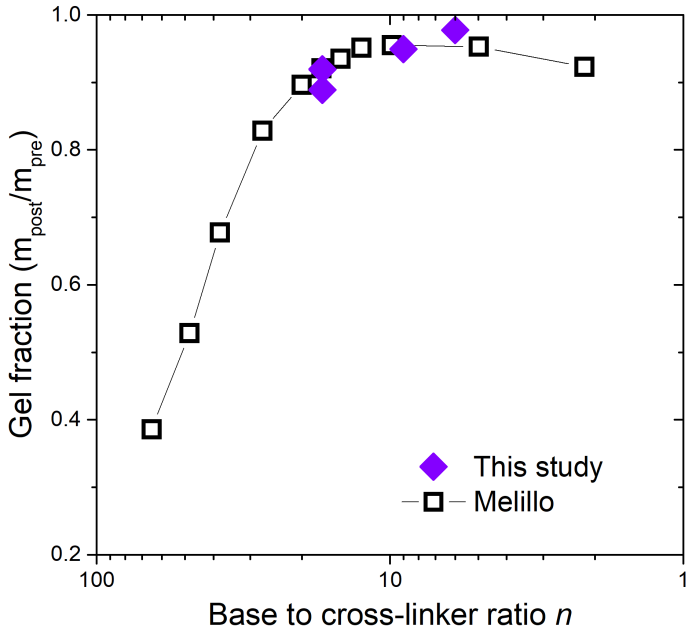

Figure 2.8: Gel fraction $\frac{m_{\text{post}}}{m_{\text{pre}}}$ determined from measurements of the mass lost after Sylgard 184 PDMS was soaked in toluene, a good solvent, for 24 h. Data from Ref. [121] using Soxhlet extraction are also shown. Good agreement is observed with mass losses of 2%–10% for the base:cross-linker range of 6:1–17:1 used in this study.

fraction values together with those from Melillo,[121] where the removal of unreacted material from Sylgard 184 PDMS was done via Soxhlet extraction with toluene over 24 h on PDMS that had been cured at 70 °C for 24 h. Our measured gel fractions ranged from 0.90 to 0.98 for PDMS made with ratios of 17:1, 9:1, and 6:1, in good agreement with those from Ref. [121]. Using dynamic mechanical analysis (DMA), Melillo reported no change in the storage and loss moduli between the pre- and post-extracted PDMS for the base:cross-linker range of 6:1–17:1 used in our study.[121] As shown in Figures 2.3 and 2.4 denoted with X-symbols, the measured $T_{\text{g}}(z)$ values were the same for samples where the PDMS had been soaked in good solvent to remove unreacted material.

Chapter 3

Physically Intuitive Continuum Mechanics Model for Quartz Crystal Microbalance: Viscoelasticity of Rubbery Polymers at MHz Frequencies

3.1 Synopsis

Employing a quartz crystal microbalance (QCM) as a MHz-viscoelastic sensor requires extracting information from higher harmonics beyond the Sauerbrey limit, which can be problematic for rubbery polymer films that are highly dissipative because of the onset of anharmonic side bands and film resonance. Data analysis for QCM can frequently obscure the underlying physics or involve approximations that tend to break down at higher harmonics. In this study, modern computational tools are leveraged to solve a continuum physics model for the QCM's acoustic shear wave

propagation through a polymer film with zero approximations, retaining the physical intuition of how the experimental signal connects to the shear modulus of the material. The resulting set of three coupled equations are solved numerically to fit experimental data for the resonance frequency Δf_n and dissipation $\Delta\Gamma_n$ shifts as a function of harmonic number n, over an extended harmonic range approaching film resonance. This allows the frequency-dependent modulus of polymer films at MHz frequencies, modeled as linear on a log-log scale, to be determined for rubbery polybutadiene (PB) and polydimethylsiloxane (PDMS) films, showing excellent agreement with time-temperature shifted rheometry data from the literature.

3.2 Introduction

Quartz crystal microbalances (QCMs), though originally employed primarily as mass sensors, are increasingly being used to measure the MHz-frequency viscoelastic properties of a wide range of polymer film and brush systems in the nm–μm thickness range.[128–149] The viscoelastic properties of these systems at such high frequencies are important for sound damping and acoustic impedance matching applications at ultrasonic frequencies where rubbery polymer films near their glass transition regime exhibit high loss.[150–152] To access such viscoelastic properties of materials via QCM, one needs to go beyond the well known Sauerbrey region at low harmonic numbers that is primarily sensitive to only the mass added to the QCM sensor.

At low harmonic numbers n, the frequency shift Δf_n of the QCM resonance is given by the Sauerbrey equation:[129,153]

$$\frac{\Delta f_n^{\text{Sauerbrey}}}{f_0} = -\frac{2\,f_0}{Z_{\text{q}}}\,(\rho\,h)\,n, \tag{3.1}$$

where for a film of thickness h and density ρ, (ρh) is the mass per unit area of the film placed on the sensor. The fundamental frequency f_0 at $n = 1$ and the acoustic

impedance Z_q are both properties of the quartz sensor being used. To access the film's viscoelastic properties, QCM measurements must be conducted at higher harmonics beyond the linear n-dependence of the Sauerbrey regime, as well as incorporating dissipation data, related to the bandwidth of the resonance. Going to higher harmonic numbers n, however, can be problematic, especially for more dissipative systems like rubbery polymers where the emergence of anharmonic side bands and the onset of film resonance occur at lower harmonics, imposing limits on the maximum frequency accessible. Film resonance occurs when the formation of standing acoustic waves in the film result in large amplitude oscillations.[129,139] Standard QCM analysis methods typically simplify equations to facilitate analytical solutions,[89] but this can further limit the maximum harmonic number accessible. As such, more recent methods favor numerical solutions to equations with fewer approximations.[128,129] As discussed by the Shull group,[136] the relevant quantity for evaluating deviations from the Sauerbrey regime and determining the viability of viscoelastic measurements via QCM is the ratio of the film thickness h to the wavelength of the shear wave λ_n:

$$\frac{h}{\lambda_n} = \frac{hf_n}{\mathrm{Re}(\tilde{c})} = h(nf_0)\sqrt{\frac{\rho}{|\widetilde{G}|}}\cos(\phi/2) \tag{3.2}$$

where the complex speed of sound in the material $\tilde{c} = \sqrt{\widetilde{G}/\rho}$ depends on the film's complex modulus $\widetilde{G} = G' + iG'' = |\widetilde{G}|\, e^{i\phi}$ and density ρ. Values of $\frac{h}{\lambda_n}$ from $0.05-0.20$ are found to provide the optimal range for viscoelastic measurements.[136,139] Thus, depending on the modulus of the material, the film thickness should ideally be chosen to maximize the small window of accessible harmonics spanning from the end of the Sauerbrey regime to the beginning of film resonance where QCM will be sensitive to the film's viscoelasticity.

To obtain the viscoelastic properties of a film, one of two approaches to QCM modeling is typically used. The first approach, which dates back to the late 1990s

and is the basis for the viscoelastic model in QCM-D systems, uses a continuum mechanics analysis while treating the film layers as a Kelvin-Voigt material.[130,154] The Kelvin-Voigt spring-dashpot model for a viscoelastic solid combines a spring element $\widehat{G}$ in parallel with a dashpot element $\hat{\eta}$ resulting in a frequency-independent storage modulus $G'(f) = \widehat{G}$ and a loss modulus with a linear dependence on frequency $G''(f) = 2\pi f\hat{\eta}$.[89,130] Depending on the material in question, this generic frequency dependence for a viscoelastic material can be inappropriate at the frequency range of the QCM,[89,128] as such recent methods typically incorporate a more general frequency dependence in an extended Voigt model.[128,130,155] The second approach treats the load on the QCM using an acoustic multilayer formalism developed and refined from the 1950s-1990s, where an equivalent circuit model is used to solve for the acoustic impedance of the QCM-film system from which the viscoelastic properties of the film can be extracted.[156,157] Although powerful, this method can obscure the connection between the underlying physics and the properties of the material being studied. The book by Johannsmann,[89] as well as several excellent reviews,[128–130,157,158] provide a useful summary of the history and range of systems studied with QCM operating as a MHz-frequency rheometer. In addition to these more conventional methods of QCM analysis, recent work by the Shull group has used an acoustic impedance-based model to numerically fit the ratio of frequency and dissipation shifts measured at two different harmonics to determine the viscoelastic modulus for a range of glassy and rubbery polymers.[128,134–137,139,140,159] This method is based on the Lu-Lewis[160] equation that matches the load impedance $\widetilde{Z}_L$ at the resonator's surface with that caused by the film at the quartz/film interface.[128,129]

With these modeling efforts in mind, two main challenges confront the QCM user interested in investigating the viscoelastic properties of rubbery polymer films: to maintain the underlying physics intuition of the QCM model, while not introducing approximations that limit the frequency range of the measurement. In the present

work, we leverage modern computational tools to numerically solve a physically intuitive continuum physics model for the shear wave propagation of the QCM's acoustic wave through the sample. This allows us to fit resonance frequency Δf_n and dissipation $\Delta\Gamma_n$ shifts over a range of harmonics n without any approximations to determine the frequency dependent modulus $\widetilde{G}(\omega) = G'(\omega) + iG''(\omega)$. We apply this method to rubbery films of polybutadiene (PB) and polydimethylsiloxane (PDMS), as well as glassy polystyrene (PS), comparing the QCM measured MHz-frequency viscoelasticity with time-temperature shifted rheometry data from the literature.

3.3 Experimental Methods

Polystyrene (PS) (M_w = 1920 kg/mol, $M_\mathrm{w}/M_\mathrm{n}$ = 1.26) from Pressure Chemical and polybutadiene (PB) (M_w = 375 kg/mol, $M_\mathrm{w}/M_\mathrm{n}$ = 2.4; 36% cis 1,4; 55% trans 1,4; 9% vinyl 1,2, as specified by the supplier) from Scientific Polymer Products were purchased and used as received. Both the PS and PB samples were spin-coated from toluene solutions directly onto the QCM sensor, as well as silicon pieces for film thickness determination by ellipsometry. Films were annealed under vacuum for a minimum of 14 h after spin-coating at a temperature of 120 °C for PS ($T_\mathrm{g} \approx 100$ °C) and 25 °C for PB ($T_\mathrm{g} \approx -96$ °C) to remove residual solvent and release stresses developed during spin-coating. Polydimethylsiloxane (PDMS) films cross-linked at a base to cross-linker ratio of 9:1 by mass were prepared using the Sylgard 184 kit manufactured by Dow Corning. After mixing the base and cross-linking agent for ≈1 min, the PDMS mixture was diluted with heptane for spin-coating (at ≈30 wt% of the PDMS mixture in heptane).[90] PDMS films were then cured at 70 °C for 2 hours to match the curing schedule of Refs.[42,45,90].

Film thicknesses were determined by spin-coating films sequentially onto a silicon wafer, the QCM sensor, and then another silicon wafer. Ellipsometry was used to

provide an independent measure of the film thickness on the QCM sensor by averaging the values obtained for the films on the silicon wafers. The thickness of the film on the QCM sensor was also determined by fitting the frequency Δf_n and dissipation $\Delta\Gamma_n$ shifts to the continuum physics model, where good agreement was found with the ellipsometry measurements.

Ellipsometry measurements were conducted using a J.A. Woollam M-2000 variable angle spectroscopic ellipsometer with rotating compensator. The film thickness h and index of refraction $n(\lambda)$ for the polymer layer were determined by fitting the amplitude $\Psi(\lambda)$ and phase shift $\Delta(\lambda)$ ellipsometry data, corresponding to the complex intensity ratio of p- to s-polarized light, collected at three angles of incidence (55°, 60°, and 65°) over the wavelength range λ spanning 400–1000 nm to an optical layer model using Woollam's CompleteEASE software. The optical layer model was comprised of a transparent Cauchy layer $n(\lambda) = A + \frac{B}{\lambda^2} + \frac{C}{\lambda^4}$ for the polymer film, atop a semi-infinite silicon substrate with a 1.25 nm native oxide layer.[84] For ellipsometric modeling of spin-coated PDMS films, an additional thickness non-uniformity parameter was included in the fit, with values typically between 3% and 7%.[90]

For the QCM measurements, AT-cut quartz sensors from Stanford Research Systems with a fundamental frequency f_0 of 5 MHz were used. Individual resonance peaks were collected with a vector network analyzer (Agilent 4395a) driving the system at 0 dBm, corresponding to a power of 1 mW. The circuit diagram of how the QCM sensor was connected to the network analyzer is given in Figure 3.1. All QCM measurements were done at room temperature (25 °C). For rubbery PB and PDMS films, full resonance traces were collected for a range of harmonics from $n = 1$ up to $n = 13$. The maximum harmonic number n for each film was limited by the emergence of anharmonic side peaks,[89] as described in section 3.4.3. Additional control measurements on glassy PS films were done where only the resonance frequencies f_n were measured for harmonics n =1–19.

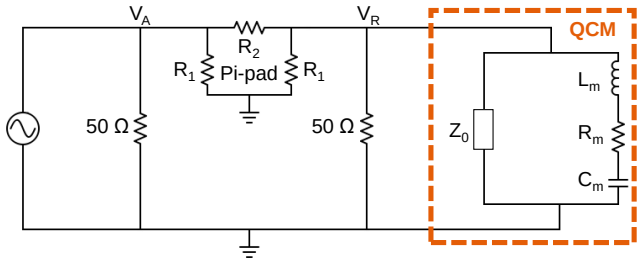

Figure 3.1: Circuit model for the QCM setup connected to the network analyzer. The QCM sensor, holder, and associated cables are highlighted by the orange dashed box. Their components consist of the motional branch elements L_m, R_m, and C_m in parallel with the electrical parasitic impedance Z_0. The network analyzer provides an oscillating voltage and measures V_A and V_R at its ports, each of which passes through a 50 Ω internal resistor to ground. A Pi-pad attenuator that includes resistors R_1 and R_2 separate V_A and V_R.

The measured resonance traces were fit to a nonlinear functional form determined from an analysis of the QCM circuit to find the resonance frequency f_n and dissipation Γ_n at each harmonic. Figure 3.1 shows the circuit diagram of the QCM equivalent circuit connected to the network analyzer with a Pi-pad attenuator consisting of resistors R_1 and R_2. The QCM equivalent circuit, identified by the dashed box in the figure, consists of a motional branch with values L_m, R_m, and C_m, describing the mechanical properties of the QCM sensor. An additional electrical branch, with a parasitic impedance Z_0 is included to account for the parasitic capacitances of the QCM's electrodes and holder, and the parasitic capacitances and inductances of the cables and connections used to connect the QCM to the network analyzer. The voltages identified as V_A and V_R are measured at the ports of the network analyzer, each of which passes through an internal resistance of 50 Ω to ground. The V_A and V_R voltages themselves are separated by a Pasternack 50 Ω, −3 dBm, Pi-pad attenuator, which was added to decrease the source power by half and to reduce electronic reflections.

The data collected from the analyzer is in the form $20\log_{10}\left|\frac{V_A}{V_R}\right|$. Solving for $\frac{V_A}{V_R}$ in the circuit diagram shown in Fig. 3.1 by adding impedances in series and parallel

gives the following functional form for the attenuator signal:

$$20\log_{10}\left|\frac{V_A}{V_R}\right| = +10\log_{10}\left[C^2 + B_n^2\, f^2 + \frac{A_n^2 + 2CA_n - B_nA_n(f^2 - f_n^2)/\Gamma_n}{1 + (f^2 - f_n^2)^2/(4\Gamma_n^2 f^2)}\right] \quad (3.3)$$

The parameter $C = 1 + R_2\left(\frac{1}{R_1} + \frac{1}{50\,\Omega}\right) = 1.41$ since $R_1 = 292.4\ \Omega$ and $R_2 = 17.6\ \Omega$. The parameters $A_n = \frac{R_2}{R_m}$ and $B_n = 2\pi R_2 Z_0$ both change with harmonic number n as the motional resistance R_m of the QCM sensor and the parasitic impedance of the circuit Z_0 vary with frequency. We additionally observed a non-zero background in the network analyzer data, which we determined to be due primarily to electromagnetic wave reflections in the cables and connections. This background is constant within the small frequency range of an individual harmonic. We therefore added a constant vertical offset term to eq. (3.3) to account for vertical shifts in the background at each harmonic. This leaves us with five fitting parameters to fit the resonance peak, where f_n corresponds to the peak frequency and Γ_n the bandwidth, A_n corresponds to the amplitude of the peak while B_n accounts for its asymmetry, and corrects for any baseline offsets.

Figure 3.2 shows resonance peaks for a 250 nm thick PB film atop the QCM sensor collected at harmonic numbers $n = 3$ ($f_3 = 3f_0 = 15$ MHz) and $n = 9$ ($f_9 = 9f_0 = 45$ MHz). Fits of eq. (3.3) to these resonance peaks give best fit parameter values of $f_3 = 15.0169$ MHz ± 0.06 Hz and $\Gamma_3 = (69.21 \pm 0.06)$ Hz, with $A_3 = 0.5162 \pm 0.0003$, $B_3 = (-3.62 \pm 0.06) \times 10^{-9}\ \Omega^2$, and $= 0.0089 \pm 0.0004$ dBm for $n = 3$, and $f_9 = 45.0432$ MHz ± 0.3 Hz and $\Gamma_9 = (691.9 \pm 0.3)$ Hz, with $A_9 = 0.04979 \pm 0.00001$, $B_9 = (-3.44 \pm 0.01) \times 10^{-9}\ \Omega^2$, and $= (-0.0322 \pm 0.0003)$ dBm for $n = 9$. Similar resonance traces were collected from other samples and fit with eq. (3.3), where the error associated with measuring any individual resonance peak was always smaller than the sample-to-sample variability. For a given polymer film, the resonance peaks collected at higher harmonics show a decreased peak amplitude A_n and increased

peak width Γ_n caused by the increased viscous dissipation at higher frequencies.

When a polymer film is added to the QCM sensor, the motional branch elements of the QCM are altered causing a shift in the resonance frequency $f_n = \frac{1}{2\pi\sqrt{L_m C_m}}$ and dissipation $\Gamma_n = \frac{R_m}{4\pi L_m}$, relative to that of the bare quartz. To determine the shifts in frequency $\Delta f_n = f_n^{\text{film+QCM}} - f_n^{\text{bare QCM}}$ and dissipation $\Delta\Gamma_n = \Gamma_n^{\text{film+QCM}} - \Gamma_n^{\text{bare QCM}}$,

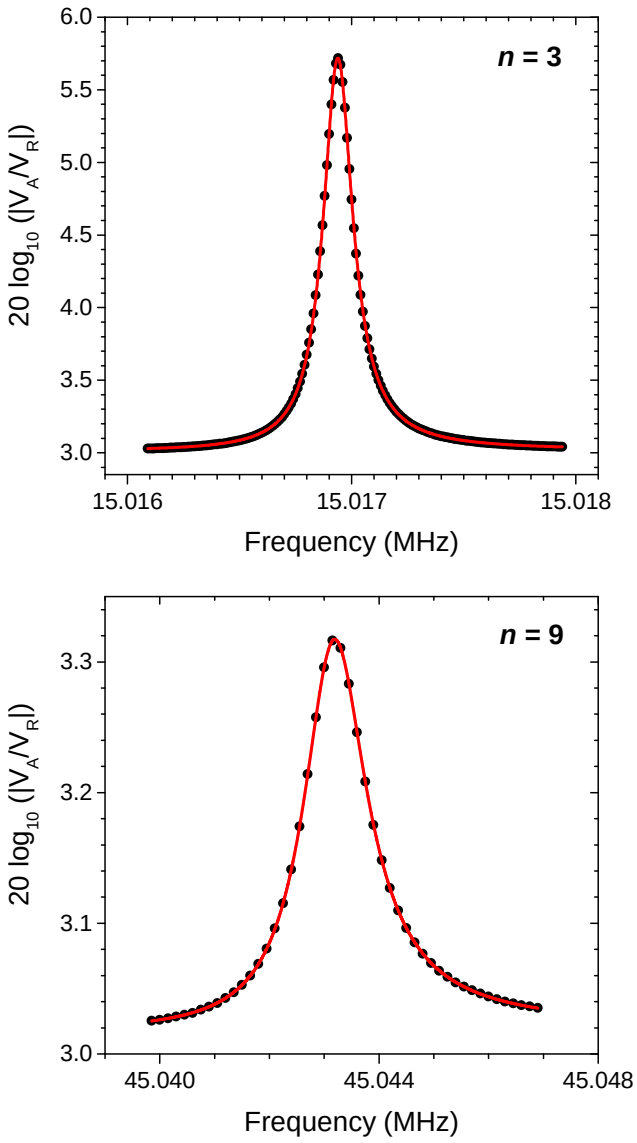

Figure 3.2: Resonance peaks for a 250 nm thick PB film on a QCM sensor at the $n = 3$ harmonic (a) and the $n = 9$ harmonic (b). The red curves represent fits of eq. (3.3) to the data (black symbols), which are used to measure the frequency f_n and dissipation Γ_n for each resonance.

measurements of the resonance peaks were collected for both the bare quartz initially giving $f_n^{\text{bare QCM}}$ and $\Gamma_n^{\text{bare QCM}}$, and then the same quartz sensor with the film added giving $f_n^{\text{film+QCM}}$ and $\Gamma_n^{\text{film+QCM}}$. These frequency and dissipation shifts, Δf_n and $\Delta\Gamma_n$, between the film-loaded and bare quartz QCM sensors are the main parameters we are interested in for the analysis with our continuum physics model.

3.4 Results and Discussion

3.4.1 Continuum physics model and numerical fitting

We present a continuum physics QCM model for a linear viscoelastic polymer film with a complex, frequency dependent shear modulus $\widetilde{G}(\omega) = G'(\omega) + iG''(\omega)$ that preserves the simple intuitive physics of the sample geometry and can be solved numerically without any approximations using current scientific computer programs such as Mathematica. This model is quantitatively equivalent to the more commonly used Lu-Lewis equation that is also solved numerically,[128,129] but physicists familiar with continuum mechanics may find this derivation more intuitive. For a viscoelastic film atop AT-cut quartz crystals, the QCM oscillation can be readily treated as a one-dimensional shear wave propagating away from the QCM surface, as the thickness shear mode in the plane of the film is dominant and compressional oscillations can be ignored. This is commonly referred to as the parallel plate model, where energy trapping considerations are ignored, see Ref. [129] for a more complete discussion.

Figure 3.3 illustrates our sample geometry with axes for the model, where we treat the shear wave as propagating in the z-direction and oscillating in the y-direction. The shear wave displacement in the $\hat{y}$-direction for the polymer film $\vec{u}_{\text{f}}$ and quartz

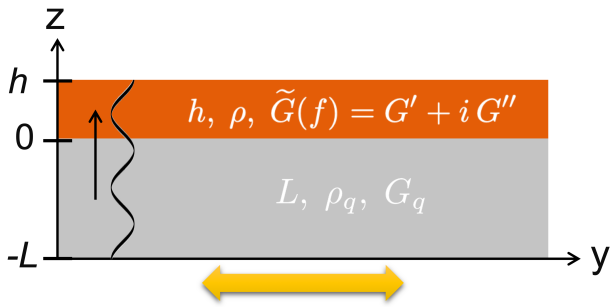

Figure 3.3: Layer geometry for the continuum physics model illustrating the one-dimensional shear wave propagating from the QCM quartz surface into the polymer film along the z-direction. A polymer film of thickness h, density ρ, and shear modulus $\widetilde{G}(f) = G'(f) + iG''(f)$ is placed atop the quartz resonator of thickness L, density ρ_{q}, and shear modulus G_{q}.

crystal $\vec{u}_{\mathrm{q}}$ can be written as

$$\vec{u}_{\mathrm{f}}(z,t) = e^{-i\widetilde{\omega}t}\left(A_{\mathrm{f}}\, e^{i\widetilde{k}_{\mathrm{f}}z} + B_{\mathrm{f}}\, e^{-i\widetilde{k}_{\mathrm{f}}z}\right)\hat{y} \quad \text{(film layer)} \tag{3.4}$$

$$\vec{u}_{\mathrm{q}}(z,t) = e^{-i\widetilde{\omega}t}\left(A_{\mathrm{q}}\, e^{i\widetilde{k}_{\mathrm{q}}z} + B_{\mathrm{q}}\, e^{-i\widetilde{k}_{\mathrm{q}}z}\right)\hat{y} \quad \text{(quartz layer)} \tag{3.5}$$

where $\tilde{k}_i = 2\pi\tilde{f}/\tilde{c}_i$ is the complex wave vector, and A_i and B_i are the wave amplitudes of the forward propagating and reflected waves, respectively.

The complex angular frequency $\widetilde{\omega} = 2\pi\tilde{f} = 2\pi(f_n + i\Gamma_n)$ contains the information about the resonance frequency f_n and dissipation Γ_n of the film+quartz system at each harmonic number n. These resonance frequencies and dissipations of the film+quartz system are defined in the model based on the bare quartz oscillation as $f_n = nf_0 + \Delta f_n$ and $\Gamma_n = n\Gamma_0 + \Delta\Gamma_n$, allowing us to directly extract the frequency and dissipation shifts Δf_n and $\Delta\Gamma_n$. These quantities will then be fit to the experimentally determined values from the resonance traces, where Δf_n corresponds to the shift in peak position and $\Delta\Gamma_n$ corresponds to the change in peak width relative to that measured for the bare quartz.

The displacement in the polymer film for the transverse shear wave emanating

from the quartz surface will satisfy the wave equation for an incompressible material[87]

$$\rho \frac{\partial^2 \vec{u}_\mathrm{f}}{\partial t^2} = \widetilde{G} \nabla^2 \vec{u}_\mathrm{f} \tag{3.6}$$

and similarly for the quartz layer. The speed for this shear wave is the transverse speed of sound $\tilde{c} = \sqrt{\frac{\widetilde{G}}{\rho}}$ that depends on the material's shear modulus and density. Assuming Hooke's law for the linear viscoelastic polymer film under small shear displacement, the shear stress tensor for the continuous material under shear deformation can be written as[87]

$$\sigma_{yz} = 2\,\widetilde{G}\,U_{yz}, \tag{3.7}$$

where U_{yz} is the yz component of the strain tensor

$$U_{yz} = \frac{1}{2}\left(\frac{\partial u_z}{\partial y} + \frac{\partial u_y}{\partial z}\right). \tag{3.8}$$

For the AT-cut quartz sensor, the predominant oscillation is the thickness shear mode that is traveling in the z-direction and polarized in the y-direction, allowing us to neglect any compressional oscillation in the z-direction so that $u_z = 0$. This simplifies the strain and stress tensors to

$$U_{yz} = \frac{1}{2}\frac{\partial u_y}{\partial z} \quad \text{and} \quad \sigma_{yz} = \widetilde{G}\,\frac{\partial u_y}{\partial z} \tag{3.9}$$

where $u_y = \vec{u}_\mathrm{f}$ in the polymer film. Similar equations exist for the quartz layer where $u_y = \vec{u}_\mathrm{q}$, and ρ_q and G_q are normally written in terms of the acoustic impedance $Z_\mathrm{q} = \sqrt{\rho_\mathrm{q} G_\mathrm{q}} = 8.8 \times 10^9$ g m^{-2} Hz for AT-cut quartz.[89]

To solve the system, we apply standard boundary conditions at the interfaces between the layers. Continuity of displacement at the film/quartz interface (no-slip

boundary condition) gives

$$u_{\mathrm{f}}(z,t)\Big|_{z=0} = u_{\mathrm{q}}(z,t)\Big|_{z=0}$$
$$A_{\mathrm{f}} + B_{\mathrm{f}} = A_{\mathrm{q}} + B_{\mathrm{q}}. \tag{3.10}$$

Stress continuity (Newton's third law) at the film/quartz interface gives

$$\sigma_{\mathrm{f}}(z,t)\Big|_{z=0} = \sigma_{\mathrm{q}}(z,t)\Big|_{z=0}$$
$$\sqrt{\rho\,\widetilde{G}}\,(A_{\mathrm{f}} - B_{\mathrm{f}}) = Z_{\mathrm{q}}\,(A_{\mathrm{q}} - B_{\mathrm{q}}), \tag{3.11}$$

while the top film/air and bottom quartz/air interfaces will be stress free giving

$$\sigma_{\mathrm{f}}(z,t)\Big|_{z=h} = 0$$
$$A_{\mathrm{f}} - B_{\mathrm{f}}\,\exp\left[-i4\pi h\sqrt{\frac{\rho}{\widetilde{G}}}\,(f_n + i\Gamma_n)\right] = 0 \tag{3.12}$$

and

$$\sigma_{\mathrm{q}}(z,t)\Big|_{z=-L} = 0$$
$$A_{\mathrm{q}} - B_{\mathrm{q}}\,\exp\left[i\frac{2\pi}{f_0}\,(f_n + i\Gamma_n)\right] = 0. \tag{3.13}$$

For computational simplicity, we are ignoring the tiny stress contribution due to air at these interfaces, which we estimate using Navier-Stokes to be less than a 0.03% correction on the frequency shift. Note, eq. (3.13) was simplified by recognizing that the thickness of the quartz crystal $L = \frac{\lambda_0}{2}$ is related to the fundamental frequency $f_0 = \frac{c_{\mathrm{q}}}{\lambda_0}$ such that $\frac{L}{c_{\mathrm{q}}} = \frac{1}{2f_0}$. This system of equations can then be further simplified by using eq. (4.3) to eliminate one of the displacement amplitudes, which we did to remove A_{f}. In addition, we also normalized the remaining amplitudes by setting

$A_q = 1$ nm.

The continuum physics model can only account for the frequency Δf_n and dissipation $\Delta\Gamma_n$ shifts due to the presence of the polymer film relative to the idealized bare quartz resonance of $f_n = nf_0$ with $\Gamma_0 = 0$. As such eqs. (4.7) and (3.13) need to be recast in terms of $\Delta f_n = f_n - nf_0$ and $\Delta\Gamma_n = \Gamma_n - \Gamma_0 \approx \Gamma_n$ by replacing $(f_n + i\Gamma_n) = (nf_0 + \Delta f_n + i\Delta\Gamma_n)$. Experimental factors associated with the circuit cables and QCM sensor mounting that might impact the frequency and dissipation measured in practice will be accounted for by determining the experimental frequency Δf_n and dissipation $\Delta\Gamma_n$ shifts relative to those measured directly for the bare quartz at each resonance:

$$\Delta f_n = f_n^{\text{film+QCM}} - f_n^{\text{bare QCM}} \tag{3.14}$$

$$\Delta\Gamma_n = \Gamma_n^{\text{film+QCM}} - \Gamma_n^{\text{bare QCM}} \tag{3.15}$$

Thus for the continuum physics model, this leaves us with a system of three complex equations that can be solved numerically using standard root finding methods to determine the complex frequency shift $\Delta\widetilde{f}_n = \Delta f_n + i\Delta\Gamma_n$ for a given polymer film of thickness h, density ρ, and a complex frequency-dependent shear modulus $\widetilde{G}(f_n)$:

$$\sqrt{\rho\,\widetilde{G}}\,(1 + B_q - 2B_f) - Z_q\,(1 - B_q) = 0 \tag{3.16}$$

$$1 + B_q - B_f\left(1 + \exp\left[-i4\pi h\sqrt{\frac{\rho}{\widetilde{G}}}\,(nf_0 + \Delta f_n + i\Delta\Gamma_n)\right]\right) = 0 \tag{3.17}$$

$$1 - B_q \exp\left[i\frac{2\pi}{f_0}\,(\Delta f_n + i\Delta\Gamma_n)\right] = 0 \tag{3.18}$$

To account for small variations in the fundamental frequency f_0 based on the particular cut of a given QCM sensor, the value of f_0 in the model is taken to be the experimentally measured value for the bare quartz crystal prior to adding the polymer film.

For the set of three equations (3.16)–(3.18), the harmonic number n functions as the independent variable, while Δf_n and $\Delta\Gamma_n$ are the dependent variables. A chi-squared minimization fitting routine is used to minimize the deviation between the experimentally measured Δf_n and $\Delta\Gamma_n$ values with those calculated numerically solving eqs. (3.16)–(3.18) in Mathematica at each harmonic number n. The density of the polymer film ρ is treated as a constant with values for each polymer determined from the literature, leaving the polymer film thickness h and shear modulus $\widetilde{G}(f_n) = G'(f_n) + iG''(f_n)$ as the fitting parameters to determine for each polymer film.

The chi-squared minimization was performed using the gradient-descent local minimization routine FindMinimum in Mathematica, which executed a Levenberg-Marquardt routine. As long as the initial guesses for the fit parameters were physically reasonable, the local minimum obtained matched a computationally longer global minimization algorithm (NMinimize). The fitting errors for the best fit parameter values obtained were determined by calculating the maximum range of each parameter along the χ^2 distribution corresponding to one standard deviation (a 68.3% confidence interval).

To account for the frequency-dependent viscoelastic nature of the polymer shear modulus $\widetilde{G}(f_n) = G'(f_n) + iG''(f_n)$, while limiting the number of fitting parameters needed, we take advantage of the narrow frequency range of the QCM (5 MHz to 65 MHz) and treat the frequency dependence as linear on a log modulus versus log frequency scale. This type of simplification has been done by others previously.[89,136] Given that $f_n = nf_0 + \Delta f_n \approx nf_0$, we can write

$$G'(f_n) \approx G'(n) = G'_0\, n^{\beta'} \tag{3.19}$$

$$G''(f_n) \approx G''(n) = G''_0\, n^{\beta''} \tag{3.20}$$

which for log-log axes gives

$$\log_{10} G'(n) = \beta' \log_{10} n + \log_{10} G'_0 \tag{3.21}$$

$$\log_{10} G''(n) = \beta'' \log_{10} n + \log_{10} G''_0 \tag{3.22}$$

G'_0 and G''_0 correspond to the values of the storage and loss modulus at the first harmonic $n = 1$ (5 MHz). β' and β'' represent the slope of the storage and loss modulus frequency dependence on a log-log scale within the QCM frequency range. To minimize the number of fit parameters, we used time-temperature shifted rheological data from the literature to determine β' and β'' for each rubbery polymer based on the local slope of $\log_{10} G'$ and $\log_{10} G''$ versus $\log_{10} f$ data in the QCM frequency range, as described in sections 3.4.3 and 3.4.4. Thus, this leaves three fitting parameters, G'_0, G''_0, and h, for the continuum physics model to define the frequency and dissipation shifts Δf_n and $\Delta\Gamma_n$.

3.4.2 Continuum physics model applied to glassy polystyrene films

As a simple test case, we begin by applying our continuum physics model to glassy polystyrene (PS) films. At room temperature (25 °C), PS is well within its glassy plateau region at MHz frequencies with negligible dissipation such that the shear modulus of PS can be treated as simply a constant storage shear modulus $\widetilde{G}(f) = G'$, independent of frequency. Justification for this choice of analysis is included in the Appendix, along with representative resonance traces for PS. Focusing on only the frequency shifts Δf_n, resonance peaks were collected for a 1.37 μm thick PS film at harmonic numbers $n = 1$ to 19. The resonance frequencies of the bare QCM resonator were also measured at the same harmonic numbers $n = 1$ to 19 prior to the polymer film being added to the QCM sensor. The resonance frequency shifts

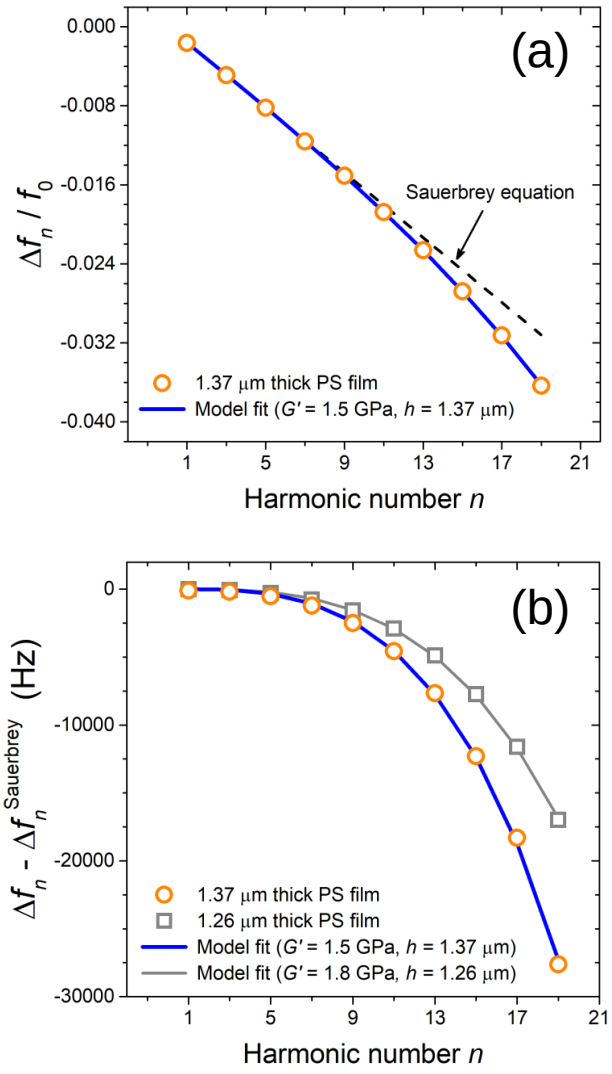

Figure 3.4: (a) Resonance frequency shifts Δf_n, normalized by the fundamental frequency f_0, measured by QCM at 25 °C over the harmonic range $n = 1$ to 19 (5 MHz to 95 MHz) for a PS film with a thickness of 1.37 μm (orange circles). These data were fit with our continuum physics model (blue curve) to determine the glassy shear modulus G' and film thickness h, giving $G' = 1.53 \pm 0.10$ GPa and $h = 1.37 \pm 0.01$ μm. The linear Sauerbrey region at low harmonics is indicated by the black dashed line, which is a linear fit to the data for the first three harmonics $n = 1, 3, 5$. (b) Frequency shifts Δf_n relative to the expected frequency shift from purely mass loading given by the Sauerbrey equation $\Delta f_n^{\text{Sauerbrey}}$, plotted as a function of harmonic number n for the 1.37 μm thick PS film and a second 1.26 μm thick PS film (gray squares). The continuum physics model fit (gray curve) to the data from this second sample give best fit values of $G' = 1.83 \pm 0.07$ GPa and $h = 1.265 \pm 0.004$ μm.

were then defined as $\Delta f_n = f_n^{\text{film+QCM}} - f_n^{\text{bare QCM}}$. Figure 3.4a plots these Δf_n values, normalized by the fundamental frequency $f_0 = 5$ MHz of the bare quartz, as a function of harmonic number n. To focus on the viscoelastic response of the film, we subtract off the frequency shift expected for the Sauerbrey regime $\Delta f_n^{\text{Sauerbrey}}$ from purely mass loading, plotting $\Delta f_n - \Delta f_n^{\text{Sauerbrey}}$ in Figure 3.4b. A second 1.26 μm thick PS sample is also included.

Our continuum physics model presented in section 3.4.1 was used to fit these experimental values of Δf_n as a function of harmonic number n to obtain the glassy shear modulus for PS giving $G' = 1.53 \pm 0.10$ GPa and a film thickness of $h = 1.37 \pm 0.01$ μm, assuming a constant density for PS of $\rho = 1.04$ g/cm^3 obtained from the literature.[122] This film thickness value determined from fitting the QCM data to the continuum physics model agrees well with the value of 1.33 ± 0.10 μm independently determined by ellipsometry. Measurements were repeated for a 1.26 μm thick PS film, where fits of the frequency shift Δf_n data gave best fit values of $G' = 1.83 \pm 0.07$ GPa and $h = 1.265 \pm 0.004$ μm. Both these QCM measurements on two separate PS films show good reproducibility. The glassy shear modulus values measured for PS with QCM over the frequency range of 5 MHz to 95 MHz agree well with literature values for glassy PS storage modulus determined by QCM ($G' \approx 1/J' = 1.7$ GPa)[133] and measurements of the shear wave speed at 1 MHz ($G' = \rho c_s^2 = 1.3$ GPa and 1.4 GPa).[161–163] The agreement between our data and the model's fit, as well as the agreement between our G' values and those from the literature for glassy PS, verifies that our QCM experimental setup and modeling accurately describe the frequency response of a film with a glassy shear modulus on top of the QCM crystal.

3.4.3 Continuum physics model applied to rubbery polybutadiene films

We now apply our continuum physics model to a fully viscoelastic rubbery polymer film, polybutadiene (PB), which is in its glass transition regime at 25 °C in the QCM MHz frequency range.[164–168] We therefore model the storage and loss moduli using equations (3.21)-(3.22), which treat the frequency dependence of the shear modulus as linear on a log-log scale.

To minimize the number of fit parameters, we determined the local slope of $\log(G')$ and $\log(G'')$ versus $\log(f)$ within the QCM frequency range, corresponding to the exponents β' and β'' in eqs. (3.21)-(3.22), by fitting rheological data from the literature.[164,165,167,168] These literature studies measured $G'(\omega)$ and $G''(\omega)$ (where $\omega = 2\pi f$) for PB samples at frequencies up to 100 rad/s (≈16 Hz) at different temperatures, then used time-temperature superposition to shift the moduli to a single reference temperature resulting in a collective frequency range spanning 10^{-3} to 10^{+11} Hz. We digitized the data in the QCM frequency range from these studies corresponding to PB samples with molecular weights ranging from $M_w = 130$ kg/mol (Colby et al.[164]) to $M_w = 1200$ kg/mol (Liu et al.[168]). The data from Colby et al.[164] and Liu et al.[168] both used a reference temperature of 25 °C for their time-temperature superposition, while Palade et al.[165] and Wang et al.[167] used −85 °C and 40 °C reference temperatures, respectively. To superimpose the data from these literature studies on a single plot and compare them with our QCM results collected at room temperature (≈ 25 °C), we shifted the data from Palade et al.[165] and Wang et al.[167] to a reference temperature of 25 °C using the shift factors from their papers. We then performed linear fits to the $\log(G')$ and $\log(G'')$ versus $\log(f)$ data from each study for the frequency range from 5 MHz to 45 MHz (corresponding to QCM harmonic range of $n = 1$ to 9) resulting in best fit average and standard deviation values of $\beta' = 0.50 \pm 0.03$ for the storage and $\beta'' = 0.74 \pm 0.01$ for the loss moduli exponents. The small errors

in β' and β'' illustrate the excellent agreement in the frequency dependence of the storage and loss moduli of PB over a wide range of molecular weights in the 5–45 MHz frequency range at the 25 °C reference temperature, within the glass transition regime. Given this consistency in β' and β'' values, it is reasonable to assume that these exponent values for the storage and loss moduli should apply well to our study's PB with a molecular weight of $M_w = 375$ kg/mol measured at room temperature by QCM within the glass transition regime. We therefore fix these exponent values of β' and β'' in our continuum model and fit our QCM data for the storage G_0' and loss G_0'' moduli offsets corresponding to $G'(n)$ and $G''(n)$ at $n = 1$ (5 MHz) in eqs. (3.21)-(3.22), along with the film thickness h.

QCM measurements were conducted on PB films for a variety of film thicknesses ranging from 250 nm to 730 nm. Thicker films up to 2 μm were also investigated, but clear reliable resonance peaks could not be obtained. For each film measured, resonance traces were collected for a range of harmonics spanning from $n = 1$ up to $n = 13$. These resonance peaks were then fit with eq. 3.3, as described in the experimental methods section, to obtain the resonance frequency f_n and dissipation Γ_n at each harmonic n. Representative resonance traces for the harmonics at $n = 3$, 9, and 11 are shown in Figure 3.5a for a 250 nm thick PB film. Corresponding reference traces of the bare quartz crystal were also collected at each harmonic to determine the frequency shift $\Delta f_n = f_n^{\text{film+QCM}} - f_n^{\text{bare QCM}}$ and dissipation shift $\Delta\Gamma_n = \Gamma_n^{\text{film+QCM}} - \Gamma_n^{\text{bare QCM}}$. These values of Δf_n and $\Delta\Gamma_n$ are then plotted as a function of harmonic number n in Figure 3.5b, with similar results for a 510 nm thick PB film shown in Figure 3.5c. To focus on the viscoelastic response of these rubbery films, the frequency shift Δf_n is referenced to the frequency shift expected from the Sauerbrey equation resulting solely from the mass contribution $\Delta f_n^{\text{Sauerbrey}}$, as given by eq. (3.1).

As the harmonic number increases, especially for thicker films, anharmonic side

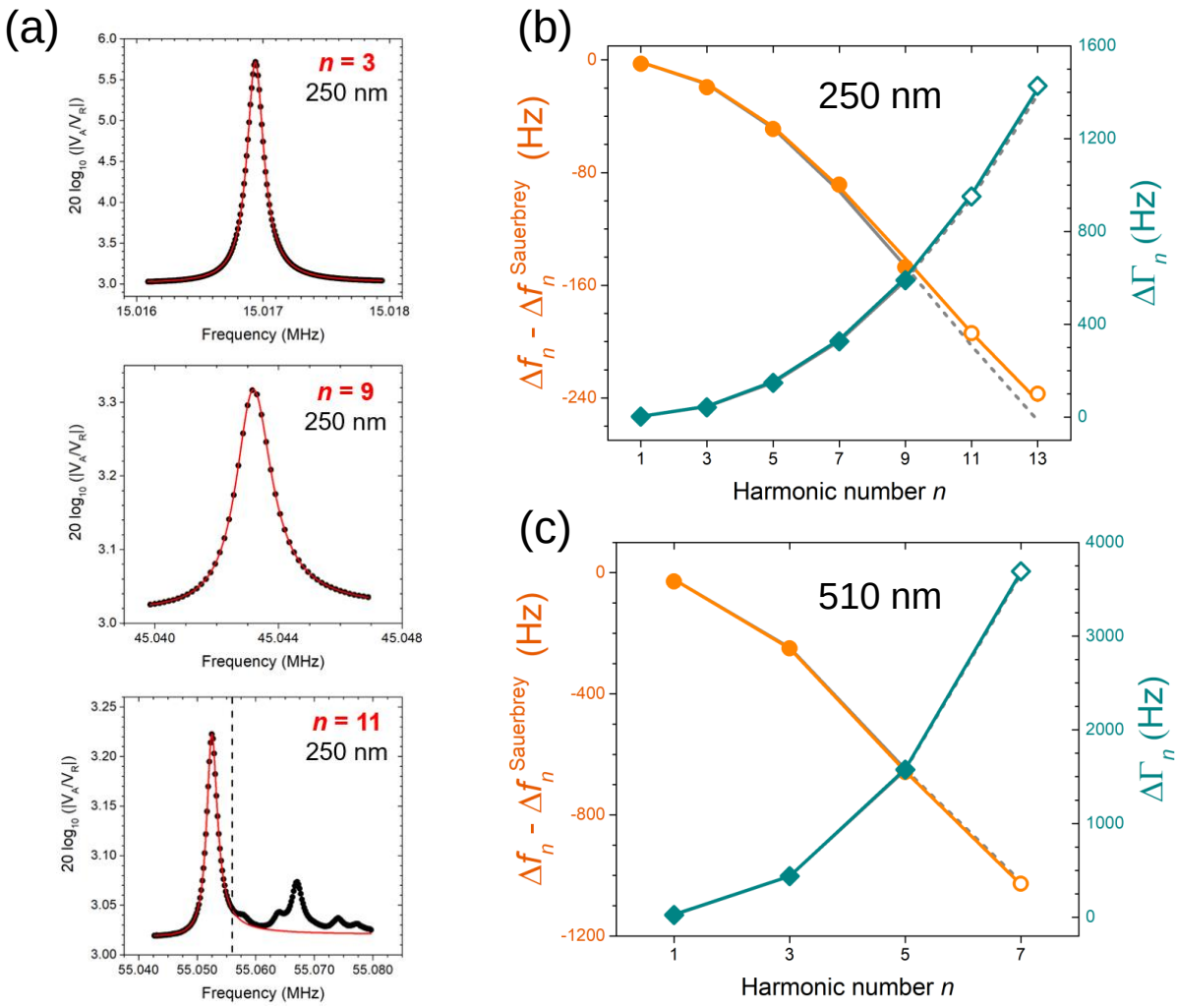

Figure 3.5: (a) Resonance traces of the $n = 3$, 9, and 11 harmonics for a 250 nm PB film on a QCM. The symbols are the data collected with the network analyzer and the red curves are fits using eq. (3.3). The dashed vertical line in the $n = 11$ resonance plot corresponds to the maximum frequency used in fitting the resonance. Resonance frequency shifts Δf_n (orange circles, left axis) and dissipation shifts $\Delta\Gamma_n$ (teal diamonds, right axis) for a 250 nm (b) and 510 nm (c) PB film. The symbols are the experimental data and the curves the continuum physics model fits to these data, where the frequency shift Δf_n has been referenced to that expected from the Sauerbrey equation $\Delta f_n^{\text{Sauerbrey}}$, which accounts only for the mass contribution. The solid colored curves are a fit to both the solid and open symbols, while the gray solid and dashed curves are a fit to the solid symbols that are then extrapolated to higher harmonics, see text for details.

peaks become present near the main resonance peak of interest. These side peaks are initially visible as side features far from the main resonance peak, but at sufficiently

high harmonics, they eventually merge with the main resonance peak, rendering the fitting for f_n and Γ_n unreliable. Because of the caution often expressed about the presence of anharmonic side peaks,[89] it is common in the QCM literature to simply discard any resonance curves with side peaks in the vicinity of the main resonance peak or limit data to below some maximum harmonic number. In our measurements, we have identified resonance traces at higher n for which anharmonic side peaks appear to be present, but where we believe the main resonance peak can still be reliably fit to obtain f_n and Γ_n. An example of such a resonance trace is shown in Fig. 3.5a for the $n = 11$ harmonic of the 250 nm PB film. By limiting the fitting range to the main resonance peak, to the left of the vertical dashed line in the figure, we were able to obtain good fits to the main resonance peak. However, given the caution expressed with such traces, we have denoted the shifts obtained from the f_n and Γ_n values determined in this manner by open symbols in Figs. 3.5b and 3.5c. The solid symbols are for Δf_n and $\Delta\Gamma_n$ shifts obtained from traces where no side peaks are present near the main resonance peak, such as those shown in Fig. 3.5a for $n = 3$ and 9. We also find the resonance shifts at the fundamental harmonic $n = 1$ to be extremely reproducible and as reliable as the resonance shifts measured at $n = 3$, as such we have included the $n = 1$ data in our analysis.

In order to access the modulus of the polymer film, there would be benefits to maximizing the number of harmonics measured because the QCM resonance becomes more sensitive to the sample's viscoelasticity at higher harmonics. As we are solving our continuum physics model for the QCM numerically, we are not restricted to only low harmonics far from the film resonance condition, as would be necessary when using several of the approximations commonly used in QCM analysis. Thus, we can use our continuum physics model as a way of verifying the consistency of the frequency and dissipation shifts obtained from the higher harmonics with some adjacent side peaks present to the main resonance. We can do this by first using

the continuum physics model to fit only the solid symbols in Figs. 3.5b and 3.5c, where no side peaks are present, and then extrapolating the model with these best fit parameters to higher harmonics to see how they compare with the Δf_n and $\Delta\Gamma_n$ values obtained when some adjacent side peaks are present (open symbols). From such a comparison, we find that the measured Δf_n and $\Delta\Gamma_n$ values (open symbols) are within 0.8% of the predicted values based on an extrapolation of the model. This good agreement suggests a consistency that justifies the inclusion of the higher harmonics (open symbols) where adjacent side peaks are present, but for which we believe the resonance and dissipation values can be accurately determined from the resonance trace. As such, we have chosen to fit the entire harmonic range measured (both open and solid symbols) to determine our best fit values for the storage and loss modulus of the polymer films by QCM. By comparing the curvature of the $\Delta f_n - \Delta f_n^{\text{Sauerbrey}}$ data as a function of harmonic number n with model predictions, we can identify these open symbols as occurring just near the start of the film resonance condition.

As described in section 3.4.1, the continuum physics model calculates the frequency and dissipation shifts Δf_n and $\Delta\Gamma_n$ as a function of harmonic number n expected for a polymer film supported on the QCM crystal based on its film thickness h, and storage $G'(n) = G'_0 n^{\beta'}$ and loss $G''(n) = G''_0 n^{\beta''}$ modulus values. By using literature data to fix the frequency dependence, exponent values β' and β'', we are left with only three fit parameters h, G'_0 and G''_0 that can be determined from fits of Δf_n and $\Delta\Gamma_n$ as a function of harmonic number n. The density of high molecular weight PB is between 0.894 and 0.896 g/cm^3 at room temperature;[164] in this study, we use the value of $\rho = 0.895$ g/cm^3 for our continuum model. For the 250 nm PB film shown in Fig. 3.5b, the best fit values determined from a fit of all the data to our continuum physics model gives $h = 246 \pm 1$ nm for the film thickness, and $G'_0 = 2.64 \pm 0.66$ MPa and $G''_0 = 5.08 \pm 0.27$ MPa for the storage and loss modulus. For the 510 nm thick PB film shown in Fig. 3.5c, the best fit values are

$h = 510 \pm 2$ nm, and $G'_0 = 3.54 \pm 0.07$ MPa and $G''_0 = 4.07 \pm 0.08$ MPa. These film thickness values determined by QCM are in good agreement with the independently measured values by ellipsometry of $h = 244 \pm 3$ nm and $h = 531 \pm 16$ nm. Data were also collected for a thicker PB film of 730 nm thickness where fits of the QCM data for harmonics $n = 1$, 3, and 5 to the continuum physics model gave best fit values of $h = 732 \pm 6$ nm, and $G'_0 = 3.75 \pm 0.12$ MPa and $G''_0 = 4.12 \pm 0.19$ MPa, where again the QCM determined film thickness agreed well with the value independently measured by ellipsometry of $h = 765 \pm 4$ nm. To within experimental error, we do not observe any meaningful thickness dependence to the moduli values measured by QCM within the measured range of 250–730 nm.

Figure 3.6 graphs these best fit values of $G'(n) = G'_0 n^{0.50}$ and $G''(n) = G''_0 n^{0.74}$ for the three PB film thicknesses measured: 250 nm, 510 nm, and 730 nm. The error bars plotted include the fitting error of G'_0 and G''_0 added in quadrature to the uncertainty in G'_0 and G''_0 due to the range in the exponent values $\beta' = 0.50 \pm 0.03$ and $\beta'' = 0.74 \pm 0.01$. To facilitate comparison with the literature rheometry data for PB, the values are graphed as $\log G'(f)$ and $\log G''(f)$ versus the logarithm of the frequency $f = nf_0$. The literature data described above and used to determine the exponents β' and β'' over the QCM frequency range are also plotted for reference.[164,165,167,168] The QCM-determined moduli correspond to room-temperature measurements conducted between a total frequency range of 5 MHz to 65 MHz for three samples of different film thicknesses. The lower-frequency rheometry data was measured over a frequency range of approximately 10^{-3} to 10^{+1} Hz at a range of different temperatures, and then time-temperature shifted to higher frequencies corresponding to a reference temperature of 25 °C. Excellent agreement is obtained between the QCM MHz data and the lower-frequency rheometry data in agreement with time-temperature superposition. Such good agreement between QCM and lower-frequency rheological measurements have also been reported by others.[136,140,169]

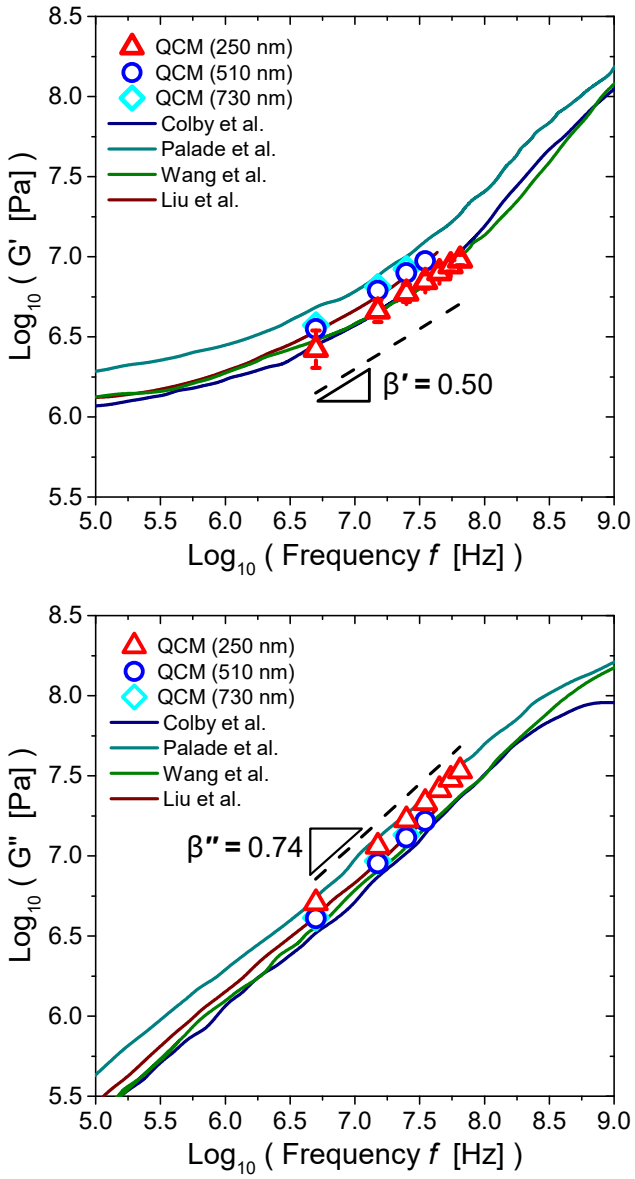

Figure 3.6: Log-log plot of storage $G'(f)$ and loss $G''(f)$ moduli for PB at 25 °C. Open symbols are the QCM data measured for PB (M_w = 375 kg/mol) films with thicknesses of 250 nm (red triangles), 510 nm (blue circles), and 730 nm (cyan diamonds). Curves depict the literature rheometry data time-temperature shifted up to the MHz frequencies of the QCM.[164,165,167,168] The dashed lines show the local slope from 5–45 MHz averaged over all the literature studies giving the exponent values $\beta' = 0.50 \pm 0.03$ and $\beta'' = 0.74 \pm 0.01$.

3.4.4 Continuum physics model applied to rubbery PDMS films

As a second case, we apply our continuum physics model to another rubbery viscoelastic polymer film, polydimethylsiloxane (PDMS), which is also in its glass transition regime at room temperature in the QCM MHz frequency range.[117] The storage and loss moduli are again modeled using eqs. (3.21)-(3.22), treating the frequency dependence of the shear modulus as linear on a log-log scale. For PDMS, we use the popular Sylgard 184 elastomer kit to make cross-linked PDMS samples (9 to 1 base to cross-linker ratio by mass) with a zero frequency elastic modulus $E \approx 1.95 \pm 0.19$ MPa.[45,90]

Again to minimize the number of fit parameters in eqs. (3.21)-(3.22), we use literature data to estimate values for the exponents β' and β'' representing the local slope of $\log(G')$ and $\log(G'')$ versus $\log(f)$ within the QCM frequency range. Unfortunately, even though PDMS is commonly used in various fields such as microfluidics,[170] cell biology,[120,171] soft robotics,[172] and 3D printing,[173] viscoelastic master curves with a wide span of frequencies are scarce. We were able to find DMA data for the same Sylgard 184 PDMS elastomer we use published by Tiwari et al., where they measured the frequency-dependent Young's modulus $E(\omega)$ from -140 °C to 120 °C in 5 °C increments, and then time-temperature shifted the data to create a master curve at a reference temperature of 20 °C.[117] Although this study by Tiwari et al. used slightly different curing conditions and base to cross-linker ratio, our previous literature compilation of Sylgard 184 PDMS Young's modulus values suggests these small differences are not significant, and the Tiwari et al. modulus curve should be a decent representation for our PDMS.[90]

To obtain the storage exponent β' for QCM shear measurements, we converted their Young's modulus $E(\omega)$ data to shear modulus using the simple relation $G'(\omega) = \frac{E(\omega)}{3}$ that assumes Poisson's ratio $\nu = 0.5$. This is a good approximation for rubbery

PDMS ($\nu = 0.495$ for Sylgard 184 PDMS[174]), but will cause some discrepancy at higher frequencies when the material is nearly glassy. The MHz frequency range for our PDMS QCM measurements ($5 - 35$ MHz) falls within the glass transition regime of PDMS at room temperature. The Tiwari et al. data actually have a gap in this regime because of crystallization issues, thus we have interpolated the $G'(\omega)$ data (see Fig. 3.8) using a simple linear interpolation to connect the rubbery and glassy regimes and estimate a reasonable value for the elastic exponent as $\beta' = 0.32 \pm 0.08$. As loss modulus $G''(\omega)$ data are not available, we performed the Kramers-Kronig transformation on the storage modulus data by Tiwari et al.[117] to obtain $\log G''(f)$ as a function of $\log(f)$ data from which to estimate a β'' value. As outlined in Ref. [175], the Kramers-Kronig transformation for polymer master curves from $G'(f)$ to $G''(f)$ is given by

$$G''(f) = \frac{2f}{\pi} \int_0^\infty \frac{G'(u) - G'(f)}{u^2 - f^2} du, \tag{3.23}$$

assuming Boltzmann's superposition principle is valid. Even though the Tiwari et al. data already span 30 decades in frequency, we extended the data to infinity assuming a flat glassy and rubbery plateau to account for the limits of integration. The value of β'' determined by fitting the resulting $\log G''$ as a function of $\log f$ curve in the $5-35$ MHz frequency range used for QCM measurements of PDMS was $\beta'' = 0.2 \pm 0.1$.

We performed QCM measurements on PDMS films with film thicknesses of 450 nm, 550 nm, and 960 nm. Data on thicker films up to 2 μm were also collected, but lacked clear reliable resonance peaks that could be fit. For the PDMS films, resonance traces over the harmonic range from $n = 1$ to $n = 7$ were collected and fit using eq. (3.3) to obtain f_n and Γ_n. Figure 3.7a shows representative resonance traces for a 450 nm thick PDMS film at harmonic numbers $n = 3$, 5, and 7. As expected, we observe that anharmonic side peaks emerge at higher harmonics, which eventually merge with and obscure the main resonance peak. As in the PB case, we have identified resonance traces for PDMS samples where we believe the main resonance peak can still be reli-

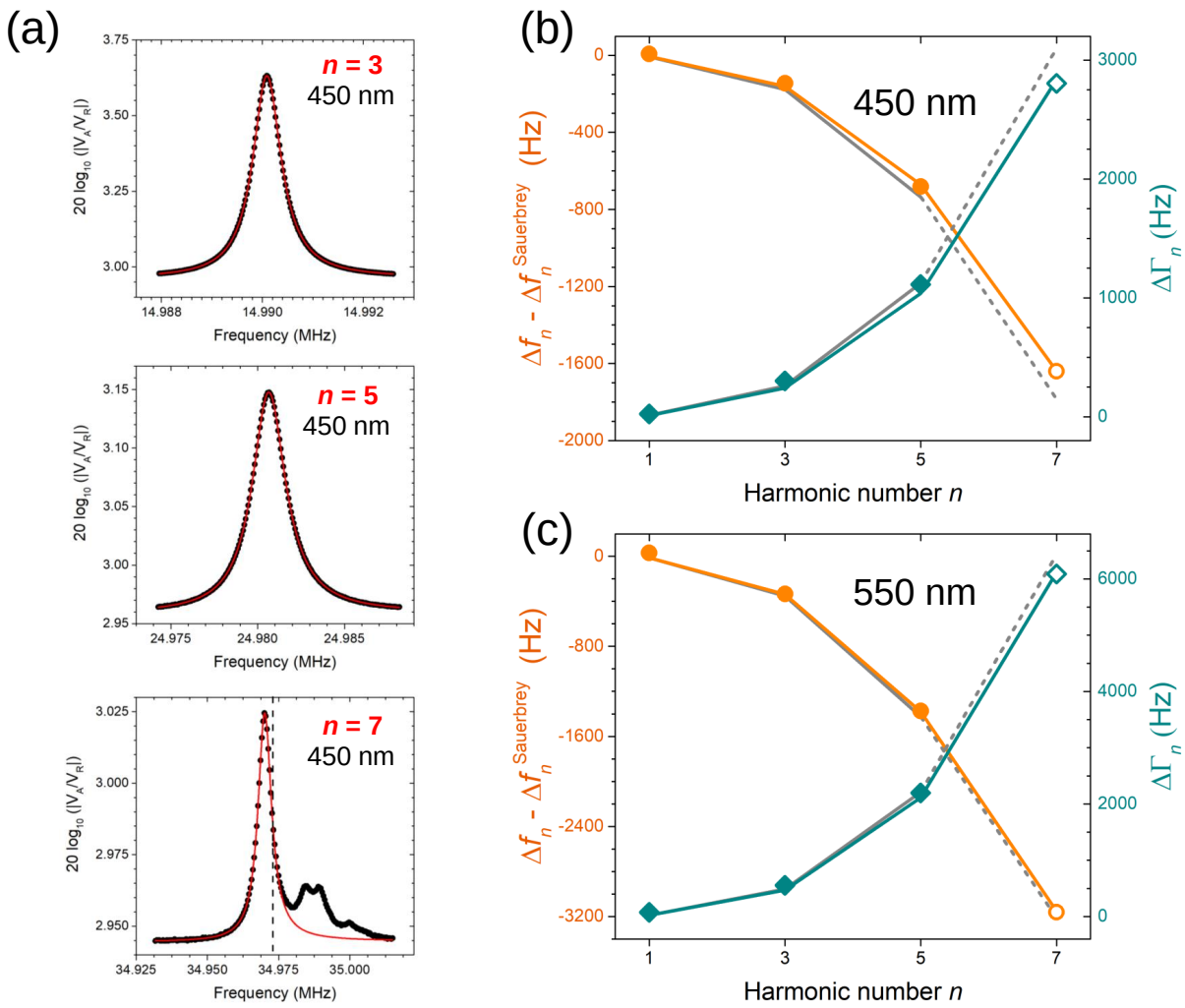

Figure 3.7: (a) QCM resonance traces measured for a 450 nm thick PDMS film at the $n = 3$, 5, and 7 harmonics (symbols), with fits to eq. (3.3) shown as red curves. For the $n = 7$ resonance, data were only fit up to the vertical dashed line. (b) and (c) plot the frequency Δf_n (orange circles, left axis) and dissipation $\Delta\Gamma_n$ (teal diamonds, right axis) shifts for 450 nm and 550 nm thick PDMS films, relative to the expected Sauerbrey mass contribution shift $\Delta f_n^{\text{Sauerbrey}}$. The solid colored curves are a fit to both the solid and open symbols, while the gray solid and dashed curves are a fit to the solid symbols that are then extrapolated to higher harmonics.

ably fit to obtain f_n and Γ_n by limiting the fitting range, like that shown in Fig. 3.7a for $n = 7$. Resonance shifts obtained from such traces have been denoted with open symbols in Fig. 3.7b and 3.7c, where solid symbols indicate resonance traces with no anharmonic side peaks present. Similar to the PB data, fits of our continuum

physics model to the Δf_n and $\Delta\Gamma_n$ resonance shifts using only the data without any anharmonic side peaks (solid symbols) and then extrapolated to higher harmonics, agree well with the open symbols. Thus, we have again chosen to report results that include fits to both the solid and open symbols.

Figures 3.7b and 3.7c graph the frequency and dissipation shifts relative to that of the bare quartz, determined as $\Delta f_n = f_n^{\text{film+QCM}} - f_n^{\text{bare QCM}}$ and $\Delta\Gamma_n = \Gamma_n^{\text{film+QCM}} - \Gamma_n^{\text{bare QCM}}$, for 450 nm and 550 nm thick PDMS films. To emphasize the viscoelastic response of these rubbery films, the measured resonance shifts Δf_n and $\Delta\Gamma_n$ for the PDMS films are again plotted relative to the expected shift from only added mass $\Delta f_n^{\text{Sauerbrey}}$ based on the Sauerbrey equation, eq. (3.1). We fit these data (both solid and open symbols) to our continuum physics model to obtain the storage $G'(n) = G'_0 n^{\beta'}$ and loss $G''(n) = G''_0 n^{\beta''}$ moduli, and film thickness h for the PDMS films. In

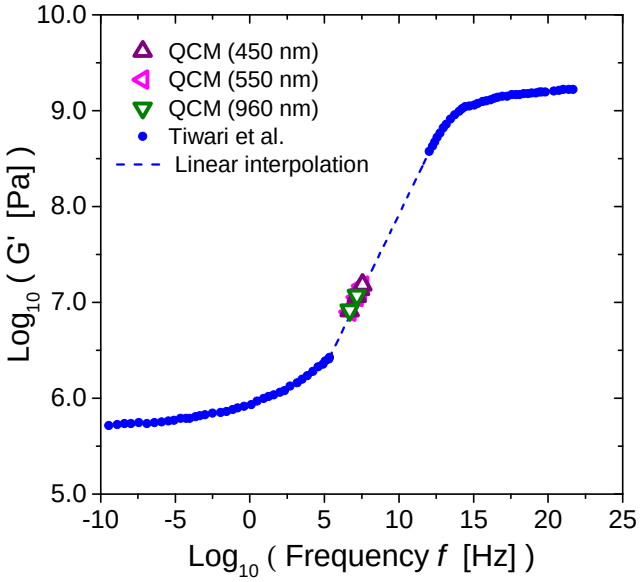

Figure 3.8: Log-log plot of the storage modulus $G'(f)$ for PDMS. Open symbols are the QCM data we measured for Sylgard 184 PDMS films with thicknesses of 450 nm (purple upward-pointing triangles), 550 nm (pink sideward-pointing triangles), and 960 nm (green downward-pointing triangles) in the frequency range of 5 MHz to 35 MHz and at 25 °C. DMA data by Tiwari et al.[117] for Sylgard 184 PDMS, time-temperature shifted to a reference temperature of 20 °C, is also plotted for comparison. The dashed line is a linear interpolation between the rubbery and glassy regimes of the Tiwari et al. data giving a slope of $\beta' = 0.32$.

eqs. (3.21)-(3.22), the exponents were held fixed at $\beta' = 0.32$ and $\beta'' = 0.2$ that we determined from the literature. The density of Sylgard 184 PDMS was taken to be $\rho = 1.1$ g/cm^3.[176] The best fit values from our continuum physics model to all the Δf_n and $\Delta\Gamma_n$ data as a function of harmonic number n are $G_0' = 8.19 \pm 0.81$ MPa, $G_0'' = 12.7 \pm 2.7$ MPa, and $h = 452 \pm 9$ nm for the 450 nm thick PDMS film; $G_0' = 7.99 \pm 0.37$ MPa, $G_0'' = 11.1 \pm 1.7$ MPa, and $h = 548 \pm 12$ nm for the 550 nm thick PDMS film; and $G_0' = 8.29 \pm 0.16$ MPa, $G_0'' = 10.28 \pm 0.89$ MPa, and $h = 960 \pm 10$ nm for the 960 nm thick PDMS film. These film thickness values determined by QCM are in good agreement with the independently measured values by ellipsometry of $h = 468 \pm 3$ nm, $h = 580 \pm 16$ nm, and $h = 972 \pm 4$ nm. As for the PB films, we do not observe any thickness dependence to the moduli values measured by QCM to within experimental error.

In Figure 3.8, we graph the best fit values of the storage modulus for the PDMS films measured by QCM by plotting $G'(n) = G_0' n^{\beta'}$, where the error associated with the fitting and the uncertainty in the exponents β' and β'' are smaller than the symbol size. The DMA data by Tiwari et al.[117] are plotted for comparison. We observe excellent agreement between the storage modulus values measured by QCM for PDMS film thicknesses of 450 nm, 550 nm, and 960 nm in the frequency range of 5 MHz to 35 MHz with the Tiwari et al. DMA data.

3.5 Conclusions

In this study, we have presented a full solution to the shear wave propagation of a MHz QCM acoustic signal through a polymer film subject to the boundary conditions of displacement and stress continuity at the interfaces, retaining the physical intuition of the continuum physics of wave propagation. By leveraging modern computational techniques, we are able to solve the resulting set of three coupled equations without

any approximations. Viscoelastic QCM measurements were performed on rubbery polymer films of PB and PDMS near their glass transition regimes, as well as control measurements on glassy PS films. The measured frequency Δf_n and dissipation $\Delta\Gamma_n$ shifts over an extended range of harmonic numbers n were numerically fit to determine the storage $G'(f_n)$ and loss $G''(f_n)$ moduli of the polymer, as well as the film thickness h, from the QCM data. These film thickness values determined from the QCM measurements were found to agree well with values determined by ellipsometry. The frequency dependence of the modulus was treated as linear on a log-log scale over the frequency range of the QCM (5–65 MHz corresponding to n = 1–13) as $\log_{10} G' = \beta' \log_{10} n + \log_{10} G'_0$ and $\log_{10} G'' = \beta'' \log_{10} n + \log_{10} G''_0$. To minimize the number of fitting parameters, the β' and β'' values representing the local slope of the log modulus vs. log frequency data over the QCM frequency range were determined from literature data. The measured storage $G'(f_n)$ and loss $G''(f_n)$ moduli from QCM in the MHz frequency regime for polymer films ranging in thickness from 250 nm to 1.4 μm agreed well with literature rheometry data taken on bulk samples over a frequency range of 10^{-3} to 10^{+1} Hz that were time-temperature shifted to higher frequencies. Thus, QCM MHz-frequency viscoelasticity measurements can be used to verify the validity of time-temperature superposition,[128,140] which has been reported to break down at time scales corresponding to MHz frequencies for some polymers.[177]

Taking advantage of the fact that we are numerically solving the resonance frequency Δf_n and dissipation $\Delta\Gamma_n$ shifts exactly, we examine the reliability of data collected at higher harmonics near film resonance. Higher harmonics that approach film resonance are typically avoided because of the belief that the presence of anharmonic side bands make the data unreliable. We test this by comparing the measured Δf_n and $\Delta\Gamma_n$ values at higher harmonics with the expected values based on an extrapolation of the continuum physics model from the data collected at lower harmonics. For QCM resonance traces where we believe the resonance peak can be adequately

fit, we find that the measured Δf_n and $\Delta\Gamma_n$ data agree well with the model, even if anharmonic side bands are adjacent to the resonance peak.

3.6 Appendix

Experimental Setup

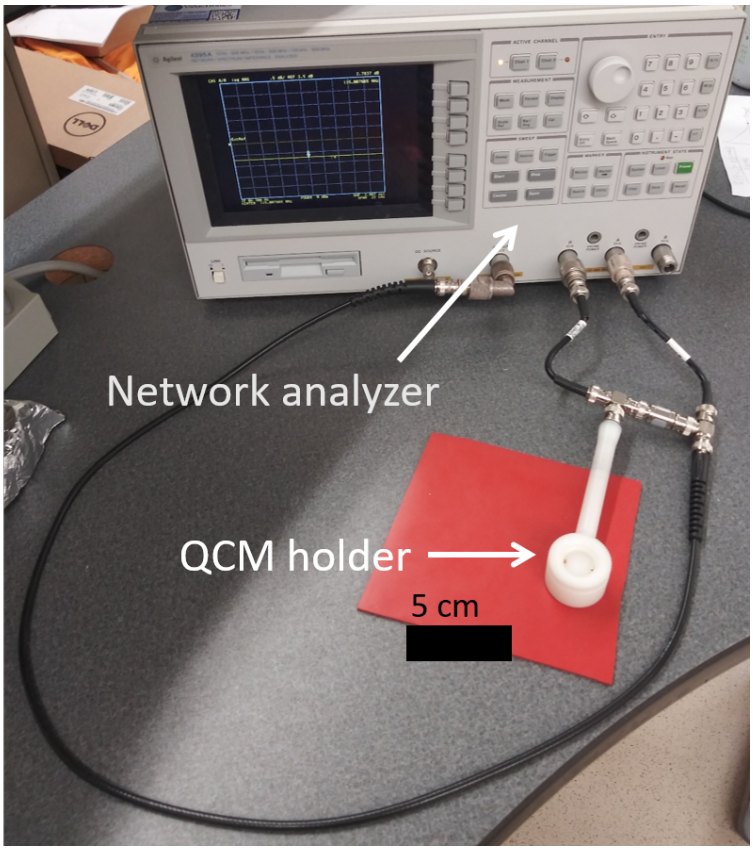

Figure 3.9: Photograph of the experimental setup of the QCM sensor connected to the network analyzer.

Polystyrene Data Tables and Resonance Traces

1.37 μm thick polystyrene film:

Harmonic n	Δf_n (Hz)	$\Delta\Gamma_n$ (Hz)	
1	-8214.7	0.2	$f_0 = 5.010151$ MHz
3	-24530.6	0.9	$G_0' = 1.53 \pm 0.10$ GPa*
5	-41066.0	2.9	$h = 1.37 \pm 0.01$ μm*
7	-57994.5	8.8	*Values determined from fitting n = 1-19
9	-75484.9	18.6	
11	-93784.1	37.6	$h = 1.33 \pm 0.10$ μm by ellipsometry
13	-113090.1	55.0	
15	-133941.2	105.2	
17	-156168.2	181.9	
19	-181714.2	274.9	
21	-210668.8	474.7	

1.26 μm thick polystyrene film:

Harmonic n	Δf_n (Hz)	$\Delta\Gamma_n$ (Hz)	
1	-7510.1	3.7	$f_0 = 5.008344$ MHz
3	-22572.8	0.3	$G_0' = 1.83 \pm 0.07$ GPa*
5	-37781.1	-3.0	$h = 1.265 \pm 0.004$ μm*
7	-53253.3	-2.6	*Values determined from fitting n = 1-19
9	-69055.5	24.2	
11	-85379.9	17.8	$h = 1.33 \pm 0.10$ μm by ellipsometry
13	-102358.4	41.9	
15	-120189.8	61.0	
17	-139079.8	102.3	
19	-159436.0	181.0	
21	-181573.9	295.7	

The best fit parameters presented in the polystyrene data tables are fitting only the frequency shift data Δf_n for the shear modulus G_0', assuming a frequency independent modulus (exponent $\beta' = 0$), as described in the main text. The assumption of a frequency independent modulus can be justified by fitting the frequency Δf_n and dissipation $\Delta\Gamma_n$ shift data to a complex modulus of the form $\widetilde{G} = |\widetilde{G}|\, e^{i\phi}$. When this is done, the phase angle $\phi = \arctan\left(\frac{G''}{G'}\right)$ is found to be very small, $\phi = 0.0079$ radians $= 0.45$ degrees, or equivalent to an exponent $\beta' = 0.005$. See Refs.[128,136] in the main text by the Shull group for a more detailed description of the phase angle ϕ.

Figure 3.10 (a) shows resonances traces for the 1.37 μm thick polystyrene (PS) film for harmonic numbers $n = 3$, 15, and 19. Figure 3.10 (b)-(c) graph the experimental frequency Δf_n and dissipation $\Delta\Gamma_n$ shifts for the 1.37 μm thick and 1.26 μm thick PS samples. The frequency shifts Δf_n are referenced to the expected frequency shifts $\Delta f_n^{\text{Sauerbrey}}$ from purely mass loading given by the Sauerbrey equation to focus on the viscoelastic response of the film. The curves show the fits of the continuum physics model to these data fitting both Δf_n and $\Delta\Gamma_n$ to a complex modulus of the form $\widetilde{G} = G' + iG''$ with no frequency dependence, and the film thickness h. Best-fit values for the 1.37 μm film are $h = 1.37 \pm 0.01$ μm, $G' = 1.53 \pm 0.12$ GPa, and $G'' = 12.0 \pm 40.4$ MPa, and best-fit values for the 1.26 μm film are $h = 1.265 \pm 0.005$ μm, $G' = 1.83 \pm 0.08$ GPa, and $G'' = 15.5 \pm 28.8$ MPa. These values of G' and h are in good agreement with those found in the main text when fitting only the frequency shift data Δf_n with fitting parameters of G' and h. The values of G'' are consistent with those determined from $G'' = G' \tan(\phi)$ when fitting the complex modulus as $\widetilde{G} = |\widetilde{G}|\, e^{i\phi}$. We note that the loss modulus values G'' have a very large error for both PS samples, which is likely due to the PS samples having a very low phase angle ϕ, leading to very small dissipation shifts $\Delta\Gamma_n$ for PS that are an order of magnitude smaller than those observed for rubbery PB and PDMS films. As such, we have chosen to only fit the storage modulus G' and film thickness h for PS in the main text.

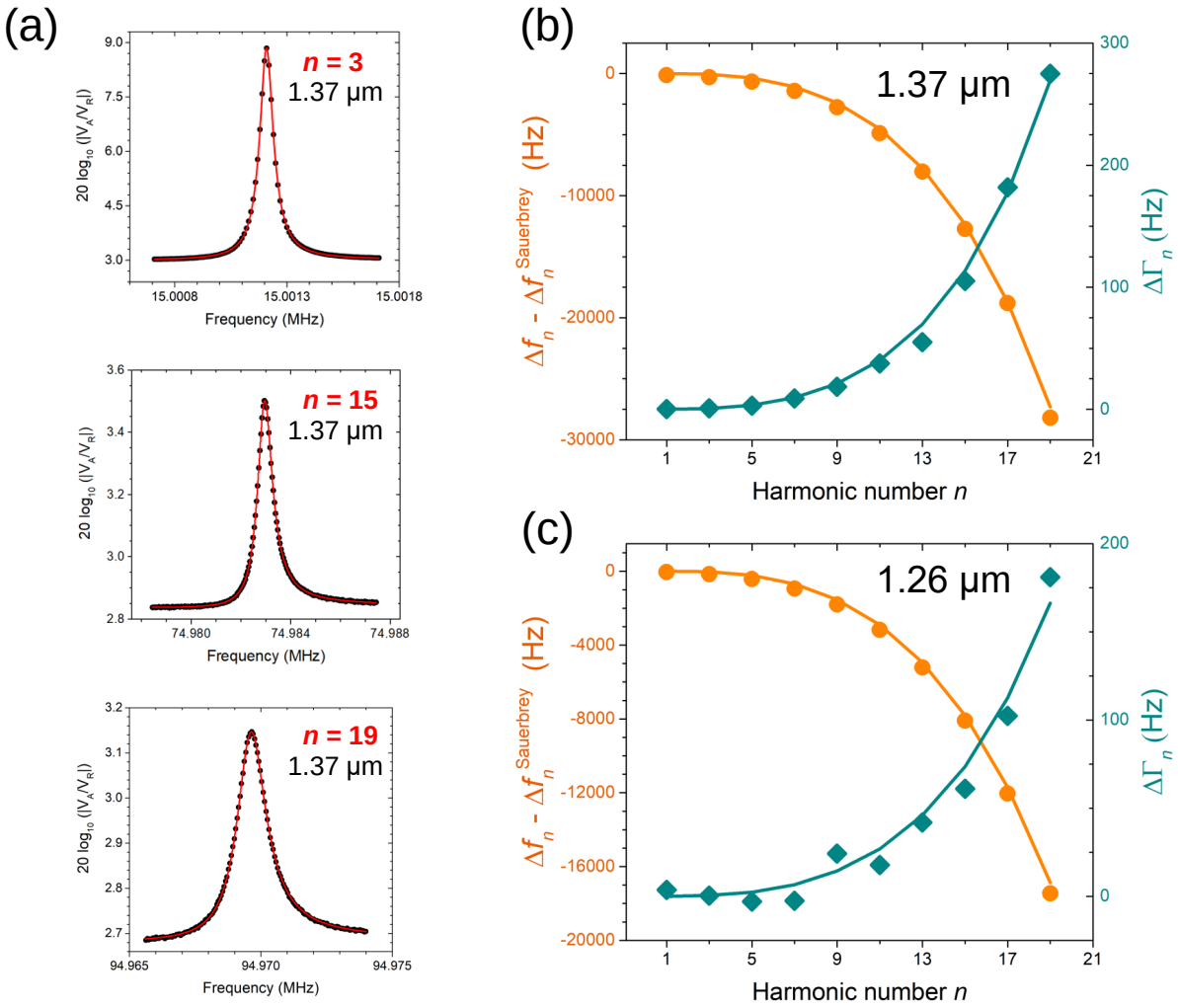

Figure 3.10: (a) Resonance traces at the $n = 3$, 15, and 19 harmonics for the 1.37 μm thick PS film. Black symbols are the data collected with the network analyzer and the red curves are fits using eq. (3.3). Resonance frequency shifts Δf_n (orange circles, left axis) and dissipation shifts $\Delta\Gamma_n$ (teal diamonds, right axis) for the 1.37 μm (b) and 1.26 μm (c) thick PS films. Symbols correspond to the experimental data, while the curves are fits of the continuum physics model to these data. The frequency shift Δf_n data are referenced to that expected from the Sauerbrey equation $\Delta f_n^{\text{Sauerbrey}}$.

Data Tables for Polybutadiene

250 nm thick polybutadiene film:

Harmonic n	Δf_n (Hz)	$\Delta\Gamma_n$ (Hz)	
1	-1259.5	1.9	$f_0 = 5.008271$ MHz
3	-3789.5	42.4	$G_0' = 2.64 \pm 0.66$ MPa
5	-6332.5	147.0	$G_0'' = 5.08 \pm 0.27$ MPa
7	-8885.4	326.5	$h = 246 \pm 1$ nm
9	-11457.3	589.9	
11	-14017.5	951.1	$h = 244 \pm 3$ nm by ellipsometry
13	-16573.9	1427.6	

510 nm thick polybutadiene film:

Harmonic n	Δf_n (Hz)	$\Delta\Gamma_n$ (Hz)	
1	-2632.4	25.4	$f_0 = 5.009164$ MHz
3	-8059.7	437.6	$G_0' = 3.54 \pm 0.07$ MPa
5	-13674.4	1574.2	$G_0'' = 4.07 \pm 0.08$ MPa
7	-19250.0	3691.1	$h = 510 \pm 2$ nm
			$h = 531 \pm 16$ nm by ellipsometry

730 nm thick polybutadiene film:

Harmonic n	Δf_n (Hz)	$\Delta\Gamma_n$ (Hz)	
1	-3832.6	78.5	$f_0 = 5.009164$ MHz
3	-11883.3	1364.3	$G_0' = 3.75 \pm 0.12$ MPa
5	-20035.9	5077.2	$G_0'' = 4.12 \pm 0.19$ MPa
			$h = 732 \pm 6$ nm
			$h = 765 \pm 4$ nm by ellipsometry

Data Tables for PDMS

450 nm thick PDMS film:

Harmonic n	Δf_n (Hz)	$\Delta\Gamma_n$ (Hz)	
1	-2815.1	25.4	$f_0 = 5.000419$ MHz
3	-8614.1	437.6	$G_0' = 8.19 \pm 0.81$ MPa
5	-14796.0	1574.2	$G_0'' = 12.7 \pm 2.7$ MPa
7	-21401.4	3691.1	$h = 452 \pm 9$ nm
			$h = 468 \pm 3$ nm by ellipsometry

550 nm thick PDMS film:

Harmonic n	Δf_n (Hz)	$\Delta\Gamma_n$ (Hz)	
1	-3396.5	74.8	$f_0 = 5.000158$ MHz
3	-10616.7	555.2	$G_0' = 7.99 \pm 0.37$ MPa
5	-18510.3	2195.2	$G_0'' = 11.1 \pm 1.7$ MPa
7	-27152.5	6089.5	$h = 548 \pm 12$ nm
			$h = 580 \pm 16$ nm by ellipsometry

960 nm thick PDMS film:

Harmonic n	Δf_n (Hz)	$\Delta\Gamma_n$ (Hz)	
1	-6102.0	151.0	$f_0 = 5.000158$ MHz
3	-19942.0	3003.9	$G_0' = 8.29 \pm 0.16$ MPa
			$G_0'' = 10.28 \pm 0.89$ MPa
			$h = 960 \pm 10$ nm
			$h = 972 \pm 4$ nm by ellipsometry

Chapter 4

Annealing Matters: Modulus Profile Developed on Annealing a Dissimilar Polymer-Polymer Interface Measured by QCM

4.1 Synopsis

Recent work by our group has demonstrated that small changes in the composition profile between dissimilar polymer domains associated with annealing can strongly alter the dynamical coupling across these domains.[70,90] In contrast, other studies have reported that polymer-liquid interfaces behave similar to the interface between a polymer and a hard substrate.[85,86] Collecting these ideas, we hypothesize that the mechanism underlying strong dynamic coupling across dissimilar polymer-polymer interfaces may be related to impedance matching, where similar moduli and densities,

and larger interfacial widths translate to more transmission of vibrational (phonon) modes or acoustic waves through the interface. We show using a quartz crystal microbalance (QCM) that MHz-frequency shear waves are transmitted differently through a polystyrene (PS) / polybutadiene (PB) interface depending on whether the interface has been minimally annealed or annealed to equilibrium. Using a continuum physics layer model we show that the data are inconsistent with the notion of only the compositional interfacial width increasing, and that there is instead a longer-ranged altered viscoelastic profile of width $W_G \approx 150$ nm that is produced during the interface annealing.

4.2 Introduction

In polymer blends, smaller domain sizes can lead to better performance, with properties of the interfaces often being responsible for various material property changes.[178] Early attempts to simplify the physics by using a simplified geometry studied the polymer/air interface by measuring the glass transition temperature T_g of polymer thin films either exposed to air on both sides ("free standing"),[57,179,180] or placed on a substrate ("supported films").[9,10,12,15] While being a simple geometry, the polymer/air interface has been studied extensively and has unearthed a plethora of polymer physics. The consensus among experiment, theory, and simulations is that a reduction in the number of nearest neighbors near the free surface enhances the local mobility of the polymer.[9,10,15] The effect of this increased mobility has been modeled in terms of a decrease in the energy barrier height to rearrangements, a change in free volume, or as a percolating front of increased mobility.[17] An attractive interaction with a substrate, by contrast, hinders the local mobility of the polymer. Measurements of the bulk T_g of a polymer on a substrate, then, include averages over the gradients in the local mobility near the free surface and substrate.[17,110]

The interface between two dissimilar polymers has been less studied than the freestanding or the supported film cases, partly due to the greater difficulty in experimentally measuring and theoretically treating the polymer-polymer interface vs. the polymer-air interface, and partly due to the polymer-air interface still continuing to provide more open questions. Computational modeling of polymer-polymer interfaces are typically restricted to making assumptions of a much shorter composition profile than experimental systems that have compositional interfacial widths w_I typically between $1 - 10$ nm. Theoretically, the presence of a polymer-air interface presents a simple stress-free boundary condition at the free surface, while polymer-polymer interfaces introduce a more complicated boundary condition.[17]

In 2015, Baglay and Roth experimentally measured the local $T_g(z)$ near a glassy-rubbery PS/PnBMA interface using a localized fluorescence probe method.[69] They found a broad spatial range of perturbations to local $T_g(z)$ spanning distances over a total of 350-400 nm. This profile was fit with a hyperbolic tangent function of the form $\phi(z) = \frac{1}{2}\left[1 + \tanh\left(\frac{2z}{W_{T_g}}\right)\right]$, providing a $T_g(z)$ interfacial width $W_{T_g} = 231 \pm 5$ nm. Similar results of large ranges of local $T_g(z)$ perturbation were found in a subsequent study[70] that measured the local $T_g(z)$ using a similar method in PS next to other polymers with both higher and lower bulk T_gs than PS. These and other local $T_g(z)$ studies[72,73,90,109] identified three key components making up the changes in the magnitude and spatial extent in shifts from bulk T_g in glassy PS near rubbery polymer domains. First, the interface must be sufficiently annealed. Without fully annealing the interface, the $T_g(z)$ profile is truncated considerably.[70,90] Second, the local $T_g(z)$ profile in PS is strongly influenced by the rubbery modulus of the neighboring rubbery domain,[90] as discussed in Chapter 2. Third, a more narrow composition profile reduces the length scales of $T_g(z)$ perturbation,[90] as discussed in Chapter 2. It therefore appears that the key control parameters determining the increase in $T_g(z)$ profile width W_{T_g} on annealing are the compositional interfacial width w_I and the

relative moduli of the polymer domains. Gathering these factors, we suggested in Ref. [90] that something akin to acoustic impedance matching may be the underlying mechanism controlling perturbations to local $T_g(z)$. In acoustic impedance matching, a mismatch in the modulus or density between layers causes increased reflections of acoustic waves at the interface. A gradual change in the density or shear modulus produces increased transmission across the interface as well, so that a larger interfacial width in composition w_I or modulus W_G leads to increased transmission of acoustic waves.

This concept of impedance matching between high and low moduli polymeric materials determining perturbations to T_g finds additional support in dewetting measurements of the film-averaged $T_g(h)$ of PS floating on liquid glycerol and an ionic liquid.[85,86] These measurements found that the $T_g(h)$ of PS floating on a liquid followed a similar behavior as the $T_g(h)$ for PS on silicon rigid substrates. These results illustrate that it is not only the absolute moduli of the materials that affect the $T_g(h)$, since the modulus of glycerol is effectively zero while the modulus of silicon is $O(10^9)$ Pa. Instead, these results may be understood as caused by the small compositional interfacial width of the PS/liquid (~ 0.5 nm) leading to no coupling of T_g dynamics across the PS/liquid or PS/solid interface.

Collectively, these studies provide a basis for the view that glassy-rubbery polymer interfaces are not only altering the local mobility of the polymers, but are also altering the boundary conditions and transmission of density waves traveling through the system. With this mechanism in mind, here we measure the effect of interface formation through annealing on the shear wave propagation in a polymer bilayer of PS and PB using a QCM. Using a continuum physics layer model extended from that developed in Chapter 3, we relate the QCM measurements to a long ranged perturbation of the modulus near the PB/PS interface. The length scales of this modulus interface are much larger than the compositional interfacial width w_I, and

are instead comparable to the $T_g(z)$ interfacial width W_{T_g}. This result of comparable length scales between the modulus and local $T_g(z)$ profiles provides strong evidence that a long-ranged modulus gradient may be responsible for the long-ranged local $T_g(z)$ perturbations observed in Refs. [69, 70, 73, 90].

4.3 Experimental Methods

Polystyrene (PS) (M_w = 1920 kg/mol, M_w/M_n = 1.26) was purchased from Pressure Chemical and used as received. Polybutadiene (PB) (M_w = 375 kg/mol, M_w/M_n = 2.4; 36% cis 1,4; 55% trans 1,4; 9% vinyl 1,2, as specified by the supplier) from Scientific Polymer Products was purchased and washed three times by dissolving in tetrahydrofuran (THF) and precipitating in chilled methanol.[73] The PS layer was spin-coated directly from a toluene solution onto the QCM sensor, as well as silicon pieces for film thickness determination by ellipsometry. The PS on the QCM was annealed under vacuum for a minimum of 14 h after spin-coating at a temperature of 120 °C to remove residual solvent and release stresses developed during spin-coating. QCM measurements were then collected on this PS film to determine the film thickness. The PB layer was spin-coated from a toluene solution onto freshly-cleaved mica, then immediately floated onto room temperature deionized water and captured from below with the annealed PS layer atop the QCM. The PB/PS bilayer was then placed in a 25 °C vacuum oven for a minimum of 14 h to relax the PB film and remove any air gaps between the PB and PS layers. QCM measurements were then collected after annealing the bilayer in a vacuum oven for different annealing times at 120 °C.

4.4 Results and Discussion

Previous measurements of the local $T_g(z)$ of PS in PSF/PS[69] and PS/PDMS[90] systems have shown the necessity of sufficient annealing to promote coupling of $T_g(z)$

dynamics across the immiscible polymer-polymer interface. The extent to which a similar effect of annealing on promoting increased mechanical coupling in the form of a long ranged gradient in viscoelasticity is the subject of this chapter, with the aim to connect the length scales of the $T_g(z)$ profile with those of a shear modulus $G(z)$ profile near the interface. This connection between length scales would provide additional evidence that local $T_g(z)$ perturbations are caused by acoustic density wave transmission through the interface, which are modulated by the mismatch in impedances (moduli) of the layers and the width of both the composition profile and the modulus profile.

Figure 4.1 (A) depicts a schematic of the local $T_g(z)$ profile across the PB/PS bilayer system based on the measurements by Kasavan et al.[73] A composition profile drawn not to scale is shown as the sharp grey dashed curve, which should have an interfacial width estimated from the value[60] of χ at 120 °C of $w_I \approx 5$ nm, using the relation $w_I = \frac{2b}{\sqrt{6\chi}}$, where b is the statistical segment length. While only the local $T_g(z)$ on the PS side of the PS/PB system was measured in Ref. [73], there was a strong similarity in the length scales of $T_g(z)$ perturbation in PS between the PS/PB and PS/PnBMA systems, where a full profile is available for PS/PnBMA.[69] In fact, the length scale of $T_g(z)$ perturbation was measured in various PS/polymer systems and was found to depend primarily on whether the PS was adjacent to a lower bulk T_g polymer ("soft confinement," with $T_g(z)$ profile length scales of $z \approx 225 - 250$ nm) or whether the PS was adjacent to a higher bulk T_g polymer ("hard confinement," with $T_g(z)$ profile length scales of $z \approx 100 - 125$ nm). We can therefore estimate that the difference between the $T_g(z)$ profiles of the PS/PB and PS/PnBMA systems will be primarily that the overall magnitude of the $T_g(z)$ profile in PS/PB will be larger than for PS/PnBMA, since the $T_g(z)$ needs to transition from the lower bulk T_g polymer PB ($T_g^{\text{bulk}} = -96$ °C) instead of PnBMA ($T_g^{\text{bulk}} = 21$ °C). Figure 4.1 (B) highlights the question that we seek to address of whether there is also a long length

scale in a modulus profile W_G that develops on annealing, which may relate to the length scale of the $T_g(z)$ profile. Figure 4.1 (C) shows the polymer bilayer of PB and PS used in this study. The left bilayer corresponds to a minimally annealed bilayer, for which we expect a sharp profile in modulus due to insufficient acoustic coupling across the layers and a small w_I. The right bilayer shows the broader modulus profile expected to develop with annealing at 120 °C, which likely relates to the previously measured buildup of the $T_g(z)$ profile.[70,73,90]

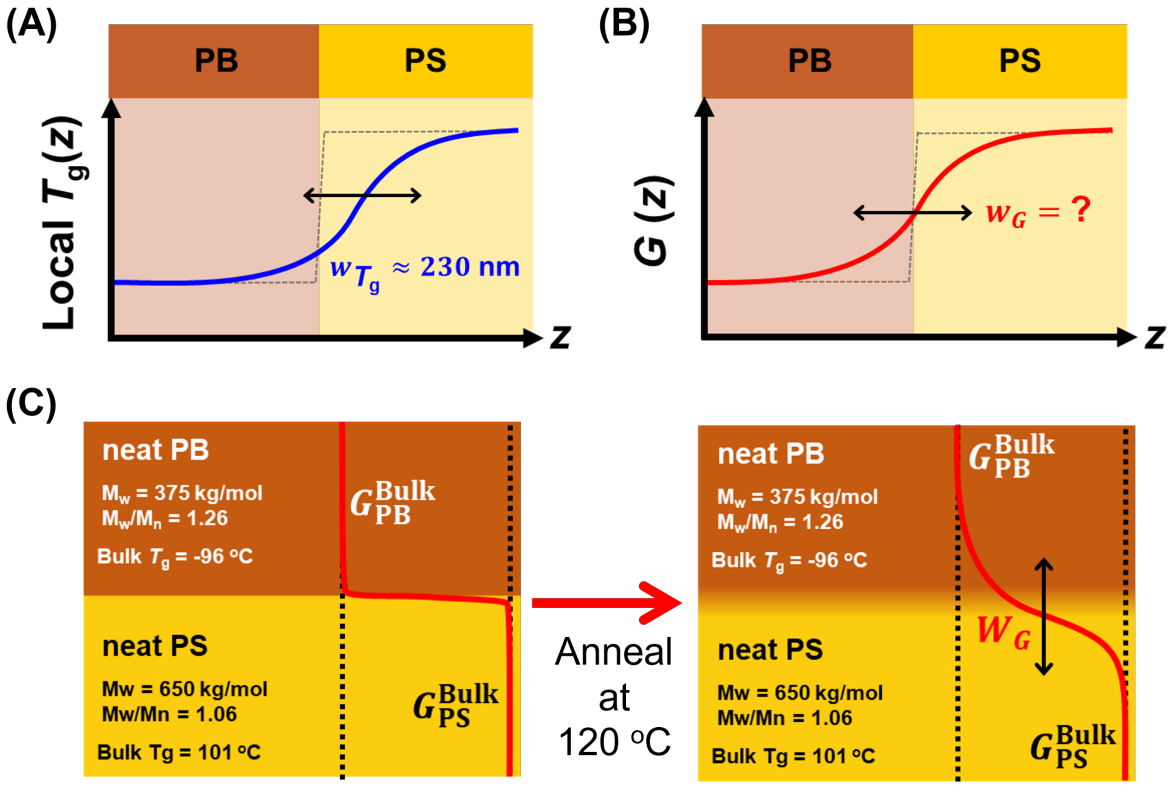

Figure 4.1: (A) Expected local $T_g(z)$ profile based on local fluorescence probe measurements on PS/PB and PS/PnBMA systems.[69,70,73] The blue $T_g(z)$ profile is much broader than the composition profile shown in grey, with a $T_g(z)$ interfacial width $W_{T_g} \approx 230$ nm.[69,70,73] The $T_g(z)$ profile is also shifted to the glassy PS side. (B) A gradient in the local shear modulus profile $G(z)$ may be responsible for causing the $T_g(z)$ profile, and this work will aim to measure the width of this gradient W_G. (C) Polymer bilayer of PB and PS used in this study. With minimal annealing, we expect a sharp profile in modulus due to insufficient coupling across the layers, and upon annealing we expect a buildup of the modulus profile, related to the building up of the $T_g(z)$ profile.[70]

Measurements of the moduli and thicknesses of the PB/PS bilayers were performed using a QCM. QCM measurements were conducted at room temperature (25 °C) using AT-cut quartz sensors from Stanford Research systems, with a fundamental frequency f_0 of 5 MHz. Resonance peaks were collected using an Agilent 4395a vector network analyzer at 0 dBm, corresponding to a source power of 1 mW.[181] We used an analytical fitting function to fit the resonance peaks to obtain the resonance frequency f_n and dissipation Γ_n at the fundamental frequency $n = 1$ of the quartz oscillation and at higher odd harmonics n, as discussed in Chapter 3. The bare quartz resonance frequency and dissipation at each harmonic number were subtracted from the loaded quartz values to obtain $\Delta f_n = f_n^{\text{film+QCM}} - f_n^{\text{bare QCM}}$ and $\Delta\Gamma_n = \Gamma_n^{\text{film+QCM}} - \Gamma_n^{\text{bare QCM}}$. The frequency and dissipation shifts can be collected to form a complex frequency shift $\Delta\tilde{f}_n = \Delta f_n + i\Delta\Gamma_n$, where i is the imaginary unit.

At low harmonic numbers n and for thin, sufficiently rigid layers deposited on the QCM, the QCM is primarily sensitive to the thickness of the layers, for a given density. At sufficiently large n and for thicker or lower modulus films, film resonance occurs, which results in unreliable measurements.[89] Therefore, the thickness of layers deposited on the QCM must be chosen such that the frequency shifts fall within a window between the end of the Sauerbrey regime and before film resonance.[139] For our measurements, we aimed to achieve film thicknesses of PS in the range $1.0 - 1.3$ μm, and film thicknesses of PB in the range $250 - 450$ nm. For these bilayer samples, we expect resonance peaks for lower harmonics to be relatively unperturbed, because lower harmonics are more sensitive to added mass, and the mass should not be varying significantly with annealing. Resonance peaks at higher harmonics, however, are more sensitive to the viscoelastic properties of the sample, and should therefore be altered if there is a change in viscoelastic properties with annealing.

Figure 4.2 shows the $n = 1$ and $n = 7$ resonance peaks for a PB/PS bilayer sample prior to and after annealing at 120 °C for 100 min. The thicknesses of the PB and PS

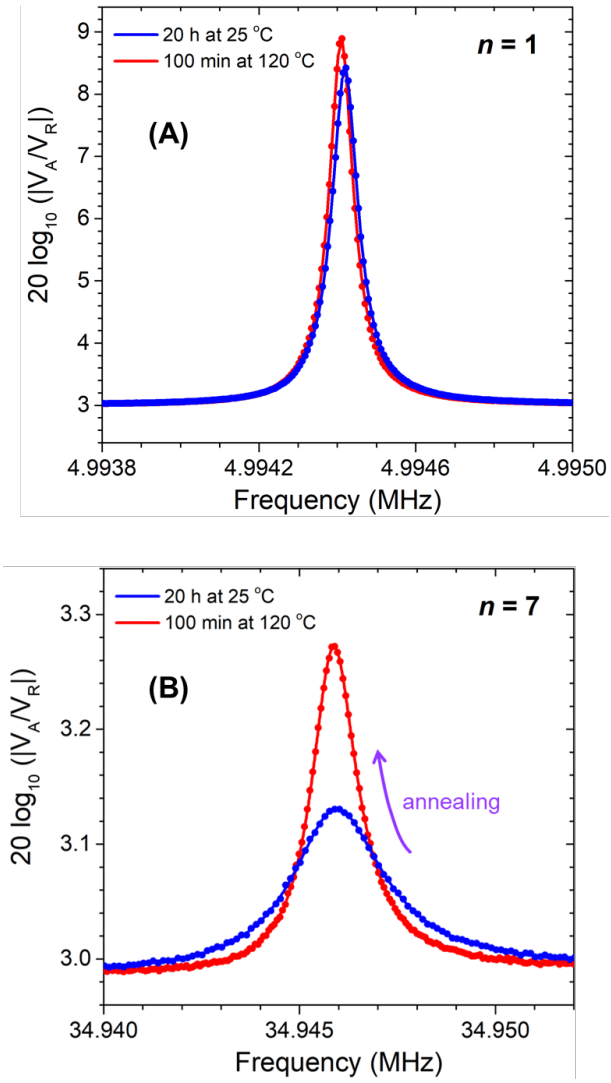

Figure 4.2: Resonance frequency traces of a PB/PS bilayer collected with QCM after minimal annealing at 25 °C for 20 h (A) and after annealing at 120 °C for 100 min (B). The $n = 1$ (5 MHz) resonance displays only a small shift on annealing because the QCM is more sensitive to the film's mass at this frequency, while the $n = 7$ (35 MHz) resonance demonstrates a strong decrease in dissipation Γ_7 (becomes more narrow) with annealing at 120 °C.

layers determined by ellipsometry were 306 ± 2 nm and 1170 ± 70 nm, respectively. The $n = 1$ peak is primarily sensitive to added mass, while the $n = 7$ peak, which was the highest harmonic collected for the sample, is the most sensitive to changes in the viscoelastic properties of the film. The resonance frequency f_1 and dissipation Γ_1 for the fit to the $n = 1$ harmonic were, for the minimally annealed sample held

at only 25 °C for 20 h, $f_1 = 4.99442$ MHz $\pm$ 0.06 Hz and $\Gamma_1 = (26.65 \pm 0.06)$ Hz. After annealing the sample at 120 °C for 100 min, these values shifted slightly to $f_1 = 4.99441$ MHz $\pm$ 0.06 Hz and $\Gamma_1 = (29.82 \pm 0.06)$ Hz. The absence of a large shift in the resonance frequency and dissipation at $n = 1$ on annealing at 120 °C is not surprising, since annealing should not be changing the mass or film thickness appreciably. The sample composition itself should only be varying in the sense of producing an interface with equilibrium interfacial width $w_I \approx 5$ nm. In contrast, the resonance peak at the $n = 7$ harmonic, where the QCM is most sensitive to the viscoelastic properties of the sample, shows a pronounced evolution to a more sharply peaked (smaller dissipation) curve on annealing, related to greater mechanical coupling across the layers and greater shear wave transmission. Specifically, the resonance frequency f_7 and dissipation Γ_7 for the fit to the $n = 7$ harmonic were, for the minimally annealed sample held at only 25 °C for 20 h, $f_7 = 34.94588$ MHz $\pm$ 6 Hz and $\Gamma_7 = (1155 \pm 5)$ Hz. After annealing the sample at 120 °C for 100 min, the resonance frequency changed slightly to $f_7 = 34.94585$ MHz $\pm$ 2 Hz, while the dissipation of the $n = 7$ harmonic decreased by 40% to $\Gamma_7 = (692 \pm 2)$ Hz. This observation is consistent with an increased transmission of the acoustic shear waves across the interface with annealing.

Figure 4.3 shows the dissipation shift as a function of annealing time t_a at 120 °C for the highest harmonic measured of $n = 7$, $\Delta\Gamma_7(t_a)$, for a PB/PS bilayer and additional control measurements of a PS/PS bilayer and a single layer PB film. The $t_a = 0$ min data correspond to the minimally annealed case of 25 °C for 20 h. The dissipation shift decreases monotonically for the PB/PS bilayer for all annealing times with a trend that is especially pronounced for annealing times ≤ 100 min. Control measurements on a PS/PS bilayer display an initial small $\Delta\Gamma_7$ decrease related to the PS/PS layers intermixing, followed by a plateau in $\Delta\Gamma_7$ with annealing time at 120 °C. Control measurements on a single layer PB film show a plateau in $\Delta\Gamma_7$ up to

approximately $t_a = 100$ min, then a pronounced decrease of at least $\approx 30\%$ at times $t_a > 100$ min. This decrease in $\Delta\Gamma_7$ for the single layer PB film is likely linked to chemical degradation, resulting in an altered viscoelasticity of the layer. As a very low molecular weight polymer, PB routinely comes with a small molecule additive that stabilizes the polymer against degredation. However, our previous study[73] found that this additive can act as a plasticizer, which is why we washed the PB to remove the additive. At 120 °C, PB is more than 200 °C above its bulk T_g, thus over an extended period of time at such an elevated temperature it can easily degrade. Since the decrease in dissipation shift of the PB/PS bilayer at very long annealing times at 120 °C may be influenced by chemical degradation of PB, we limited the maximum annealing time to $t_a = 100$ min, corresponding to the maximum annealing time of the PB/PS bilayer. We chose this time because $\Delta\Gamma_7$ at $t_a = 100$ min is less than a 10% percent change from the minimally annealed $\Delta\Gamma_7$ for PB single layer films, and because for the PB/PS bilayer, the trend in $\Delta\Gamma_7$ is similar up to and including $t_a = 100$ min, while the trend then continues with a lower slope at times $t_a > 100$ min.

4.4.1 Continuum Physics Model

The continuum physics layer model that will be used here to fit the Δf_n and $\Delta\Gamma_n$ experimental data is an extension from that developed in Chapter 3. The essential ingredients are that the QCM and layers atop the QCM are treated as continuum layers described by a complex, frequency-dependent shear modulus $\widetilde{G}(f) = G'(f) + iG''(f)$, density ρ, and film thickness h. The density is held constant at a value determined from the literature. The QCM produces a shear wave that obeys continuity of stress and displacement across the layers, and zero stress boundary conditions at the free surfaces. These continuity equations are numerically solved for the frequency and dissipation shifts Δf_n and $\Delta\Gamma_n$ at each harmonic n.

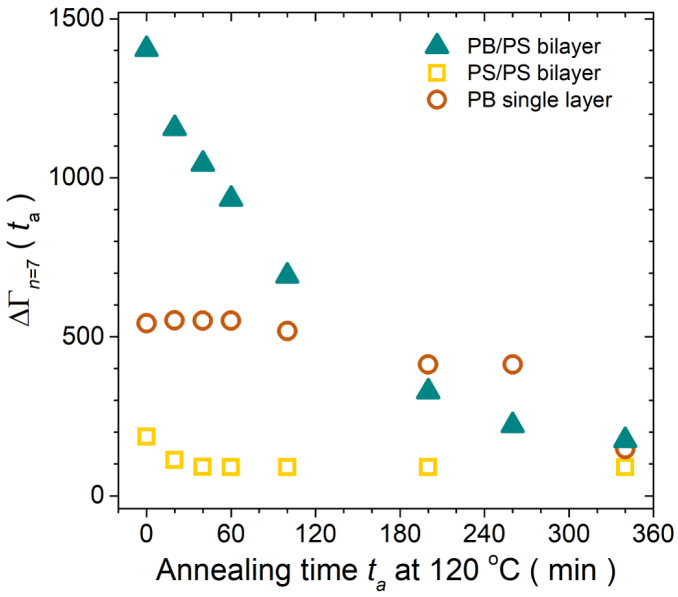

Figure 4.3: Dissipation shift as a function of cumulative annealing time t_a at 120 °C for the $n = 7$ harmonic $\Delta\Gamma_7(t_a)$ for a PB/PS bilayer and control measurements of a PS/PS bilayer and single layer PB film. The dissipation shift decreases monotonically for the PB/PS bilayer over a large range of t_a. An initial dissipation shift decrease was observed for a PS/PS bilayer corresponding to the PS/PS layers intermixing. A single layer PB control displayed a decrease in dissipation shift at sufficiently high annealing times $t_a > 100$ min, which is likely linked to chemical degradation.

For the specific cases of PS and PB, the modulus of PS at room temperature and MHz frequencies is approximately constant and can be well fit by a single frequency independent storage modulus parameter G'_{PS}.[181] The density of PS is held fixed at $\rho = 1.04$ g/cm^3.[122,181] The modulus of PB at room temperature and in the frequency range between 5 MHz to 45 MHz (corresponding to the QCM harmonic range of $n = 1$ to 9) was previously established to depend on the harmonic number (frequency) as $\widetilde{G}(f) = G'(f) + iG''(f) = G'_0 n^{\beta'} + iG''_0 n^{\beta'}$ (see Chapter 3).[181] The values for the storage modulus exponent β' and the loss modulus exponent β'' were determined in Ref. [181] by fitting literature data as $\beta' = 0.50 \pm 0.03$ and $\beta'' = 0.74 \pm 0.01$, where excellent agreement was found between the storage and loss moduli for PB determined by QCM with that from literature studies that were collected at lower frequency then time temperature shifted to MHz frequencies for a 25 °C reference temperature. The

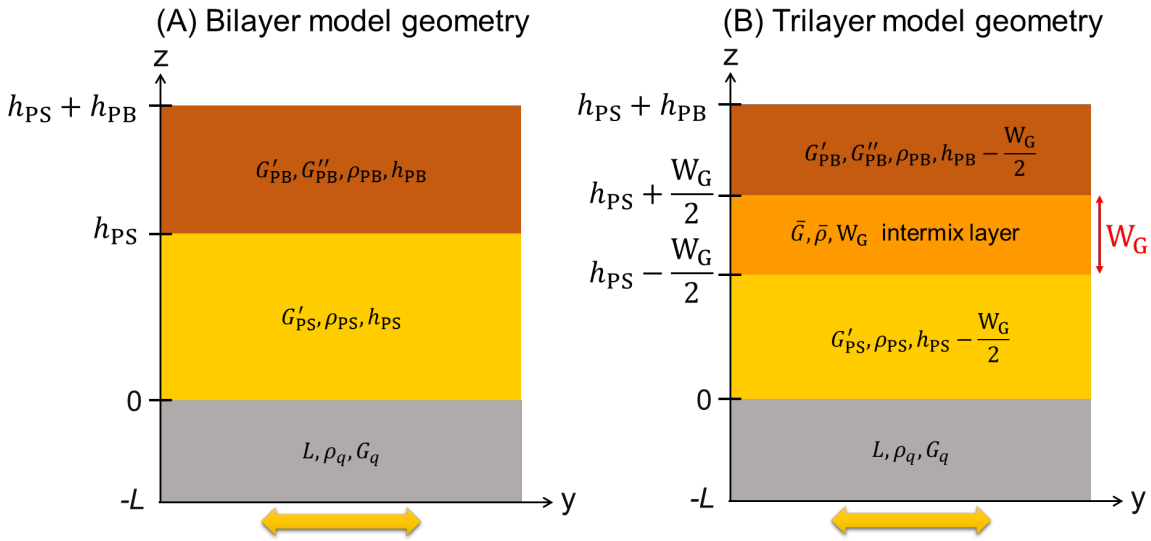

Figure 4.4: Continuum model layer geometry for bilayers and trilayers of PS and PB on a QCM. Each layer is described by a thickness, density, and shear modulus. For the trilayer geometry, an intermixing layer of thickness W_G was placed between the PS and PB layers. This intermixing layer was given a modulus and density that are the average of the PS and PB moduli and densities.

density of PB is held fixed at $\rho = 0.895$ g/cm^3.[164,181]

Here we extend the continuum physics model presented in Chapter 3 to treat bilayer and trilayer film geometries. Figure 4.4 shows the layer model geometry for these cases. The addition of a layer provides additional equations of displacement and stress continuity for each interface. The displacement and shear moduli for a layer j are given by

$$\vec{u}_j(z,t) = e^{-i\tilde{\omega}t}\left(A_j\, e^{i\tilde{k}_j z} + B_j\, e^{-i\tilde{k}_j z}\right)\hat{y} \quad , \tag{4.1}$$

$$\sigma_{yz} = \widetilde{G}_j\,\frac{\partial u_y}{\partial z} \tag{4.2}$$

For the bilayer shown in Figure 4.4 (A), continuity of displacement at the PS/quartz

interface at $z = 0$ (no-slip boundary condition) gives

$$\begin{aligned} u_{\mathrm{PS}}(z,t)\Big|_{z=0} &= u_{\mathrm{q}}(z,t)\Big|_{z=0} \\ A_{\mathrm{PS}} + B_{\mathrm{PS}} &= A_{\mathrm{q}} + B_{\mathrm{q}}, \end{aligned} \tag{4.3}$$

and continuity of displacement at the PB/PS interface ($z = h_{\mathrm{PS}}$) gives

$$\begin{aligned} u_{\mathrm{PB}}(z,t)\Big|_{z=h_{\mathrm{PS}}} &= u_{\mathrm{PS}}(z,t)\Big|_{z=h_{\mathrm{PS}}} \\ A_{\mathrm{PB}}e^{ik_{\mathrm{PB}}h_{\mathrm{PS}}} + B_{\mathrm{PB}}e^{-ik_{\mathrm{PB}}h_{\mathrm{PS}}} &= A_{\mathrm{PS}}e^{ik_{\mathrm{PS}}h_{\mathrm{PS}}} + B_{\mathrm{PS}}e^{-ik_{\mathrm{PS}}h_{\mathrm{PS}}}. \end{aligned} \tag{4.4}$$

Stress continuity (Newton's third law) at the PS/quartz interface ($z = 0$) gives

$$\begin{aligned} \sigma_{\mathrm{PS}}(z,t)\Big|_{z=0} &= \sigma_{\mathrm{q}}(z,t)\Big|_{z=0} \\ \sqrt{\rho_{\mathrm{PS}}\, G'_{\mathrm{PS}}}\,(A_{\mathrm{PS}} - B_{\mathrm{PS}}) &= Z_{\mathrm{q}}\,(A_{\mathrm{q}} - B_{\mathrm{q}}), \end{aligned} \tag{4.5}$$

where $\sqrt{\rho_{\mathrm{PS}}\, G'_{\mathrm{PS}}}$ is the acoustic impedance of PS, and Z_{q} is the known acoustic impedance for AT-cut quartz: $Z_{\mathrm{q}} = \sqrt{\rho_{\mathrm{q}} G_{\mathrm{q}}} = 8.8 \times 10^9$ g m^{-2} Hz.[89,181]. The relation $k = \frac{\omega}{c} = \omega\sqrt{\frac{\rho}{G}}$ was used to substitute for the wavevector prefactors that are gained after taking derivatives of the displacement. Stress continuity at the PB/PS interface ($z = h_{\mathrm{PS}}$) gives

$$\begin{aligned} \sigma_{\mathrm{PB}}(z,t)\Big|_{z=h_{\mathrm{PS}}} &= \sigma_{\mathrm{PS}}(z,t)\Big|_{z=h_{\mathrm{PS}}} \\ \sqrt{\rho_{\mathrm{PB}}\, \widetilde{G}_{\mathrm{PB}}}[A_{\mathrm{PB}}e^{ik_{\mathrm{PB}}h_{\mathrm{PS}}} - B_{\mathrm{PB}}e^{-ik_{\mathrm{PB}}h_{\mathrm{PS}}}] &= \sqrt{\rho_{\mathrm{PS}}\, G'_{\mathrm{PS}}}[A_{\mathrm{PS}}e^{ik_{\mathrm{PS}}h_{\mathrm{PS}}} - B_{\mathrm{PS}}e^{-ik_{\mathrm{PS}}h_{\mathrm{PS}}}], \end{aligned} \tag{4.6}$$

where $\sqrt{\rho_{\mathrm{PB}}\, \widetilde{G}_{\mathrm{PB}}}$ is the acoustic impedance of PB. The PB film/air and bottom

quartz/air interfaces are stress free, giving

$$\sigma_{\mathrm{PB}}(z,t)\Big|_{z=(h_{\mathrm{PS}}+h_{\mathrm{PB}})} = 0$$
$$A_{\mathrm{PB}} - B_{\mathrm{PB}}\,\exp\left[-i4\pi(h_{\mathrm{PS}}+h_{\mathrm{PB}})\sqrt{\frac{\rho_{\mathrm{PB}}}{\widetilde{G}_{\mathrm{PB}}}}\,(f_n+i\Gamma_n)\right] = 0, \tag{4.7}$$

and

$$\sigma_{\mathrm{q}}(z,t)\Big|_{z=-L} = 0$$
$$A_{\mathrm{q}} - B_{\mathrm{q}}\,\exp\left[i\frac{2\pi}{f_0}\,(f_n+i\Gamma_n)\right] = 0. \tag{4.8}$$

To solve Equations (4.3)-(4.8), we first normalized the amplitudes by setting $A_{\mathrm{q}} =$ 1 nm. We also input an initial guess for the PB modulus $\widetilde{G}_{\mathrm{PB}}$ and thickness h_{PB} and the PS modulus G'_{PS} and thickness h_{PS}. For a given harmonic number n, we then solved Equations (4.3)-(4.8) (6 equations) numerically for the six unknowns, all of which are complex: $\Delta\widetilde{f}_n = \Delta f_n + i\Delta\Gamma_n$, B_{q}, A_{PS}, B_{PS}, A_{PB}, B_{PB}. To fit the experimental data with our continuum physics model to determine the moduli and film thickness of the PB and PS layers, chi-squared minimization was performed using the gradient-descent local minimization routine FindMinimum in Mathematica, which performs a Levenberg-Marquardt routine. The resulting best fit parameters were the storage and loss moduli prefactors G'_0 and G''_0 and the film thickness of the PB layer, and the modulus G'_{PS} and film thickness of the PS layer.

The bilayer geometry shown in Figure 4.4 (A) was used to model the systems that had not yet been annealed at 120 °C. This minimally annealed sample held at only 25 °C for 20 h will have a sharp PB/PS interface $w_I \lesssim 1$ nm, and therefore should not have a long-ranged perturbation to the local modulus. The fitting protocol used to fit these bilayer data was to first fix the PS thickness to that determined from fitting the single layer PS film on the QCM collected before floating the PB on top of

the PS. For the PB layer, we held $\beta' = 0.50$ and $\beta'' = 0.74$ fixed and fit for $G_0^{'}$, $G_0^{''}$, and h. The fitting parameters for a bilayer were therefore the frequency-independent glassy plateau modulus of the PS $G_{\rm PS}^{'}$, and the storage and loss moduli terms $G_0^{'}$ and $G_0^{''}$ and film thickness h for PB.

These same samples were then annealed at 120 °C for different lengths of time t_a. It was found that the bilayer model did not fit the data, but instead a trilayer model indicative of a broad modulus profile $G(z)$ was needed to fit the data. The trilayer model shown in Figure 4.4 mimics a broad $G(z)$ profile by using a trilayer model with an intermediate layer of average modulus $\widetilde{G}_{\rm av}$ between that of PB and PS. For the trilayer system corresponding to a bilayer annealed at 120 °C, the values of the bulk PB and PS moduli were held fixed at the values determined from fitting the minimally annealed bilayer data. The intermediate interfacial layer consisted of a layer with modulus that is the average of $\widetilde{G}_{\rm PB}$ and $G_{\rm PS}^{'}$: $\widetilde{G}_{\rm av} = \frac{\widetilde{G}_{\rm PB}+G_{\rm PS}^{'}}{2}$, and a density which is the average of the densities of PB and PS: $\rho_i = \frac{\rho_{\rm PB}+\rho_{\rm PS}}{2}$. The only fit parameter for the trilayer model, therefore, is the layer width W_G, and the internal parameters of the displacement amplitudes in the interfacial layer A_i and B_i.

Figure 4.5 shows the dissipation shifts $\Delta\Gamma_n$ as a function of harmonic number n for a PB/PS bilayer sample with $h_{\rm PS} = 1100$ nm, determined by fitting the PS single layer, and $h_{\rm PB} = 360$ nm, determined by fitting the minimally-annealed PB/PS bilayer. These values of the film thicknesses are in good agreement with separate ellipsometry measurements of $h_{\rm PS} = 1171 \pm 69$ nm and $h_{\rm PB} = 306 \pm 3$ nm. The blue curve corresponds to a fit of the minimally annealed Δf_n and $\Delta\Gamma_n$ data with the bilayer continuum physics layer model shown in Figure 4.4 (A). From the bilayer fit, the modulus of the PS was $G' = 1.72$ GPa, in good agreement with our previous measurements[181] of the PS modulus of G' ranging from $1.5 - 1.8$ GPa. The PB moduli and film thickness values determined from the bilayer fit were $G_0^{'} = 3.50$ MPa, $G_0^{''} = 3.70$ MPa, and $h = 359$ nm. These values of the moduli are in good agreement

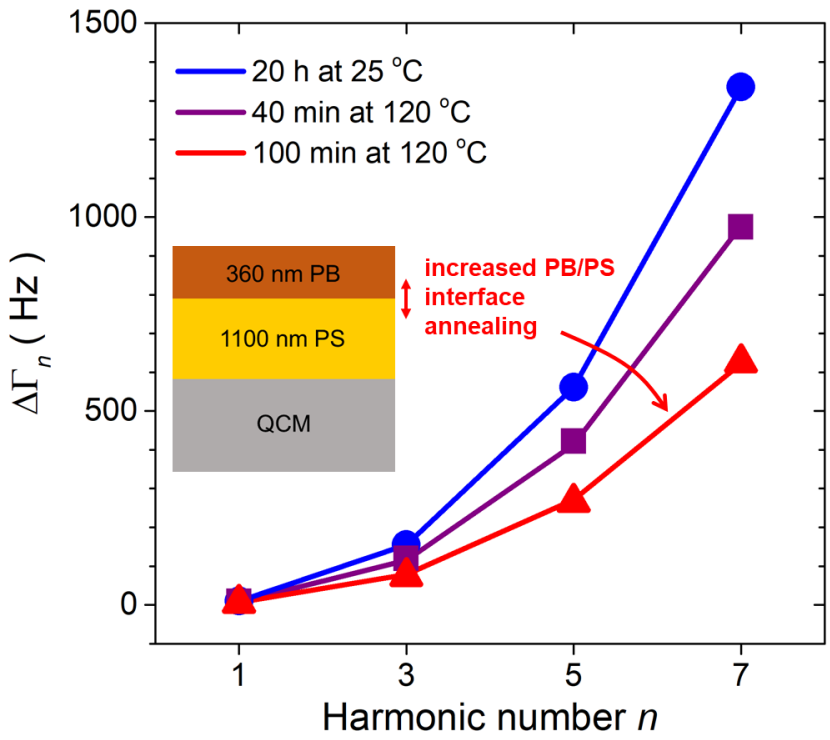

Figure 4.5: Dissipation shift $\Delta\Gamma_n$ decreases on annealing a bilayer of 360 nm PB atop an 1100 nm PS layer. Symbols represent experimental dissipation shifts measured as a function of harmonic number n collected after varying the annealing time at 120 °C of the PB/PS sample. The blue symbols correspond to data collected after minimally annealing the sample at 25 °C for 20 h. The blue curve is a fit to the minimally annealed PB/PS sample data using the bilayer continuum physics model. The purple and red curves are fits to the experimental data with a trilayer continuum physics model consisting of a bulk PB and bulk PS layer that sandwich an intermixed layer of thickness W_G with average modulus and density of the bulk PB and PS layers.

with previous measurements of the PB moduli[181] of G_0' ranging from $2.64 - 3.75$ MPa and G_0'' ranging from $4.07 - 5.08$ MPa. However, when we tried fitting the 120 °C annealed data with a simple bilayer model, the resulting moduli values were deemed unreliable, deviating by more than 30% from the bulk values. Specifically, these moduli values were $G'_{\mathrm{PS}} = 1.1$ GPa, and for PB, $G_0' = 5.0$ MPa and $G_0'' = 8.7$ MPa. The large deviations between these values and values measured of single layer PB and PS films[181] indicates that the bilayer model is not sufficient to treat data from PB/PS samples annealed at 120 °C.

We instead found that a trilayer model depicted in Figure 4.4 (B) that included an intermixing layer was necessary to treat QCM data collected for PB/PS bilayers annealed at 120 °C. The purple and red curves in Figure 4.5 are fits using the trilayer model to the 120 °C experimental data, where a best-fit intermixing layer thickness $W_G = 67$ nm was found for $t_a = 40$ min, and $W_G = 153$ nm for $t_a = 100$ min. These values of W_G can be understood as a coarse-grained measure of the width of the local modulus profile $G(z)$, which may in reality follow a hyperbolic tangent function similar to the $T_g(z)$ profile.[69] These large values of W_G are in contrast with the considerably shorter compositional interfacial width w_I calculated from the interaction parameter[60,182] $\chi = 0.032$ at the annealing temperature of 120 °C using $w_I = \frac{2b}{\sqrt{6\chi}} \approx 2.8$ nm, where the average value of the statistical segment lengths[182] of PS ($b_{\mathrm{PS}} = 0.68$ nm) and PB ($b_{\mathrm{PB}} = 0.53$ nm) was used. Capillary waves tend to increase values of the interfacial width by a couple of nm,[63] so that the interfacial width for this PB/PS system annealed to equilibrium is likely closer to $w_I \approx 5$ nm, still much smaller than the W_G values obtained above. By extension, the $G(z)$ profile is significantly more broad than the composition profile, with the length scales of the $G(z)$ profile more closely related to the length scales of the $T_g(z)$ profile than the composition profile.

The broad $G(z)$ profile implied by the large length scales of W_G reduces the impedance mismatch locally across the polymer domains, since the local impedance is directly related to the local modulus. The development of a broad $G(z)$ profile across dissimilar polymer domains by annealing therefore suggests an increase in the transmission of vibrational modes across the interface. This increased transmission of vibrational modes may then perturb the local vibrational modes in the polymer domains, which have been shown to be predictors of structural relaxations associated with the glass transition.[123,124,183–185] The inherently long-ranged nature of sound waves and associated vibrational modes may also provide an explanation for the

long-ranged nature of the perturbations to the local $T_g(z)$ and $G(z)$ profiles. The presence of a long-ranged viscoelastic gradient near the PB/PS interface formed on annealing may also result in perturbations to the local $T_g(z)$ near the interface by altering the energy barrier height to α-relaxations. In this picture, a reduced local modulus may facilitate cage breaking events, in a manner analogous to the cage-breaking mechanism in the Shoving[36,37] and ECNLE[17,28–35] models that have been applied to bulk glasses, as well as freestanding and supported polymer films.

4.5 Conclusions

Previous studies by our group[70,90] have demonstrated that small changes in the composition profile between dissimilar polymer domains associated with annealing can strongly alter the dynamical coupling across these domains, as measured by the local glass transition temperature $T_g(z)$. In contrast, other studies have reported that the film-averaged T_g of polymers supported on liquid interfaces behave similar to the T_g of polymers supported on rigid substrates.[85,86] We proposed in Chapter 3 that the mechanism underlying strong dynamic coupling across dissimilar polymer-polymer interfaces may be related to acoustic impedance matching, where similar moduli and densities and larger interfacial widths between layers translate into more transmission of acoustic vibrational modes through the interface. These vibrational modes may then interact with local "soft spots," resulting in alterations to local α-relaxations.[123,124,183–185] With this mechanism of acoustic vibrational mode transmission potentially being responsible for local $T_g(z)$ perturbation near interfaces in mind, we have used a QCM to demonstrate that MHz-frequency acoustic shear waves are transmitted differently through a PB/PS interface depending on whether the interface was minimally annealed at 25 °C for 20 h or annealed at 120 °C for times up to 100 min. Extending the continuum physics layer model for QCM described in

Chapter 3, we have shown that the 120 °C annealed bilayer data are inconsistent with the notion of only the compositional interfacial width w_I increasing, and that there is instead a longer-ranged altered viscoelastic profile of width $W_G \approx 150$ nm produced during the interfacial annealing. This large value of W_G implies a long range of perturbation to the local modulus profile $G(z)$ near the PB/PS interface, with similar length scales as the width of the local $T_g(z)$ profile. This similarity in length scales between the modulus $G(z)$ and $T_g(z)$ gradient provides further evidence that increased transmission of vibrational modes across dissimilar polymer-polymer interfaces occurring on annealing is likely responsible for the broad $T_g(z)$ and $G(z)$ gradients across the interface indicating a long range coupling of dynamics. This broad $G(z)$ profile reduces the impedance mismatch locally across the polymer domains, since the local impedance is directly related to the local modulus. This increased transmission of vibrational modes may be associated with perturbations to the local vibrational modes in the material, which can alter structural relaxations associated with the glass transition.[123,124,183–185]

Chapter 5

Summary and Conclusions

In this dissertation, I have used a modified fluorescence method[82] to measure the local glass transition temperature $T_g(z)$ of multilayer polymer films, and have developed a quartz crystal microbalance (QCM) method to measure the MHz-frequency modulus of single layer and bilayer films. These measurements have collectively addressed the question of how the modulus of a polymer domain impacts the local $T_g(z)$ in an adjacent polymer domain, and they have demonstrated that the mechanism causing long-ranged perturbations to the local $T_g(z)$ near dissimilar polymer-polymer interfaces may be the propagation of vibrational modes across the interface, where the transmission of these modes through the interface is assisted by a broad shear modulus $\widetilde{G}(z)$ profile across the interface that is developed after sufficient annealing of the interface.

Studies on thin polymer films have demonstrated a range of property changes with decreasing film thickness caused by interface effects,[15,17,38,91,92] including polymer-polymer interfaces.[69,70,77,82,92–101] The tuning of the properties of multicomponent materials requires an understanding of how these interface effects perturb local properties. To isolate the effect of individual interfaces in multicomponent systems, studies of simplified geometries with a single interface are often used. This simplified geom-

etry renders both experimental and theoretical methods more tractable and provides insight into the fundamental physics of polymer-polymer interfaces.

In 2015, Baglay and Roth used a local fluorescence probe method to obtain a profile of the local glass transition temperature $T_g(z)$ near a glassy-rubbery polystyrene (PS) / poly(n-butyl methacrylate) (PnBMA) interface.[69] They found this profile in local dynamics to be much more broad than the composition profile in addition to being asymmetric, with the local $T_g(z)$ in PS converging to bulk T_g at a larger distance from the interface than the $T_g(z)$ in PnBMA. Follow-up work demonstrated a similar $T_g(z)$ behavior for a range of weakly immiscible polymer pairs,[70,73] and it was revealed that the spatial range of $T_g(z)$ perturbation in PS depended on whether the neighboring polymer domain had a higher T_g^{bulk} ("hard confinement", with perturbations to PS $T_g(z)$ extending to $z \approx$ 100–125 nm), or lower T_g^{bulk} ("soft confinement," with perturbations to PS $T_g(z)$ extending to $z \approx$ 225–250 nm). An additional observation in Ref. [70] was that these broad $T_g(z)$ profiles only formed upon annealing the dissimilar polymer-polymer interface to equilibrium, suggesting that some factor relating to the formation of the polymer-polymer interface was responsible for the coupling of T_g dynamics across the interface.

These studies that mapped the local $T_g(z)$ across dissimilar polymer-polymer interfaces with interfacial widths $w_I \approx 5-7$ nm created a number of open questions in the field. First, what causes the large length scale of perturbation to local $T_g(z)$ near polymer-polymer interfaces? This question relates to what is the relevant parameter describing hard or soft confinement, since the breadth of the $T_g(z)$ profile of PS under soft confinement was approximately double that of PS under hard confinement. Theory and simulations suggested that the relevant parameter in perturbations to $T_g(z)$ near interfaces may have been the glassy plateau shear modulus through the Debye-Waller factor,[77] but there did not exist an experimental study that measured the effect of systematically varying the modulus of a polymer domain on the local $T_g(z)$

in an adjacent polymer domain. A second open question was why is annealing of the dissimilar polymer-polymer interface required to obtain these large length scales of local $T_g(z)$ perturbation? Annealing of the interface leads to an increased interfacial width, interfacial roughness, and chain connectivity across the interface. While the effects of interfacial roughness[71] and chain connectivity[72] had been experimentally investigated, the role of interfacial width on influencing the coupling of T_g dynamics across the interface was an open question.

One of my significant contributions to the literature was demonstrating that the local $T_g(z)$ in PS is strongly sensitive to the modulus of the neighboring polydimethylsiloxane (PDMS) domain, which I tuned by varying the cross-link density of the PDMS. In Chapter 2, I used the localized fluorescence method developed in Ref. [82] to measure profiles of the local glass transition temperature $T_g(z)$ within PS next to PDMS domains. By changing the base to cross-linker ratio, I varied the cross-link density and therefore the Young's modulus of the PDMS. I found that the local $T_g(z)$ in PS at a distance of $z = 50$ nm away from the PS/PDMS interface shifted by 40 K as the PDMS modulus was varied from 0.9–2.6 MPa, demonstrating a strong sensitivity of the glass forming dynamics to the rigidity of the neighboring domain.

Chapter 2 helped address the open question in the literature of what role the modulus plays in altering local T_g dynamics. Interestingly, the cross-link ratios of PDMS used should not have altered the glassy shear modulus, and instead should only have varied the low frequency modulus. The strong sensitivity of the local $T_g(z)$ in PS to the low frequency modulus of PDMS suggests that there is a key component missing in some current theories of the glass transition and simulations, which point to the Debye-Waller factor (related to the high-frequency glassy shear modulus) as the key parameter in influencing T_g perturbations near interfaces. This work therefore points to a potentially fruitful new avenue for theories and simulations to investigate the effects of the low frequency modulus and associated longer wavelength phenomena

relating to structural relaxation associated with the glass transition.

Also in Chapter 2, I found that the extent the $T_g(z)$ perturbation persists away from the PS/PDMS interface is $z \approx 65$–90 nm before bulk T_g is recovered, which is much shorter for this strongly immiscible system compared with the weakly immiscible systems studied by Baglay and Roth. We attributed this reduced length scale to the smaller interfacial width of the PS/PDMS system of $w_I \approx 1.5$ nm compared to the systems studied by Baglay and Roth with interfacial widths ranging from $w_I \approx 5 - 7$ nm. This finding suggests that the interfacial width, along with the relative moduli of the layers, plays a key role in determining the spatial extent of the $T_g(z)$ profile near immiscible polymer-polymer interfaces and provided strong evidence that the broader interfacial width is the main reason that annealing an immiscible polymer-polymer interface is required to obtain a broad $T_g(z)$ profile.

Since the publication corresponding to Chapter 2, our work has been cited by four reviews examining the causes of T_g perturbations by interfaces.[186–189] In Refs. [186–188] our work is cited by virtue of its being the only experimental study that has measured the influence of the modulus of a polymer domain on the local $T_g(z)$ of an adjacent polymer domain. Ref. [189] cited our work with other works as an example of the use of the local fluorescence probe method to determine the local $T_g(z)$ in polymer systems.

Gathering the results of a large effect of modulus of a domain on the local $T_g(z)$ in an adjacent domain, together with the importance of annealing in obtaining long length scales of perturbations to $T_g(z)$, we suggested in Chapter 2 that the mechanism behind the modulus of a polymer domain perturbing the local $T_g(z)$ in an adjacent polymer domain may be related to impedance matching, where acoustic wave transmission through a dissimilar polymer-polymer interface is controlled by the relative impedances $\widetilde{Z} = \sqrt{\rho \widetilde{G}}$ of the domains and the breadth of the density and modulus profiles. To directly measure the acoustic wave transmission and modulus profile near

dissimilar polymer-polymer interfaces, I designed an electrical circuit that incorporated a QCM and developed a continuum physics model in collaboration with the Burton Lab at Emory.

Standard QCM analysis methods typically simplify equations to facilitate analytical solutions,[89] but this can limit the maximum harmonic number accessible, as these analytical solutions become invalid as film resonance is approached at higher harmonics. This limitation becomes especially problematic for thick, rubbery polymer films, for which the onset of film resonance occurs at lower harmonics. In addition, the standard method of QCM analysis uses an acoustic multilayer formalism, in which an equivalent circuit model is used to solve for the acoustic impedance of the QCM-film system from which the viscoelastic properties of the film can be extracted.[156,157] Although powerful and intuitive for those with a strong circuit background, this method can obscure the connection between the underlying physics and the properties of the material being studied.

In Chapter 3, I presented a physically intuitive continuum physics model that numerically solves a system of equations stemming from standard continuum physics boundary conditions of displacement and stress continuity across interfaces. The solutions to these equations are the resonance frequency and dissipation shifts Δf_n and $\Delta\Gamma_n$ at each odd harmonic n that occur on loading the QCM with a film. This continuum model was then fit to experimental data I collected of rubbery polybutadiene (PB) and PDMS films, as well as glassy PS films, to determine the frequency-dependent complex shear moduli $\widetilde{G}(\omega) = G'(\omega) + iG''(\omega)$ at MHz frequencies and the film thicknesses h of the films. The storage and loss moduli of PB and PDMS, which are both in the rubber-to-glass transition at the MHz frequencies of the QCM oscillator, were modeled as linear on a log-log scale with the frequency/harmonic number: $G' = G'_0(n)^{\beta'}$ and $G'' = G''_0(n)^{\beta''}$. This assumption of the frequency dependence of the storage and loss moduli is valid in the relatively narrow frequency range of the QCM

($\sim$ 5 MHz-65 MHz), and is a more realistic treatment of the modulus of a viscoelastic solid than the Kelvin-Voigt model of a solid occasionally used in QCM modeling.[89] Values for the exponents β' and β'', corresponding to the slopes of the log(modulus) vs. log(frequency) between 5 MHz-65 MHz were determined by fitting to literature data that had been collected with lower frequency (approximately 10^{-3} to 10^{+1} Hz) rheometry at a range of different temperatures, and then time-temperature shifted to higher frequencies corresponding to a reference temperature of 25 °C. Excellent agreement between the direct measurements of the MHz-frequency moduli by QCM and these time-temperature shifted literature values were found for the measured systems of PB and PDMS, as well as for the glassy plateau shear modulus of PS.

With the QCM method for determining the modulus and thickness of films in the MHz-frequency regime established in Chapter 3, I returned in Chapter 4 to the problem of measuring the propagation of acoustic waves and of potentially connecting the $T_g(z)$ profile with a local modulus $G(z)$ profile that relates to an acoustic impedance profile near dissimilar polymer-polymer interfaces. By extending the QCM method and continuum physics model to treat a bilayer film, I found that MHz-frequency shear waves produced by a QCM are transmitted differently through a PB/PS interface depending on whether the interface has been minimally annealed at 25 °C or annealed at 120 °C, which should produce an interfacial width of at most $w_I \approx 5$ nm for this weakly immiscible system.

Using a continuum physics layer model, I showed that the data for a PB/PS bilayer that had undergone minimal annealing of 25 °C for 20 h were fit well with a bilayer model. This was expected, as in this case we would not expect the $T_g(z)$ profile, and by extension the $G(z)$ profile, to be well developed, and the moduli of each layer should not be appreciably perturbed from their bulk values near the interface. In contrast, data from the same sample after having been annealed at 120 °C required treatment with a trilayer model. In this trilayer model, bulk PB and

PS layers with moduli determined from fitting the minimally annealed bilayer data sandwiched an interfacial layer of thickness W_G, which represents the spatial extent of the local modulus profile near the PB/PS interface. The modulus of this interfacial layer was modeled as the average of the bulk PB and PS moduli determined from fitting the minimally annealed bilayer data, and the density of the interfacial layer was taken to be the average of the densities of PB and PS. Fitting this trilayer model to data collected for a sample that had been annealed at 120 °C for W_G, I found that W_G systematically increased with annealing time at 120 °C, with the value at the longest annealing time of 100 min at 120 °C of $W_G = 153$ nm. This finding implies that the breadth of the modulus profile for this immiscible polymer bilayer system annealed at 120 °C is similar to the breadth of local $T_g(z)$ profiles,[69,70,90] both of which are considerably larger than the composition profile width of the PB/PS system annealed to equilibrium of $w_I \approx 5$ nm.

The broad $G(z)$ profile that is developed on annealing at temperatures above the highest T_g^{bulk} of the system reduces the impedance mismatch locally across the polymer domains, since the local impedance is directly related to the local modulus. The increased transmission of vibrational modes associated with a locally reduced impedance mismatch may be associated with perturbations to the local vibrational modes in the material, which can alter structural relaxations associated with the glass transition.[123,124,183–185] Alterations to the local modulus may also facilitate cage breaking events, in a manner analogous to the cage-breaking mechanism in the Shoving[36,37] and ECNLE[17,28–35] models.

The results of my PhD work have left a number of open questions. First, what is the shape of the modulus profile near a dissimilar polymer-polymer interface? Is the profile asymmetric, like the $T_g(z)$ profile?[69] This might be investigated by extending our continuum physics layer model into one that approximates continuous modulus or density profiles by decomposing the profile into a series of thin slabs with varying

moduli. The modulus of each layer could be chosen to follow a linear or hyperbolic tangent profile, and matrices used to represent the acoustic properties of each layer. The solution of this matrix system could then yield the parameters that define the modulus gradient, such as the width and slope of the gradient and whether the profile is shifted to one side of the interface. I have developed the necessary matrix math of this model and Alex Couturier, the most recent member of the Roth Lab, will further develop the model and fit it to experimental data. An additional adaptation of the continuum physics model that may be worth exploring is to incorporate reflection and transmission coefficients within the model, to be able to quantify the reflection and transmission of MHz-frequency shear waves propagating through a dissimilar polymer-polymer interface. One can imagine a plot of the transmission coefficient as a function of annealing time or of interfacial width as being useful to understand at what annealing time or interfacial width the transmission or reflection saturates. Another open question is to what extent do results from the MHz-frequency shear wave propagation through a dissimilar polymer-polymer interface as measured by QCM relate to the propagation of vibrational modes relevant for altering the local T_g dynamics? Perhaps other forms of acoustic measurements, such as those performed at different frequencies than MHz frequencies, or perhaps those that produce compression waves, could be worthwhile to apply to bilayer systems, with the goal of extracting a modulus profile near the interface. A similar continuum physics model to that developed in Chapters 3 and 4 for QCM could be developed for these other acoustic measurement methods, and perhaps differences in the length scale or shape of the modulus profile as measured by these other methods could identify a frequency range or a mode of oscillation that relate most directly to the local $T_g(z)$ profile width or shape.

Bibliography

[1]C. B. Roth and R. R. Baglay, *Polymer Glasses*, edited by C. B. Roth (CRC Press, Taylor & Francis Group, Boca Raton, FL, 2016).

[2]E. R. Weeks, J. C. Crocker, A. C. Levitt, A. Schofield, and D. A. Weitz, "Three-Dimensional Direct Imaging of Structural Relaxation Near the Colloidal Glass Transition", Science **287**, 627–631 (2000).

[3]G. Adam and J. H. Gibbs, "On the Temperature Dependence of Cooperative Relaxation Properties in Glass-Forming Liquids", Journal of Chemical Physics **43**, 139–146 (1965).

[4]E. Hempel, G. Hempel, A. Hensel, C. Schick, and E. Donth, "Characteristic Length of Dynamic Glass Transition Near Tg for a Wide Assortment of Glass-Forming Substances", Journal of Physical Chemistry B **104**, 2460–2466 (2000).

[5]M. D. Ediger, "Spatially Heterogeneous Dynamics in Supercooled Liquids", Annual Review of Physical Chemistry **51**, 99–128 (2000).

[6]S. L. Simon and G. B. McKenna, *Polymer Glasses*, edited by C. B. Roth (CRC Press, Taylor & Francis Group, Boca Raton, FL, 2016).

[7]P. C. Hiemenz and T. P. Lodge, *Polymer Chemistry*, 2nd (CRC Press, Boca Raton, FL, 2007).

[8]J. M. Caruthers and G. A. Medvedev, *Polymer Glasses*, edited by C. B. Roth (CRC Press, Taylor & Francis Group, Boca Raton, FL, 2016).

[9]J. L. Keddie, R. A. L. Jones, and R. A. Cory, "Swelling Behavior of Partially Cross-Linked Polymers: A Ternary System", Macromolecules **38**, 4447–4455 (2005).

[10]J. L. Keddie, R. A. Jones, and R. A. Cory, "Interface and Surface Effects on the Glass-Transition Temperature in Thin Polymer Films", Faraday Discussions **98**, 219–230 (1994).

[11]C. B. Roth and J. R. Dutcher, "Glass Transition and Chain Mobility in Thin Polymer Films", Journal of Electroanalytical Chemistry **584**, 13–22 (2005).

[12]J. H. van Zanten, W. E. Wallace, and W.-l. Wu, "Effect of Strongly Favorable Substrate Interactions on the Thermal Properties of Ultrathin Polymer Films", Physical Review E **53**, R2053–R2056 (1996).

[13]A. Silberberg, "Distribution of Conformations and Chain Ends Near the Surface of a Melt of Linear Flexible Macromolecules", Journal of Colloid and Interface Science **90**, 86–91 (1982).

[14]D. M. Sussman, W.-S. Tung, K. I. Winey, K. S. Schweizer, and R. A. Riggleman, "Entanglement Reduction and Anisotropic Chain and Primitive Path Conformations in Polymer Melts Under Thin Film and Cylindrical Confinement", Macromolecules **47**, 6462–6472 (2014).

[15]C. J. Ellison and J. M. Torkelson, "The Distribution of Glass-Transition Temperatures in Nanoscopically Confined Glass Formers", Nature Materials **2**, 695–700 (2003).

[16]R. J. Lang and D. S. Simmons, "Interfacial Dynamic Length Scales in the Glass Transition of a Model Freestanding Polymer Film and their Connection to Cooperative Motion", Macromolecules **46**, 9818–9825 (2013).

[17]K. S. Schweizer and D. S. Simmons, "Progress Towards a Phenomenological Picture and Theoretical Understanding of Glassy Dynamics and Vitrification Near

Interfaces and Under Nanoconfinement", Journal of Chemical Physics **151**, 240901 (2019).

[18]V. Lubchenko and P. G. Wolynes, "Theory of Structural Glasses and Supercooled Liquids", Annual Review of Physical Chemistry **58**, 235–266 (2007).

[19]B. A. Pazmiño Betancourt, J. F. Douglas, and F. W. Starr, "String Model for the Dynamics of Glass-Forming Liquids", Journal of Chemical Physics **140**, 204509 (2014).

[20]P. Z. Hanakata, J. F. Douglas, and F. W. Starr, "Interfacial Mobility Scale Determines the Scale of Collective Motion and Relaxation Rate in Polymer Films", Nature Communications **5**, 1–8 (2014).

[21]T. Salez, J. Salez, K. Dalnoki-Veress, E. Raphaël, and J. A. Forrest, "Cooperative Strings and Glassy Interfaces", Proceedings of the National Academy of Sciences **112**, 8227–8231 (2015).

[22]R. P. White and J. E. G. Lipson, "Polymer Free Volume and Its Connection to the Glass Transition", Macromolecules **49**, 3987–4007 (2016).

[23]R. P. White and J. E. G. Lipson, "Dynamics across a Free Surface Reflect Interplay between Density and Cooperative Length: Application to Polystyrene", Macromolecules **54**, 4136–4144 (2021).

[24]J. D. McCoy and J. G. Curro, "Conjectures on the Glass Transition of Polymers in Confined Geometries", Journal of Chemical Physics **116**, 9154–9157 (2002).

[25]N. B. Tito, J. E. G. Lipson, and S. T. Milner, "Lattice Model of Dynamic Heterogeneity and Kinetic Arrest in Glass-Forming Liquids", Soft Matter **9**, 3173–3180 (2013).

[26]N. B. Tito, J. E. G. Lipson, and S. T. Milner, "Lattice Model of Mobility at Interfaces: Free Surfaces, Substrates, and Bilayers", Soft Matter **9**, 9403–9413 (2013).

[27]J. DeFelice and J. E. Lipson, "Different Metrics for Connecting Mobility and Glassiness in Thin Films", Soft Matter **15**, 1651–1657 (2019).

[28]S. Mirigian and K. S. Schweizer, "Unified Theory of Activated Relaxation in Liquids Over 14 Decades in Time", Journal of Physical Chemistry Letters **4**, 3648–3653 (2013).

[29]S. Mirigian and K. S. Schweizer, "Elastically Cooperative Activated Barrier Hopping Theory of Relaxation in Viscous Fluids. I. General Formulation and Application to Hard Sphere Fluids", Journal of Chemical Physics **140**, 194506 (2014).

[30]S. Mirigian and K. S. Schweizer, "Elastically Cooperative Activated Barrier Hopping Theory of Relaxation in Viscous Fluids. II. Thermal Liquids", Journal of Chemical Physics **140**, 194507 (2014).

[31]S. Mirigian and K. S. Schweizer, "Dynamical Theory of Segmental Relaxation and Emergent Elasticity in Supercooled Polymer Melts", Macromolecules **48**, 1901–1913 (2015).

[32]S. Mirigian and K. S. Schweizer, "Communication: Slow Relaxation, Spatial Mobility Gradients, and Vitrification in Confined Films", Journal of Chemical Physics **141**, 161103 (2014).

[33]S. Mirigian and K. S. Schweizer, "Theory of Activated Glassy Relaxation, Mobility Gradients, Surface Diffusion, and Vitrification in Free Standing Thin Films", Journal of Chemical Physics **143**, 244705 (2015).

[34]A. D. Phan and K. S. Schweizer, "Theory of the Spatial Transfer of Interface-Nucleated Changes of Dynamical Constraints and Its Consequences in Glass-Forming Films", Journal of Chemical Physics **150**, 044508 (2019).

[35]A. D. Phan and K. S. Schweizer, "Theory of Spatial Gradients of Relaxation, Vitrification Temperature and Fragility of Glass-Forming Polymer Liquids Near Solid Substrates", ACS Macro Letters **9**, 448–453 (2020).

[36]J. C. Dyre, "Source of Non-Arrhenius Average Relaxation Time in Glass-Forming Liquids", Journal of Non-Crystalline Solids **235**, 142–149 (1998).

[37]J. C. Dyre, T. Christensen, and N. B. Olsen, "Elastic Models for the Non-Arrhenius Viscosity of Glass-Forming Liquids", Journal of Non-Crystalline Solids **352**, 4635–4642 (2006).

[38]B. D. Vogt, "Mechanical and Viscoelastic Properties of Confined Amorphous Polymers", Journal of Polymer Science Part B: Polymer Physics **56**, 9–30 (2018).

[39]B. Oommen and K. Van Vliet, "Effects of Nanoscale Thickness and Elastic Nonlinearity on Measured Mechanical Properties of Polymeric Films", Thin Solid Films **513**, 235–242 (2006).

[40]P. C. Chung, E. Glynos, and P. F. Green, "The Elastic Mechanical Response of Supported Thin Polymer Films", Langmuir **30**, 15200–15205 (2014).

[41]C. M. Stafford, C. Harrison, K. L. Beers, A. Karim, E. J. Amis, M. R. Vanlandingham, H. C. Kim, W. Volksen, R. D. Miller, and E. E. Simonyi, "A Buckling-Based Metrology for Measuring the Elastic Moduli of Polymeric Thin Films", Nature Materials **3**, 545–550 (2004).

[42]C. M. Stafford, B. D. Vogt, C. Harrison, D. Julthongpiput, and R. Huang, "Elastic Moduli of Ultrathin Amorphous Polymer Films", Macromolecules **39**, 5095–5099 (2006).

[43]J. M. Torres, C. M. Stafford, and B. D. Vogt, "Elastic Modulus of Amorphous Polymer Thin Films: Relationship to the Glass Transition Temperature", ACS Nano **3**, 2677–2685 (2009).

[44]J. M. Torres, C. M. Stafford, and B. D. Vogt, "Impact of Molecular Mass on the Elastic Modulus of Thin Polystyrene Films", Polymer **51**, 4211–4217 (2010).

[45]E. A. Wilder, S. Guo, S. Lin-Gibson, M. J. Fasolka, and C. M. Stafford, "Measuring the Modulus of Soft Polymer Networks via a Buckling-Based Metrology", Macromolecules **39**, 4138–4143 (2006).

[46]Y. Liu, Y.-C. Chen, S. Hutchens, J. Lawrence, T. Emrick, and A. J. Crosby, "Directly Measuring the Complete Stress–Strain Response of Ultrathin Polymer Films", Macromolecules **48**, 6534–6540 (2015).

[47]R. K. Bay and A. J. Crosby, "Uniaxial Extension of Ultrathin Freestanding Polymer Films", ACS Macro Letters **8**, 1080–1085 (2019).

[48]P. A. O'Connell and G. B. McKenna, "Rheological Measurements of the Thermoviscoelastic Response of Ultrathin Polymer Films", Science **307**, 1760–1763 (2005).

[49]P. A. O'Connell and G. B. McKenna, "Novel Nanobubble Inflation Method for Determining the Viscoelastic Properties of Ultrathin Polymer Films", Review of scientific instruments **78**, 013901 (2007).

[50]X. Li and G. B. McKenna, "Ultrathin Polymer Films: Rubbery Stiffening, Fragility, and Tg Reduction", Macromolecules **48**, 6329–6336 (2015).

[51]T. B. Karim and G. B. McKenna, "Unusual Surface Mechanical Properties of Poly (α-methylstyrene): Surface Softening and Stiffening at Different Temperatures", Macromolecules **45**, 9697–9706 (2012).

[52]T. B. Karim and G. B. McKenna, "Comparison of Surface Mechanical Properties Among Linear and Star Polystyrenes: Surface Softening and Stiffening at Different Temperatures", Polymer **54**, 5928–5935 (2013).

[53]K. Van Workum and J. J. de Pablo, "Computer Simulation of the Mechanical Properties of Amorphous Polymer Nanostructures", Nano Letters **3**, 1405–1410 (2003).

[54]K. Yoshimoto, T. S. Jain, K. Van Workum, P. F. Nealey, and J. J. de Pablo, "Mechanical Heterogeneities in Model Polymer Glasses at Small Length Scales", Physical Review Letters **93**, 175501 (2004).

[55]K. Yoshimoto, T. S. Jain, P. F. Nealey, and J. J. de Pablo, "Local Dynamic Mechanical Properties in Model Free-Standing Polymer Thin Films", Journal of Chemical Physics **122**, 144712 (2005).

[56]W. Xia and S. Keten, "Interfacial Stiffening of Polymer Thin Films Under Nanoconfinement", Extreme Mechanics Letters **4**, 89–95 (2015).

[57]J. A. Forrest, K. Dalnoki-Veress, and J. R. Dutcher, "Brillouin Light Scattering Studies of the Mechanical Properties of Thin Freely Standing Polystyrene Films", Physical Review E **58**, 6109 (1998).

[58]J. Chang, K. B. Toga, J. D. Paulsen, N. Menon, and T. P. Russell, "Thickness Dependence of the Young's Modulus of Polymer Thin Films", Macromolecules **51**, 6764–6770 (2018).

[59]E. Helfand and Y. Tagami, "Theory of the Interface Between Immiscible Polymers. II", Journal of Chemical Physics **56**, 3592–3601 (1972).

[60]H. B. Eitouni and N. P. Balsara, "Thermodynamics of Polymer Blends", in *Physical Properties of Polymers Handbook*, edited by J. E. Mark, 2nd ed. (Springer, New York, 2007) Chap. 19, pp. 339–356.

[61]A. J. Nedoma, M. L. Robertson, N. S. Wanakule, and N. P. Balsara, "Measurements of the Flory–Huggins Interaction Parameter Using a Series of Critical Binary Blends", Industrial & Engineering Chemistry Research **47**, 3551–3553 (2008).

[62]C. C. Han, B. J. Bauer, J. C. Clark, Y. Muroga, Y. Matsushita, M. Okada, Q. Trancong, T. Chang, and I. C. Sanchez, "Temperature, Composition and Molecular-Weight Dependence of the Binary Interaction Parameter of Polystyrene/Poly (vinyl methyl ether) Blends", Polymer **29**, 2002–2014 (1988).

[63]R. A. L. Jones and R. W. Richards, *Polymers at Surfaces and Interfaces* (Cambridge University Press, 1999).

[64]T. G. Fox, "Influence of Diluent and of Copolymer Composition on the Glass Temperature of a Polymer System", Bull. Am. Phys. Soc. **1**, 123 (1956).

[65]W. Brostow, R. Chiu, I. M. Kalogeras, and A. Vassilikou-Dova, "Prediction of Glass Transition Temperatures: Binary Blends and Copolymers", Materials Letters **62**, 3152–3155 (2008).

[66]T. K. Kwei, "The Effect of Hydrogen Bonding on the Glass Transition Temperatures of Polymer Mixtures", Journal of Polymer Science: Polymer Letters Edition **22**, 307–313 (1984).

[67]J. Q. Pham and P. F. Green, "The Glass Transition of Thin Film Polymer/Polymer Blends: Interfacial Interactions and Confinement", Journal of Chemical Physics **116**, 5801–5806 (2002).

[68]T. P. Lodge and T. C. McLeish, "Self-Concentrations and Effective Glass Transition Temperatures in Polymer Blends", Macromolecules **33**, 5278–5284 (2000).

[69]R. R. Baglay and C. B. Roth, "Communication: Experimentally Determined Profile of Local Glass Transition Temperature across a Glassy-Rubbery Polymer Interface with a Tg Difference of 80 K", Journal of Chemical Physics **143**, 111101 (2015).

[70]R. R. Baglay and C. B. Roth, "Local glass transition temperature Tg(z) of polystyrene next to different polymers: Hard vs. soft confinement", Journal of Chemical Physics **146**, 203307 (2017).

[71]X. Huang, M. F. Thees, W. B. Size, and C. B. Roth, "Experimental Study of Substrate Roughness on the Local Glass Transition of Polystyrene", Journal of Chemical Physics **152**, 244901 (2020).

[72]X. Huang and C. B. Roth, "Optimizing the Grafting Density of Tethered Chains to Alter the Local Glass Transition Temperature of Polystyrene near Silica Substrates: The Advantage of Mushrooms over Brushes", ACS Macro Letters **7**, 269–274 (2018).

[73]B. L. Kasavan, R. R. Baglay, and C. B. Roth, "Local Glass Transition Temperature $T_g(z)$ Profile in Polystyrene next to Polybutadiene with and without Plasticization Effects", Macromolecular Chemistry and Physics **219**, 1700328 (2018).

[74]S. Mirigian and K. S. Schweizer, "Influence of Chemistry, Interfacial Width, and Non-Isothermal Conditions on Spatially Heterogeneous Activated Relaxation and Elasticity in Glass-Forming Free Standing Films", Journal of Chemical Physics **146**, 203301 (2017).

[75]C. G. Robertson, T. E. Hogan, M. Rackaitis, J. E. Puskas, and X. Wang, "Effect of Nanoscale Confinement on Glass Transition of Polystyrene Domains From Self-Assembly of Block Copolymers", Journal of Chemical Physics **132**, 104904 (2010).

[76]D. Christie, R. A. Register, and R. D. Priestley, "Direct Measurement of the Local Glass Transition in Self-Assembled Copolymers With Nanometer Resolution", ACS Central Science **4**, 504–511 (2018).

[77]R. J. Lang, W. L. Merling, and D. S. Simmons, "Combined Dependence of Nanoconfined Tg on Interfacial Energy and Softness of Confinement", ACS Macro Letters **3**, 758–762 (2014).

[78]K. Kalyanasundaram and J. K. Thomas, "Environmental Effects on Vibronic Band Intensities in Pyrene Monomer Fluorescence and Their Application in Studies of Micellar Systems", Journal of the American Chemical Society **99**, 2039–2044 (1977).

[79]B. Valeur, *Molecular Fluorescence: Principles and Applications* (Wiley-VCH, Weinheim, 2002).

[80]C. Ellison, S. Kim, D. Hall, and J. Torkelson, "Confinement and Processing Effects on Glass Transition Temperature and Physical Aging in Ultrathin Polymer Films: Novel Fluorescence Measurements", The European Physical Journal E **8**, 155–166 (2002).

[81]S. Kim, S. A. Hewlett, C. B. Roth, and J. M. Torkelson, "Confinement Effects on Glass Transition Temperature, Transition Breadth, and Expansivity: Comparison of Ellipsometry and Fluorescence Measurements on Polystyrene Films", European Physical Journal E **30**, 83–92 (2009).

[82]P. M. Rauscher, J. E. Pye, R. R. Baglay, and C. B. Roth, "Effect of Adjacent Rubbery Layers on the Physical Aging of Glassy Polymers", Macromolecules **46**, 9806–9817 (2013).

[83]H. Fujiwara, *Spectroscopic Ellipsometry: Principles and Applications* (John Wiley & Sons, 2007).

[84]X. Huang and C. B. Roth, "Changes in the Temperature-Dependent Specific Volume of Supported Polystyrene Films With Film Thickness", Journal of Chemical Physics **144**, 234903 (2016).

[85]J. Wang and G. B. McKenna, "Viscoelastic and Glass Transition Properties of Ultrathin Polystyrene Films by Dewetting from Liquid Glycerol", Macromolecules **46**, 2485–2495 (2013).

[86]J. Wang and G. B. McKenna, "A Novel Temperature-Step Method to Determine the Glass Transition Temperature of Ultrathin Polymer Films by Liquid Dewetting", Journal of Polymer Science Part B: Polymer Physics **51**, 1343–1349 (2013).

[87]B. Lautrup, *Physics of Continuous Matter*, 2nd ed. (CRC Press, Boca Raton, FL, 2011).

[88]S. Mirigian and K. S. Schweizer, "Communication: Slow Relaxation, Spatial Mobility Gradients, and Vitrification in Confined Films", Journal of Chemical Physics **141**, 161103 (2014).

[89]D. Johannsmann, *The Quartz Crystal Microbalance in Soft Matter Research: Fundamentals and Modeling* (Springer, Switzerland, 2015).

[90]Y. J. Gagnon and C. B. Roth, "Local Glass Transition Temperature Tg(z) Within Polystyrene Is Strongly Impacted by the Modulus of the Neighboring PDMS Domain", ACS Macro Letters **9**, 1625–1631 (2020).

[91]M. D. Ediger and J. A. Forrest, "Dynamics near Free Surfaces and the Glass Transition in Thin Polymer Films: A View to the Future", Macromolecules **47**, 471–478 (2014).

[92]C. B. Roth, K. L. McNerny, W. F. Jager, and J. M. Torkelson, "Eliminating the Enhanced Mobility at the Free Surface of Polystyrene: Fluorescence Studies of the Glass Transition Temperature in Thin Bilayer Films of Immiscible Polymers", Macromolecules **40**, 2568–2574 (2007).

[93]C. B. Roth and J. M. Torkelson, "Selectively Probing the Glass Transition Temperature in Multilayer Polymer Films: Equivalence of Block Copolymers and Multilayer Films of Different Homopolymers", Macromolecules **40**, 3328–3336 (2007).

[94]H. Yoon and G. B. McKenna, "Substrate Effects on Glass Transition and Free Surface Viscoelasticity of Ultrathin Polystyrene Films", Macromolecules **47**, 8808–8818 (2014).

[95]C. M. Evans, S. Narayanan, Z. Jiang, and J. M. Torkelson, "Modulus, Confinement, and Temperature Effects on Surface Capillary Wave Dynamics in Bilayer Polymer Films Near the Glass Transition", Physical Review Letters **109**, 038302 (2012).

[96]C. M. Evans, S. Kim, C. B. Roth, R. D. Priestley, L. J. Broadbelt, and J. M. Torkelson, "Role of Neighboring Domains in Determining the Magnitude and Direction of Tg-Confinement Effects in Binary, Immiscible Polymer Systems", Polymer **80**, 180–187 (2015).

[97]R. P. Sharma and P. F. Green, "Role of "Hard" and "Soft" Confinement on Polymer Dynamics at the Nanoscale", ACS Macro Letters **6**, 908–914 (2017).

[98]K.-I. Jo, Y. Oh, B. J. Sung, T.-H. Kim, M. S. Um, W. J. Choi, J. Bang, G. Yuan, S. K. Satija, and J. Koo, "Enhanced Dynamics of Confined Polymers near the Immiscible Polymer–Polymer Interface: Neutron Reflectivity Studies", ACS Macro Letters **9**, 210–215 (2020).

[99]D. D. Hsu, W. Xia, J. Song, and S. Keten, "Dynamics of Interacting Interphases in Polymer Bilayer Thin Films", MRS Communications **7**, 832–839 (2017).

[100]S. Mani and R. Khare, "Effect of Chain Flexibility and Interlayer Interactions on the Local Dynamics of Layered Polymer Systems", Macromolecules **51**, 576–588 (2018).

[101]R. R. Baglay and C. B. Roth, "Experimental Study of the Influence of Periodic Boundary Conditions: Effects of Finite Size and Faster Cooling Rates on Dissimilar Polymer–Polymer Interfaces", ACS Macro Letters **6**, 887–891 (2017).

[102]J.-H. Lee, D. Veysset, J. P. Singer, M. Retsch, G. Saini, T. Pezeril, K. A. Nelson, and E. L. Thomas, "High Strain Rate Deformation of Layered Nanocomposites", Nature Communications **3**, 1164 (2012).

[103]L. Shen, T.-P. Wang, F.-Y. Lin, S. Torres, T. Robison, S. H. Kalluru, N. B. Hernández, and E. W. Cochran, "Polystyrene- block-Polydimethylsiloxane as a Potential Silica Substitute for Polysiloxane Reinforcement", ACS Macro Letters **9**, 781–787 (2020).

[104]P. J. Beltramo, D. Schneider, G. Fytas, and E. M. Furst, "Anisotropic Hypersonic Phonon Propagation in Films of Aligned Ellipsoids", Physical Review Letters **113**, 205503 (2014).

[105]F. S. Bates, M. A. Hillmyer, T. P. Lodge, C. M. Bates, K. T. Delaney, and G. H. Fredrickson, "Multiblock Polymers: Panacea or Pandora's Box?", Science **336**, 434–440 (2012).

[106]R. Y. F. Liu, T. E. Bernal-Lara, A. Hiltner, and E. Baer, "Polymer Interphase Materials by Forced Assembly", Macromolecules **38**, 4819–4827 (2005).

[107]E. Kang, B. Graczykowski, U. Jonas, D. Christie, L. A. G. Gray, D. Cangialosi, R. D. Priestley, and G. Fytas, "Shell Architecture Strongly Influences the Glass Transition, Surface Mobility, and Elasticity of Polymer Core-Shell Nanoparticles", Macromolecules **52**, 5399–5406 (2019).

[108]Y. Tao, J. Kim, and J. M. Torkelson, "Achievement of Quasi-Nano Structured Polymer Blends by Solid-State Shear Pulverization and Compatibilization by Gradient Copolymer Addition", Polymer **47**, 6773–6781 (2006).

[109]X. Huang, M. F. Thees, W. B. Size, and C. B. Roth, "Experimental Study of Substrate Roughness on the Local Glass Transition of Polystyrene", Journal of Chemical Physics **152**, 244901 (2020).

[110]D. S. Simmons, "An Emerging Unified View of Dynamic Interphases in Polymers", Macromolecular Chemistry And Physics **217**, 137–148 (2016).

[111]J. DeFelice, S. T. Milner, and J. E. G. Lipson, "Simulating Local Tg Reporting Layers in Glassy Thin Films", Macromolecules **49**, 1822–1833 (2016).

[112]P. Z. Hanakata, B. A. P. Betancourt, J. F. Douglas, and F. W. Starr, "A Unifying Framework to Quantify the Effects of Substrate Interactions, Stiffness, and Roughness on the Dynamics of Thin Supported Polymer Films", Journal of Chemical Physics **142**, 234907 (2015).

[113]A. Kriisa, S. S. Park, and C. B. Roth, "Characterization of Phase Separation of Polystyrene/Poly(vinyl methyl ether) Blends using Fluorescence", Journal of Polymer Science Part B: Polymer Physics **50**, 250–256 (2012).

[114]J. D. Glover, C. E. McLaughlin, M. K. McFarland, and J. T. Pham, "Extracting Uncrosslinked Material From Low Modulus Sylgard 184 and the Effect on Mechanical Properties", Journal of Polymer Science **58**, 343–351 (2020).

[115]F. Carrillo, S. Gupta, M. Balooch, S. J. Marshall, G. W. Marshall, L. Pruitt, and C. M. Puttlitz, "Nanoindentation of Polydimethylsiloxane Elastomers: Effect of Crosslinking, Work of Adhesion, and Fluid Environment on Elastic Modulus", Journal of Materials Research **20**, 2820–2830 (2005).

[116]B. Trappmann, J. E. Gautrot, J. T. Connelly, D. G. T. Strange, Y. Li, M. L. Oyen, M. A. C. Stuart, H. Boehm, B. Li, V. Vogel, J. P. Spatz, F. M. Watt, and W. T. S. Huck, "Extracellular-Matrix Tethering Regulates Stem-Cell Fate", Nature Materials **11**, 642–649 (2012).

[117]A. Tiwari, L. Dorogin, A. I. Bennett, K. D. Schulze, W. G. Sawyer, M. Tahir, G. Heinrich, and B. N. J. Persson, "The Effect of Surface Roughness and Viscoelasticity on Rubber Adhesion", Soft Matter **13**, 3602–3621 (2017).

[118]Schott Corporation, *Technical Information Advanced Optics 31: Mechanical and Thermal Properties of Optical Glass* (version October 2018).

[119]J. A. Forrest and K. Dalnoki-Veress, "Sub-Glass-Transition Temperature Interface Formation Between an Immiscible Glass Rubber Pair", Journal of Polymer Science Part B: Polymer Physics **39**, 2664–2670 (2001).

[120]J. N. Lee, X. Jiang, D. Ryan, and G. M. Whitesides, "Compatibility of Mammalian Cells on Surfaces of Poly(dimethylsiloxane)", Langmuir **20**, 11684–11691 (2004).

[121]M. J. Melillo, *PDMS Network Structure-Property Relationships: Influence of Molecular Architecture on Mechanical and Wetting Properties* (Ph.D. Dissertation, North Carolina State University, 2017).

[122]J. Brandrup, E. H. Immergut, E. A. Grulke, A. Abe, and D. H. Bloch, eds., *Polymer Handbook*, 4th (Wiley, New York, 1999).

[123]A. Smessaert and J. Rottler, "Structural Relaxation in Glassy Polymers Predicted by Soft Modes: A Quantitative Analysis", Soft Matter **10**, 8533–8541 (2014).

[124]M. L. Manning and A. J. Liu, "Vibrational Modes Identify Soft Spots in a Sheared Disordered Packing", Physical Review Letters **107**, 108302 (2011).

[125]K. Spaeth, G. Kraus, and G. Gauglitz, "In-Situ Characterization of Thin Polymer Films for Applications in Chemical Sensing of Volatile Organic Compounds By Spectroscopic Ellipsometry", Fresenius' Journal of Analytical Chemistry **357**, 292–296 (1977).

[126]E. W. Cochran, D. C. Morse, and F. S. Bates, "Design of ABC Triblock Copolymers near the ODT with the Random Phase Approximation", Macromolecules **36**, 782–792 (2003).

[127]S. Nandi and H. H. Winter, "Swelling Behavior of Partially Cross-Linked Polymers: A Ternary System", Macromolecules **38**, 4447–4455 (2005).

[128]K. R. Shull, M. Taghon, and Q. Wang, "Investigations of the High-Frequency Dynamic Properties of Polymeric Systems With Quartz Crystal Resonators", Biointerphases **15**, 021012 (2020).

[129]D. Johannsmann, A. Langhoff, and C. Leppin, "Studying Soft Interfaces with Shear Waves: Principles and Applications of the Quartz Crystal Microbalance (QCM)", Sensors **21**, 3490 (2021).

[130]A. D. Easley, T. Ma, C. I. Eneh, J. Yun, R. M. Thakur, and J. L. Lutkenhaus, "A Practical Guide to Quartz Crystal Microbalance With Dissipation Monitoring of Thin Polymer Films", Journal of Polymer Science, DOI: 10.1002/pol.20210324 (2021).

[131]D. Johannsmann, K. Mathauer, G. Wegner, and W. Knoll, "Viscoelastic Properties of Thin Films Probed With a Quartz-Crystal Resonator", Physical Review B **46**, 7808–7815 (1992).

[132]A. Domack, O. Prucker, J. Rühe, and D. Johannsmann, "Swelling of a Polymer Brush Probed With a Quartz Crystal Resonator", Physical Review E **56**, 680–689 (1997).

[133]O. Wolff and D. Johannsmann, "Shear Moduli of Polystyrene Thin Films Determined With Quartz Crystal Resonators in the Sandwich Configuration", Journal of Applied Physics **87**, 4182–4188 (2000).

[134]D. A. Brass and K. R. Shull, "Membrane-Enhanced Surface Acoustic Wave Analysis of Grafted Polymer Brushes", Journal of Applied Physics **103**, 073517 (2008).

[135]G. C. DeNolf, L. Haack, J. Holubka, A. Straccia, K. Blohowiak, C. Broadbent, and K. R. Shull, "High Frequency Rheometry of Viscoelastic Coatings with the Quartz Crystal Microbalance", Langmuir **27**, 9873–9879 (2011).

[136]G. C. DeNolf, L. F. Sturdy, and K. R. Shull, "High-Frequency Rheological Characterization of Homogeneous Polymer Films with the Quartz Crystal Microbalance", Langmuir **30**, 9731–9740 (2014).

[137]L. Sturdy, F. Casadio, M. Kokkori, K. Muir, and K. R. Shull, "Quartz Crystal Rheometry: A Quantitative Technique for Studying Curing and Aging in Artists' Paints", Polymer Degradation and Stability **107**, 348–355 (2014).

[138]L. F. Sturdy, A. Yee, F. Casadio, and K. R. Shull, "Quantitative Characterization of Alkyd Cure Kinetics With the Quartz Crystal Microbalance", Polymer **103**, 387–396 (2016).

[139]K. Sadman, C. G. Wiener, R. Weiss, C. C. White, K. R. Shull, and B. D. Vogt, "Quantitative Rheometry of Thin Soft Materials Using the Quartz Crystal Microbalance with Dissipation", Analytical Chemistry **90**, 4079 (2018).

[140]D. E. Delgado, L. F. Sturdy, C. W. Burkhart, and K. R. Shull, "Validation of Quartz Crystal Rheometry in the Megahertz Frequency Regime", Journal of Polymer Science Part B: Polymer Physics **57**, 1246–1254 (2019).

[141]D. K. Reid, A. Summers, J. O'Neal, A. V. Kavarthapu, and J. L. Lutkenhaus, "Swelling and Thermal Transitions of Polyelectrolyte Multilayers in the Presence of Divalent Ions", Macromolecules **49**, 5921–5930 (2016).

[142]H. Furusawa, T. Sekine, and T. Ozeki, "Hydration and Viscoelastic Properties of High- and Low-Density Polymer Brushes Using a Quartz-Crystal Microbalance Based on Admittance Analysis (QCM-A)", Macromolecules **49**, 3463–3470 (2016).

[143]X. Tang, J. Fang, X. Du, and D.-M. Zhu, "Probing the Viscoelastic Moduli of Thin, Soft Films With a Quartz Crystal Resonator", Journal of Applied Polymer Science **134**, 44532 (2017).

[144]H. Tanoue, N. L. Yamada, K. Ito, and H. Yokoyama, "Quantitative Analysis of Polymer Brush Formation Kinetics Using Quartz Crystal Microbalance: Viscoelasticity of Polymer Brush", Langmuir **33**, 5166–5172 (2017).

[145]J. Petri and D. Johannsmann, "Determination of the Shear Modulus of Thin Polymer Films with a Quartz Crystal Microbalance: Application to UV-Curing", Analytical Chemistry **91**, 1595–1602 (2019).

[146]J. T. O'Neal, E. Y. Dai, Y. Zhang, K. B. Clark, K. G. Wilcox, I. M. George, N. E. Ramasamy, D. Enriquez, P. Batys, M. Sammalkorpi, and J. L. Lutkenhaus, "QCM-D Investigation of Swelling Behavior of Layer-by-Layer Thin Films upon Exposure to Monovalent Ions", Langmuir **34**, 999–1009 (2018).

[147]D. Lin, P. Lopez-Sanchez, N. Selway, and M. J. Gidley, "Viscoelastic Properties of Pectin/Cellulose Composites Studied by QCM-D and Oscillatory Shear Rheology", Food Hydrocolloids **79**, 13–19 (2018).

[148]A. D. Monta, F. Razan, J.-B. Le Cam, and G. Chagnon, "Using Thickness-Shear Mode Quartz Resonator for Characterizing the Viscoelastic Properties of PDMS During Cross-Linking, From the Liquid to the Solid State and at Different Temperatures", Sensors and Actuators A: Physical **280**, 107–113 (2018).

[149]M. Zhang, C. G. Wiener, P. I. Sepulveda-Medina, J. F. Douglas, and B. D. Vogt, "Influence of Sodium Salts on the Swelling and Rheology of Hydrophobically Cross-Linked Hydrogels Determined by QCM-D", Langmuir **35**, 16612–16623 (2019).

[150]L. H. Sperling, "Sound and Vibration Damping with Polymers", in *Sound and Vibration Damping with Polymers*, edited by R. D. Corsaro and L. H. Sperling (ACS Symposium Series, vol. 424, 1990), pp. 5–22.

[151]V. G. Geethamma, R. Asaletha, N. Kalarikkal, and S. Thomas, "Vibration and Sound Damping in Polymers", Resonance **19**, 821–833 (2014).

[152]V. T. Rathod, "A Review of Acoustic Impedance Matching Techniques for Piezoelectric Sensors and Transducers", Sensors **20**, 4051 (2020).

[153]G. Sauerbrey, "Verwendung von Schwingquarzen zur Wägung dünner Schichten und zur Mikrowägung", Zeitschrift für Physik **155**, 206–222 (1959).

[154]M. V. Voinova, M. Rodahl, M. Jonson, and B. Kasemo, "Viscoelastic Acoustic Response of Layered Polymer Films at Fluid-Solid Interfaces: Continuum Mechanics Approach", Physica Scripta **59**, 391–396 (1999).

[155]N. B. Eisele, F. I. Andersson, S. Frey, and R. P. Richter, "Viscoelasticity of Thin Biomolecular Films: A Case Study on Nucleoporin Phenylalanine-Glycine Repeats Grafted to a Histidine-Tag Capturing QCM-D Sensor", Biomacromolecules **13**, 2322–2332 (2012).

[156]V. E. Granstaff and S. J. Martin, "Characterization of a Thickness-Shear Mode Quartz Resonator With Multiple Nonpiezoelectric Layers", Journal of Applied Physics **75**, 1319–1329 (1994).

[157]D. Johannsmann, "Viscoelastic, Mechanical, and Dielectric Measurements on Complex Samples With the Quartz Crystal Microbalance", Physical Chemistry Chemical Physics **10**, 4516–4534 (2008).

[158]D. Johannsmann, "Viscoelastic Analysis of Organic Thin Films on Quartz Resonators", Macromolecular Chemistry and Physics **200**, 501–516 (1999).

[159]E. J. Martin, M. T. Mathew, and K. R. Shull, "Viscoelastic Properties of Electrochemically Deposited Protein/Metal Complexes", Langmuir **31**, 4008–4017 (2015).

[160]C.-S. Lu and O. Lewis, "Investigation of Film-Thickness Determination by Oscillating Quartz Resonators With Large Mass Load", Journal of Applied Physics **43**, 4385–4390 (1972).

[161]P. H. Mott, J. R. Dorgan, and C. M. Roland, "The Bulk Modulus and Poisson's Ratio of "Incompressible" Materials", Journal of Sound and Vibration **312**, 572–575 (2008).

[162]B. Hartmann, "Acoustic Properties", in *Physical Properties of Polymers Handbook*, edited by J. E. Mark (AIP Press, New York, 1996) Chap. 49, pp. 677–686.

[163]B. Hartmann and J. Jarzynski, "Immersion Apparatus for Ultrasonic Measurements in Polymers", Journal of the Acoustical Society of America **56**, 1469–1477 (1974).

[164]R. H. Colby, L. J. Fetters, and W. W. Graessley, "The Melt Viscosity-Molecular Weight Relationship for Linear Polymers", Macromolecules **20**, 2226–2237 (1987).

[165]L. I. Palade, V. Verney, and P. Attané, "Time-Temperature Superposition and Linear Viscoelasticity of Polybutadienes", Macromolecules **28**, 7051–7057 (1995).

[166]S. J. Park, P. S. Desai, X. Chen, and R. G. Larson, "Universal Relaxation Behavior of Entangled 1,4-Polybutadiene Melts in the Transition Frequency Region", Macromolecules **48**, 4122–4131 (2015).

[167]S. Wang, S.-Q. Wang, A. Halasa, and W.-L. Hsu, "Relaxation Dynamics in Mixtures of Long and Short Chains: Tube Dilation and Impeded Curvilinear Diffusion", Macromolecules **36**, 5355–5371 (2003).

[168]C.-Y. Liu, R. Keunings, and C. Bailly, "Direct Rheological Evidence of Monomer Density Reequilibration for Entangled Polymer Melts", Macromolecules **40**, 2946–2954 (2007).

[169]L. Szántó, R. Vogt, J. Meier, D. Auhl, E. Van Ruymbeke, and C. Friedrich, "Entanglement Relaxation Time of Polyethylene Melts From High-Frequency Rheometry in the Mega-Hertz Range", Journal of Rheology **61**, 1023–1033 (2017).

[170]J. M. K. Ng, I. Gitlin, A. D. Stroock, and G. M. Whitesides, "Components for Integrated Poly(dimethylsiloxane) Microfluidic Systems", Electrophoresis **23**, 3461–3473 (2002).

[171]M. Murrell, R. Kamm, and P. Matsudaira, "Substrate Viscosity Enhances Correlation in Epithelial Sheet Movement", Biophysical Journal **101**, 297–306 (2011).

[172]G. M. Whitesides, "Soft Robotics", Angewandte Chemie International Edition **57**, 4258–4273 (2018).

[173]J. Herzberger, J. M. Sirrine, C. B. Williams, and T. E. Long, "Polymer Design for 3D Printing Elastomers: Recent Advances in Structure, Properties, and Printing", Progress in Polymer Science **97**, 101144 (2019).

[174]A. Müller, M. C. Wapler, and U. Wallrabe, "A Quick and Accurate Method to Determine the Poisson's Ratio and the Coefficient of Thermal Expansion of PDMS", Soft Matter **15**, 779–784 (2019).

[175]H. C. Booij and G. P. J. M. Thoone, "Generalization of Kramers-Kronig Transforms and Some Approximations of Relations Between Viscoelastic Quantities", Rheologica Acta **21**, 15–24 (1982).

[176]L. L. Stevens, E. B. Orler, D. M. Dattelbaum, M. Ahart, and R. J. Hemley, "Brillouin-Scattering Determination Of The Acoustic Properties And Their Pressure Dependence For Three Polymeric Elastomers", Journal of Chemical Physics **127**, 104906 (2007).

[177]Y. Ding and A. P. Sokolov, "Breakdown Of Time–Temperature Superposition Principle And Universality Of Chain Dynamics In Polymers", Macromolecules **39**, 3322–3326 (2006).

[178]L. M. Robeson, *Polymer Blends: a Comprehensive Review* (Hanser Gardner Publications, Inc., Cincinnati, OH, 2007).

[179]C. B. Roth, A. Pound, S. W. Kamp, C. A. Murray, and J. Dutcher, "Molecular-Weight Dependence of the Glass Transition Temperature of Freely-Standing Poly (methyl methacrylate) Films", The European Physical Journal E **20**, 441–448 (2006).

[180]J. E. Pye and C. B. Roth, "Two Simultaneous Mechanisms Causing Glass Transition Temperature Reductions in High Molecular Weight Freestanding Polymer Films as Measured by Transmission Ellipsometry", Physical Review Letters **107**, 235701 (2011).

[181]Y. J. Gagnon, J. C. Burton, and C. B. Roth, "Physically Intuitive Continuum Mechanics Model for Quartz Crystal Microbalance: Viscoelasticity of Rubbery Polymers at MHz Frequencies", Journal of Polymer Science **60**, 244–257 (2022).

[182]J. N. Owens, I. S. Gancarz, J. T. Koberstein, and T. P. Russell, "Investigation of the Microphase Separation Transition in Low-Molecular-Weight Diblock Copolymers", Macromolecules **22**, 3380–3387 (1989).

[183]G. Kapteijns, D. Richard, and E. Lerner, "Nonlinear Quasilocalized Excitations in Glasses: True Representatives of Soft Spots", Physical Review E **101**, 032130 (2020).

[184]S. S. Schoenholz, A. J. Liu, R. A. Riggleman, and J. Rottler, "Understanding Plastic Deformation in Thermal Glasses From Single-Soft-Spot Dynamics", Physical Review X **4**, 031014 (2014).

[185]Y. Zhai, P. Luo, and Y. Z, "Role of Phonon Softening Induced by Anisotropic Fluctuations in the Enhanced Mobility at Free Glassy Surfaces", Physical Review B **103**, 085424 (2021).

[186]C. B. Roth, "Polymers Under Nanoconfinement: Where Are We Now in Understanding Local Property Changes?", Chemical Society Reviews **50**, 8050–8066 (2021).

[187]B. Li, S. Zhang, J. S. Andre, and Z. Chen, "Relaxation Behavior of Polymer Thin Films: Effects of Free Surface, Buried Interface, and Geometrical Confinement", Progress in Polymer Science **120**, 101431 (2021).

[188]S. Zhang, L. A. Galuska, and X. Gu, "Water-Assisted Mechanical Testing of Polymeric Thin-Films", Journal of Polymer Science, DOI: 10.1002/pol.20210281 (2021).

[189]H. Tian, Q. Xu, H. Zhang, R. D. Priestley, and B. Zuo, "Surface Dynamics of Glasses", Applied Physics Reviews **9**, 011316 (2022).